UNIVERSITÀ DEGLI STUDI DI BRESCIA

DOTTORATO DI RICERCA IN INGEGNERIA MECCANICA E INDUSTRIALE

CICLO XXXIII

Settore scientifico disciplinare

FIS/01 FISICA SPERIMENTALE

RISK ASSESSMENT OF RADIATION "HOT SPOTS" IN A RADIOACTIVE ION BEAM FACILITY

DOTTORANDA: Antonietta Donzella

RELATORE: Prof. Aldo Zenoni

COORDINATORE DEL DOTTORATO: Prof.ssa Laura Depero

Riassunto

I nuclei atomici sono stati per oltre un secolo oggetto di studi sperimentali rivolti all'investigazione della loro struttura e alla comprensione delle loro caratteristiche. Con la scoperta della radioattività, un numero via via maggiore di nuclei instabili si è reso disponibile, e più recentemente la comunità internazionale dei fisici nucleari ha iniziato a focalizzare la propria attenzione sui nuclei radioattivi che presentano un eccesso di protoni o neutroni rispetto agli isotopi stabili della stesse specie.

Questi nuclei "esotici" rappresentano tutt'oggi una preziosa risorsa per lo studio delle proprietà del nucleo e dei fenomeni astrofisici legati all'evoluzione stellare. Oltre a ciò, essi consentono di svolgere ricerche d'avanguardia in molteplici settori interdisciplinari, ad esempio nella scienza dei materiali o in ambito medico-diagnostico, per la produzione e lo studio di radiofarmaci innovativi.

Lo sviluppo nella generazione di fasci accelerati di ioni composti da nuclei instabili o radioattivi (Radioactive Ion Beams o RIBs) richiede complesse tecnologie di produzione. Una di queste tecniche è basata sul metodo ISOL (Isotope Separation On-Line), che consente di ottenere fasci di ioni radioattivi con un'elevata purezza isotopica. La tecnica ISOL prevede un fascio primario di ioni leggeri prodotto da un acceleratore e un bersaglio per la produzione degli isotopi di interesse, la loro estrazione per evaporazione dal bersaglio e successiva ionizzazione, infine la selezione e riaccelerazione dei fasci radioattivi.

La presenza di acceleratori di particelle per i fasci primari e la produzione di specie esotiche secondarie, possono generare situazioni di potenziale impatto radioattivo sulla persona e sull'ambiente, che vanno attentamente valutate e tenute sotto controllo. Il successo di questo tipo di installazioni dipende anche dalle molteplici soluzioni adottate per la gestione della sicurezza radiologica dell'impianto, partendo dalla fase di progettazione fino a quella di funzionamento e poi di dismissione, alla fine del ciclo di vita dell'apparato.

Attualmente nel mondo sono presenti numerosi impianti per la produzione di RIBs. Tra di essi vi è il progetto SPES (Selective Production of Exotic Species), in avanzata fase di realizzazione presso i Laboratori Nazionali di Legnaro (LNL), PD, dell'Istituto Nazionale di Fisica Nucleare (INFN). Lo scopo del progetto è quello di produrre col metodo ISOL intensi fasci di nuclei radioattivi ricchi di neutroni, con elevata purezza isotopica.

Il lavoro presentato in questa tesi è dedicato alla valutazione dei rischi di natura radiologica in alcune tra le aree più critiche dell'impianto SPES ai LNL. Viene effettuato uno studio dettagliato della radioattività e della potenziale esposizione esterna causate da alcuni "hot spot" di radiazione presenti in differenti aree dell'impianto SPES: in primo luogo il bunker contenente le linee di fascio, ma anche le zone in prossimità del sito di stoccaggio temporaneo, dove vengono movimentati i bersagli esausti dopo l'irraggiamento con fascio primario di protoni.

Lo scopo del lavoro è quello di fornire informazioni utili per attuare strategie di protezione per i lavoratori nelle diverse aree dell'impianto, per pianificare le ispezioni e le operazioni di manutenzione sulle linee di produzione e per gestire la fase di dismissione dell'apparato. Tutte queste strategie derivano dall'osservanza dei limiti di dose stabiliti dalla legge, dall'applicazione dei principi generali della radioprotezione e in particolare dal processo di ottimizzazione della protezione, che si applica a tutte le particolari situazioni di esposizione radiologica nell'ambito del progetto SPES.

I temi affrontati nella tesi possono essere considerati parte della più completa analisi dei rischi del progetto SPES. Inoltre, l'approccio utilizzato nello studio può essere applicato ed esteso al caso generale di un qualsiasi impianto per la produzione di RIBs con la tecnica ISOL. In conclusione, il lavoro si colloca nel contesto della promozione di politiche per lo sviluppo sostenibile di progetti di ricerca in fisica nucleare.

Contents

Chapter 1

Introduction

Since the beginning of the last century, atomic nuclei have been subject of physical researches aimed at investigating their structure and their behavior. Initially, only a small portion of the nuclei estimated to exist in the universe were studied, because only stable nuclei were known. Then, more and more unstable nuclei were discovered and big efforts were devoted, inside the nuclear physics community, in studying the structure and the stability of the nucleus. More recently, several projects in the world began to focus their attention on "exotic" radioactive nuclei having an excess of protons or neutrons with respect to stable isotopes.

The study of these unstable nuclei has generated new interest and new challenges, both for fundamental nuclear physics research and for applications in multiple fields of science. The knowledge of the interactions bounding together protons and neutrons inside the nucleus, the understanding of astrophysical phenomena as the stellar nucleosynthesis, but also the production of innovative radiopharmaceuticals for nuclear medicine, depend also on the possibility of producing and studying accelerated beams of radioactive ions.

The development of the so called Radioactive Ion Beams (RIBs) has passed through the use of complex technologies of production. Nowadays, there is a worldwide interest in producing accelerated beams of unstable nuclei for use in multidisciplinary applications. A number of facilities are under construction or currently in activity in Europe and worldwide.

The high biological hazard of the radioactive ion species involved imposes severe radiological safety constraints in the design and operation of the RIB facilities. Some of these safety and radiation protection issues are common to any accelerator-driven facility. Moreover, the presence of RIBs introduces additional radiological issues. The success of such type of installations will

also depend on cost-effective solutions to such problems.

The work presented in this thesis is devoted to the investigation of the radioactive hazard and environmental impact of the SPES (Selective Production of Exotic Species) project, a second generation nuclear facility for the production of RIBs, currently in an advanced construction phase at INFN-LNL (Istituto Nazionale di Fisica Nucleare, Laboratori Nazionali di Legnaro), Padua, Italy. The present work aims to provide useful information to implement strategies for the protection of the workers in different areas of the facility, to plan inspections, maintenance operations and to manage the decommissioning phase of the facility. In a more general extent, this approach can be applied to any existent of future RIB facility. Furthermore, it matches with the increasing interest in promoting policies for the sustainable development of nuclear physics research projects.

In Chapter 2, an overview of the SPES project and the related physical aspects and motivations are presented. The main applications, both in forefront nuclear physics research as well as in industry and medicine, are described, with particular emphasis to the ISOLPHARM project aimed at the development of radiopharmaceuticals with unprecedented purity and specific activity.

Chapter 3 introduces the main methods for the production of RIBs, and in particular the ISOL technique. Successively, it illustrates the design of the SPES apparatus, starting from the cyclotron driver up to the definition and control of the RIBs, downstream of the production. A preliminary mention of the radiation protection issues related to the SPES production target is made.

Chapter 4 describes the main elements of radiation protection related to possible exposure of people and of the environment to ionizing radiation. Biological aspects, definition of quantities of interest, definition of the system of the radiological protection and of its fundamental principles, ethics and environmental aspects are illustrated.

In Chapter 5 the radiation protection safety and security aspects specifically associated to the SPES project are mentioned, and the different case studies investigated in the thesis are introduced. Then, the calculation tools employed in the study, the adopted methods and their strengths are illustrated. Particular concern is devoted to the physics models which reproduce the nuclear fission process, which is the starting point for the operation of the SPES apparatus.

From Chapter 6 to Chapter 8 a comprehensive description of the case studies dealt with in this thesis work is presented. The assessment of the radiation external exposure, originating from all the radiation contributions in

the production area, is performed at different times during the whole SPES life cycle, in particular when maintenance operations on the RIB production apparatus are foreseen. The handling procedures of the exhausted production target and ion source units during their life cycle, and the system and equipment devoted to their temporary storage, are analyzed.

Chapter 9 outlines the main radiation issues for operators, population and the surrounding environment, arousing by the implementation and operation of the SPES facility, with reference to the people and environmental impact and to the sustainable development policies undertaken by the project.

Finally, in Chapter 10 summary and conclusions are drawn.

Chapter 2

Overview of the SPES project

2.1 Physics aspects of the project

The atom is the fundamental block of the matter composing our world. The atomic mass is essentially concentrated in its nucleus, which is 10^5 times smaller than the atom itself and can be imagined as an aggregate of particles called nucleons, about 2000 times heavier than the electron. The nucleons in turn are distinguished in protons, particles with positive electric charge, and neutrons, neutral particles. The number Z of protons identifies the chemical specie. Atoms of the same chemical element, with a different number N of neutrons in the nucleus, are called isotopes. Atomic species characterized by specific values of Z and N are called nuclides. The total number A of protons and neutrons in an atomic nucleus is the atomic mass number.

2.1.1 Nuclear structure

Nucleons are strongly bound to each other by the so-called "nuclear force", a short range interaction which is able to contrast the electrostatic repulsion between positively charged protons inside the nucleus. The mass of the nucleus is the sum of the masses of the Z protons and N neutrons constituent, decreased by the nuclear binding energy B, i.e. the minimum energy that would be required to overcome the attractive nuclear force and to break the nucleus in its components.

The nuclear binding energy per nucleon B/A is shown in Figure 2.1 for a wide range of nuclides. Its value peaks around A = 56 (close to the mass of

iron), where it exceeds 8 MeV [1], and is weakly decreasing for the nuclei with A > 56. These energy values are very high compared to the ones typical of atomic bonds, which are of the order a few eV, due to the intensity and clear predominance of the attractive nuclear force over the electromagnetic one at the very short nuclear distances. The range of mass around A=56 represents the region of maximum stability for the nuclei. When very light nuclei are merged with each other, they achieve greater stability (fusion), whereas heavy nuclei may achieve greater stability by splitting into smaller fragments (fission).
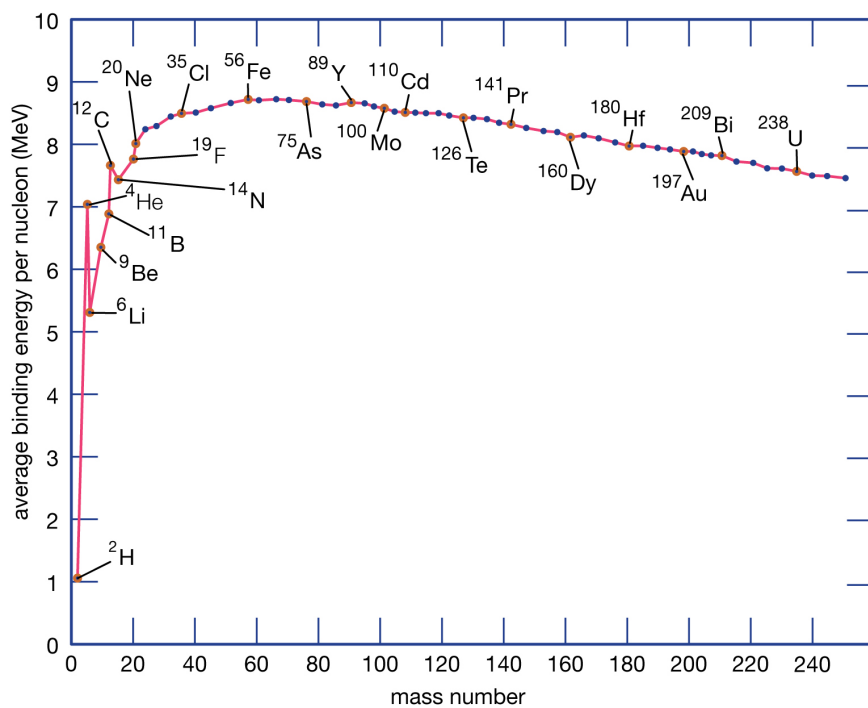
© 2012 Encyclopædia Britannica, Inc.

Figure 2.1: Binding energy as a function of the nuclear mass [1].

All the nuclides discovered up to now are included in the "chart of nuclides" (see Figure 2.2), a two-dimensional graph that represents the nuclides as a function of N and Z. The stable nuclei are characterized by balanced combinations of protons and neutrons and are positioned on the "valley of stability", identified by black squares. For these nuclei the strong interaction is able to pledge an adequate cohesion. At low N values, the stable nuclides

---

[1] 1 eV is the amount of kinetic energy gained by a single electron accelerating from rest through an electric potential difference of one volt in vacuum.

contain more or less the same number of protons and neutrons. However, as N grows, the stability valley tends to turn towards the neutron-rich region N>Z, due to the electrostatic repulsion between protons.

All the nuclides outside the stability valley are unstable or radioactive. This means that they transform into other nuclides releasing a typical spectrum of radiation. Radioactive decay is a stochastic process, but the probability of disintegration of a nuclide is constant over time and can be expressed by means of a decay constant λ. Therefore, the number of decays expected to occur in an time interval dt is proportional to the total number N_{tot} of atoms of the radionuclide present. This law can be described through the following differential equation:

$$\frac{dN_{tot}(t)}{dt} = -\lambda \ N_{tot}(t), \tag{2.1}$$

which has as solution at t = T:

$$N_{tot}(T) = N_{tot}(0) \ e^{-\lambda T}. \tag{2.2}$$

This expression gives the definition of "activity":

$$A_{tot}(t) = \ \mid \frac{dN_{tot}(t)}{dt} \mid \ = \lambda \ N_{tot}(t). \tag{2.3}$$

The activity is a quantity defined as the number of decays per unit of time of a given quantity of radioactive material. The early unit of activity was the curie (Ci), that is defined as $3.7 \cdot 10^{10}$ disintegrations per second. However, the curie is sometimes replaced by its corresponding SI unit, the bequerel (Bq), defined as one disintegration per second.

The decay constant λ is characteristic of the substance in question and represents the average number of decays of the single nucleus in the unit of time. Often, the time required to reduce to one half the initial activity, the half-life, is considered; it is related to the decay constant as follows:

$$t_{1/2} = \frac{ln \ 2}{\lambda}. \tag{2.4}$$

The half-lives of the radioactive nuclei vary from nearly instantaneous to longer than the age of the universe.

The radioactive nuclides with a neutron excess will generally decay transmuting a neutron into a proton (with the emission of an electron and an antineutrino). On the contrary, if a nuclide is characterized by a proton excess, it will decay transmuting a proton into a neutron (with the emission of a positron and a neutrino). In both reactions, there is emission of energy. These two processes, called β- decay and β+ decay respectively, are a

consequence of the "weak force", a nuclear interaction responsible for most radioactive decays. The mass number of the new atom does not change, whereas the number of protons increases of one (β- decay) or decreases of one (β+ decay).
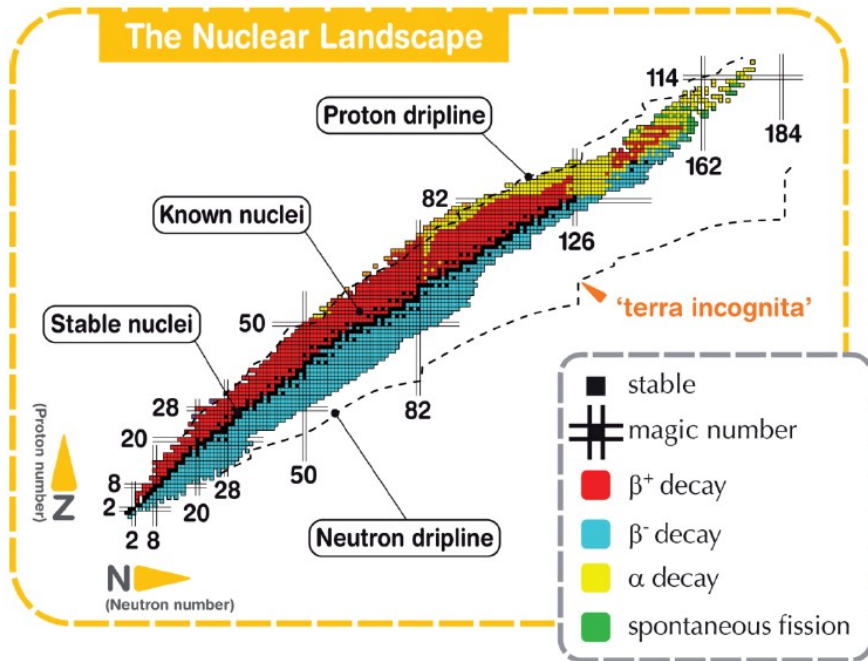
Figure 2.2: Chart of the nuclides [2].

Otherwise, a nucleus in an excited state tends to lose the excess energy emitting high frequency electromagnetic radiation due to the internal re-arrangement of the nucleons. This is the case of the γ decay. The nucleus does not change its position in the nuclide chart and, consequently, it remains the same isotope.

Again, in the heaviest nuclei the binding energy could not be strong enough to hold up together the whole nucleus permanently, so it may undergo fragmentation into two or even more light nuclei. In most cases, one of the fragments involved in the reaction is a ^{4}He nucleus (called α particle), because of its extremely stable structure. This kind of process is called α decay. In this way, the daughter nucleus will have a variation of both the number Z of protons and the number A of mass, according to: $Z_{daughter} = Z_{parent}$ - 2, $A_{daughter} = A_{parent}$ - 4.

If the daughter nucleus is not a ^{4}He nucleus, a spontaneous fission occurs, a process whereby a parent nucleus breaks into two daughter nuclei of

approximately equal masses without any external action.

Nowadays around 3600 radioactive nuclei have been studied in laboratories. However, more than 6000 unstable nuclei are expected to exist in the universe. Many of these "exotic nuclei" are located at the limits of the nuclide chart, in the so called "terra incognita", which includes the neutron-rich and the super-heavy nuclei, as shown in Figure 2.2. Beyond this boundary, the nuclei are so unstable that they immediately decay emitting nucleons.

The production of the RIBs allows nuclei which are located far from the stability valley to be investigated. Atomic nuclei with very asymmetric combinations of protons and neutrons can be produced and used in different fields of science. In Section 2.3 some of the most important applications of RIBs will be summarized.

2.1.2   Nuclear reactions

A nuclear reaction is a collision between an energetic nuclear particle or nucleus and a target nucleus. It happens when the particle succeeds to overcome the Coulomb energy barrier and therefore enter in the nuclear force range. The first nuclear reactions were observed around 1919 in the Rutherford's laboratory, using α particles emitted by a radioactive source. In these early experiments, the α particles hitting the target were re-emitted from the target nuclei in an elastic way, and this fact suggested, for the first time, the existence of the atomic nucleus. This phenomenon, called since that time "Rutherford scattering", is a particular type of nuclear reaction in which the final products are the same than the initial ones. However, in general, the final products of a nuclear reaction may be different from the initial ones or may not be uniquely defined.

The properties of the nuclear reactions depend on the nature, mass and energy of the projectile and the nature of the target. Reactions can be induced by light projectiles (A≤4) incident on heavy nuclei, or by heavy ions with mass number until 40 or more. Furthermore, nuclear reactions are classified as "low energy" reactions if the energy of the projectile is lower than 10 MeV per nucleon or less, as "medium energy" reactions in the 100 MeV-1 GeV energy range and "high energy" reactions for larger projectile energy values.

As an example, a nucleon incident on a nucleus of mass number A can be absorbed by the nucleus. The resulting "compound nucleus", that has A+1 nucleons, acquires an excitation energy equal to the kinetic energy of the incoming particle plus the new amount of binding energy of the nucleus, that generally is less stable than the previous one. Among the various pos-

sibilities, the de-excitation process can consist in the emission of a particle with the same or smaller energy than that of the nucleon absorbed. This phenomenon may not take place immediately; in fact, the excited nucleus can live a time long enough to lose any memory about the former process that created the unstable nucleus.

Often, the result of this process is the formation of radioactivity in materials. The excited nucleus can in fact decay through the radioactive phenomena described in Section 2.1.1. As an example, in the case of the SPES project, a 40 MeV primary proton beam interacts with a production target, generating neutrons by nuclear fission of the ^{238}U nuclei of the target (see Section 2.1.3). In this case, "induced activation" on the materials of the production apparatus can be caused both by direct interaction of the primary protons and by fission neutron interaction. This topic will be discussed in detail in Section 6.5.2.

Furthermore, a 40 MeV proton interaction on a ^{238}U nucleus of the SPES target can lead to proton capture with production of a Np isotope and some neutrons, as indicated in Equation 2.5:

$$ p \; + \; ^{238}U \rightarrow \; ^{239-x}Np \; + \; xn, \tag{2.5} $$
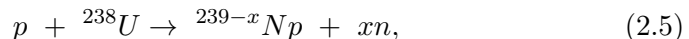
where x is an integer variable, and stands for the number of emitted neutrons after the collision. This reaction can be shorty written as ^{238}U(p,xn)$^{239-x}$Np; such notation has been used for the activation studies described in the thesis.

Each reaction channel has a certain probability to take place. This probability, normalized on the total number of reaction channels, is the reaction branching ratio. It depends on a quantity denoted as σ and called "cross section", which has the dimension of an area (it is measured in barn: 1 barn=10^{-28}m^2) and can be thought of as an area that is much larger the greater the probability of interaction.

The cross section characterizing all possible interaction processes is called "total cross section", while it is possible to distinguish different cross sections for specific processes or specific projectile nuclei, depending on the projectile energy.

2.1.3 Induced fission

At the energies involved in the SPES project, the proton mainly induces a fission reaction on the UC$_x$ target, in which a ^{238}U nucleus is split into two fragments and a few neutrons. The energy threshold to trigger the ^{238}U fission is about 10 MeV: a part of this energy is used to overcome the

Coulomb energy barrier (about 5-6 MeV, depending on the kind of nucleus), and the remaining part is needed to excite the nucleus and to make the process occur [3].
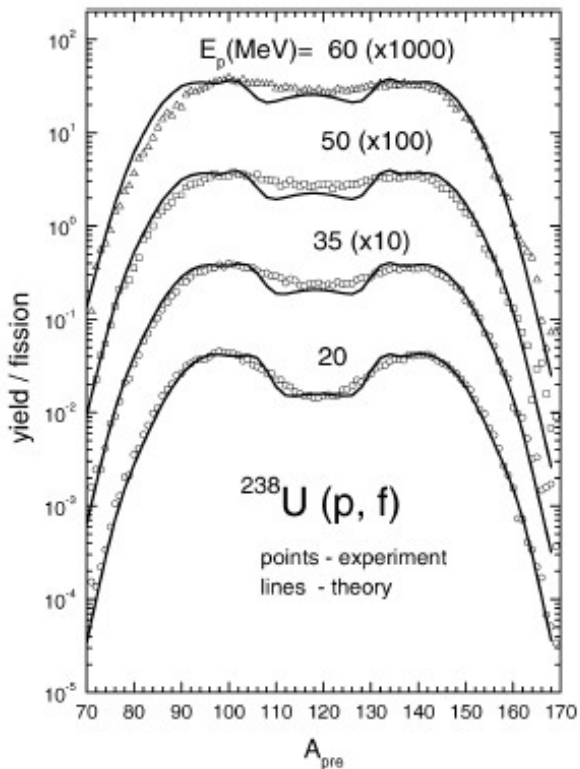
Figure 2.3: Comparison between the measured pre-neutron-emission fragment mass distributions in ^{238}U proton-induced fission at E_p=20, 35, 50 and 60 MeV (symbols) and the calculated ones (curves) [4].

Being heavy nuclei preferably neutron-rich, fission produces many lighter radioactive neutron-rich nuclei. These fragments will decay β- until they reach the valley of stability. In turn, neutrons generated after a fission process interact with the nuclei of the structures surrounding the target, generating activation in the materials. Conversely, neutrons contribute to fission in the SPES target for a percentage less than 1% [3].

In most cases, the nucleus splits into two fragments with different masses (two peak asymmetric fission spectrum). Essentially, the competition between asymmetric and symmetric terms in the fission spectrum could be connected to the presence of shell structures in the deformed nucleus. The presence of shell effects depends on the energy of the projectile: these ef-

fects lose importance with the increase of the excitation energy, leading to a symmetric fission spectrum at high excitation energies. This behavior is visible in Figure 2.3, where a comparison between experimental yields and theoretical models [4] is shown.

In general, fission is a very complex process, depending on the energy of the projectile. Despite all the progress in its understanding, still no complete theoretical model is able to describe the mass dependent and excitation energy dependent transition between symmetric and asymmetric fission in a satisfactory way [5, 6].

2.2 General description and motivations

SPES is the acronym for "Selective Production of Exotic Species". The aim of the project is to produce high intensity and high quality beams of neutron-rich radioactive nuclei to perform forefront research in interdisciplinary fields like nuclear physics, astrophysics, medicine and material sciences. The SPES project is completely financed by the Italian "Istituto Nazionale di Fisica Nucleare" (INFN) and is currently under advanced construction in one of the four main INFN laboratories in Italy, the "Laboratori Nazionali di Legnaro" (LNL), Legnaro, Padua [3, 7, 8, 9, 10, 11, 12].

An important network of collaborations, both national and international, has been constituted to complete the project, among which INFN, Laboratori Nazionali del Sud (LNS, Catania), ENEA (Bologna), Universities of Padova, Ferrara, Pavia, Trento, Brescia, LENA research reactor (Pavia) in Italy, and, in the rest of the world, HIE-ISOLDE at CERN (Switzerland) [13], ISAC at TRIUMF (Vancouver, Canada) [14], ALTO at IPN Orsay (Paris, France) [15], HRIBF at the Oak Ridge National Laboratories (USA) [16] and other RIB facilities in different countries [17, 18, 19, 20].

The SPES production method is based on the ISOL (Isotope Separation On-Line) technique [21]; this technique is explained in detail in Section 3.2. A monochromatic proton beam produced by a commercial cyclotron interacts with a multi-foil uranium carbide production target (UC_x). The target is composed of seven thin disks, 40 mm diameter and 0.8 mm thickness, with a density of about 4 g/cm^3 [22]. Radioactive neutron-rich isotopes are produced by nuclear fission induced on ^{238}U, with the aim to reach a rate of about 10^{13} fission/s in the production target. Such fission rate requires a proton beam of 40 MeV energy and 200 μA current.

The target is tightly connected to a 1+ ion source, and the Target and Ion Source (TIS) system is kept at a working temperature of about 2000 °C. In this way, the reaction products are effectively extracted from the target

by thermal processes, and reach the 1+ source. Here, they are ionized and extracted with a 40 kV voltage difference, producing a low energy radioactive beam. After an isobaric selection and a further ionization to n+, the exotic beam is injected towards a re-acceleration phase to subsequently produce high intensity and high purity RIBs.

Such a facility will produce mainly neutron-rich nuclei in a range of mass 80-160 u[2], when a uranium carbide target is used. Neutron-deficient beams will be obtained using other target materials, such as silicon carbide, currently under development.

Interest in using the RIBs produced by the SPES apparatus has been expressed by several interdisciplinary communities in different scientific and technological across-the-board aspects between nuclear physics, engineering and material science, chemistry, pharmacy. Moreover, a large interest is present in the field of medicine, to produce innovative radiopharmaceuticals to be used in therapy and diagnostics. Concerning this latter issue, in Section 2.4 the ISOLPHARM project will be briefly discussed.

2.3   Nuclear physics at SPES

The most significant physical models of the nuclear structure are based on the features of the nuclei very close to the stability region or in the proton-rich side, being they well-known and easier to produce. However, these models can hardly be validated in the neutron-rich region of the nuclide chart. Dedicated experiments with RIBs could provide more information to confirm or possibly modify some aspects of nuclear structure models, improving the understanding of nuclear fundamental interactions. In the following subsections a short description of possible contribution of RIBs in the field of fundamental and applied nuclear physics is provided.

2.3.1   Improvement and verification of the Standard Model

The study of the unstable nuclei, and in particular of the exotic nuclei, opens the way to forefront researches in nuclear physics. Of crucial importance is the proof of the validity of the Standard Model, that considers three of the four fundamental interactions, namely the strong nuclear interaction, electromagnetism and the weak nuclear interaction as unified.

All the properties and the interactions between all known particles are included in such model; however, the Standard Model cannot be seen as a

---

[2]The dalton or unified atomic mass unit (u) is defined as 1/12 of the mass of an unbound neutral atom of ^{12}C in its nuclear and electronic ground state and at rest.

complete theory for the fundamental interactions, since it is based on some assumptions that are not yet experimentally verified and some phenomena are still unexplained by the model. For example, the theory of gravitation, as described by general relativity, is not contemplated by the model.

Measurements on very exotic RIBs could provide precise information on the decay properties of some less-known nuclei, contributing to verify the fundamental assumptions of the Standard Model.

2.3.2 Neutron halos

In the "liquid drop model" of the nucleus, the radius of the atomic nucleus is described according to $R = R_0 \cdot A^{1/3}$, where R_0 is a dimensional constant and A the atomic mass number. However, the more a nucleus is far from the stability valley, the smaller is the binding energy of the last nucleons. For nuclei near to the neutron drip line, one or more neutrons with a small amount of separation energy[3] may move in special low matter density regions, external to the core containing all the other nucleons. This kind of region is associated to a nuclear halo.

One of the first halo nuclei discovered was ^{11}Li, which has two neutrons orbiting around a ^{9}Li core [23]. As it can be seen from Figure 2.4, its halo is about of the same size as the core of the ^{48}Ca isotope.
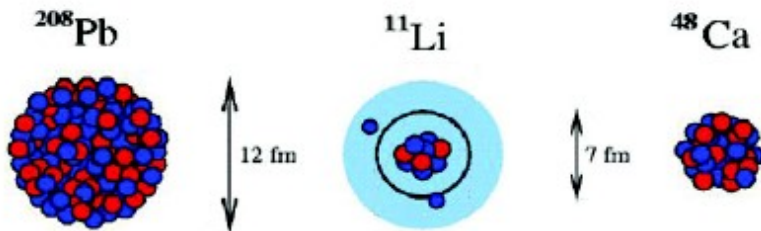
Figure 2.4: Comparison between the size of the ^{11}Li nucleus and that of other more massive nuclei.

2.3.3 Super-heavy element production

The chemical elements that can be found in Nature are just over 90. Recently, nuclear fusion allowed new heavier nuclei to be synthesized, extending

---

[3]In nuclear physics, separation energy is the energy needed to remove one nucleon from an atomic nucleus.

the periodic table up to Z = 118 or more. Such elements, indicated as super-heavy, lie around the so-called "island of stability", corresponding, on the nuclide chart, to the region around Z = 114 protons and N = 184 neutrons, which is considered particularly stable [24]. The formation of such elements can occur when neutron-rich RIBs impinge neutron-rich (stable) targets.

2.3.4 Nuclear astrophysics

Nuclear astrophysics plays an important role in the understanding of the structure of the Universe as well as of the processes involved in its origin and evolution. One of the main lines of research of this science consists in studying the stellar cycles. Stars are natural nuclear reactors in which both stable and unstable nuclei interact generating energy through nuclear reactions [25]. Sometimes the consumption of nuclear fuel proceeds regularly and these processes last billions of years; in other conditions they are explosive and last few minutes or seconds.

During the different phases of the life of a star, new chemical elements are formed, both through reactions of nucleosynthesis that follow the stability valley, and through other processes that take place in unknown regions of the nuclide chart. In order to define models able to describe such processes, essential information including lifetimes, masses and decay channels are requested for a number of key nuclides far from the stability valley.

Nuclear reactions involving unstable nuclei can be measured only through the use of radioactive beams. So, the facilities for the production of RIBs will be fundamental for the understanding of the elemental synthesis of the Universe.

2.3.5 Solid state physics

The development of smaller and smaller semiconductor materials, with the request of optimal optical and electrical characteristics, needs severe controls on defects that strongly affect their properties and their function. Since the radioactive isotopes have the same chemical properties of the stable nuclides, they can be used to probe the optical and electrical behavior of the semiconductor, according to their position inside the crystal lattice.

The technique of the "Emission Channeling" consists in the implantation of radioactive nuclei inside a solid state system and the following study of their decay, with the detection of the emitted particles or the gamma radiation. Measuring the anisotropic intensity distributions of the emitted radiation, the position occupied by the radioactive isotopes inside the

structure of the crystal can be determined with an accuracy of few tenths of Å. [26].

2.3.6   Nuclear medicine

With the discovery of the radioactivity, at the end of the nineteenth century, new lines of research were developed in the field of the treatment of a wide range of diseases, from cancer to nervous diseases, by using radioactive isotopes as radium [27]. Nowadays, nuclear medicine is a fundamental branch of medicine.

One of the most studied tools of nuclear medicine, widely used in diagnostics and therapy of tumor diseases and other pathologies, is constituted by the radiopharmaceuticals. Radiopharmaceuticals are drugs containing radionuclides which deliver a predefined amount of radiation to a target tissue.

Diagnostic radiopharmaceuticals provide a non-invasive method of assessing the disease and monitoring the efficacy of a specific therapeutic treatment [28, 29]. As an example, the "Positron Emission Tomography" (PET) is extensively used in clinical oncology for the imaging of tumours or metastases and for neuro-imaging. It is depicted in Figure 2.5.
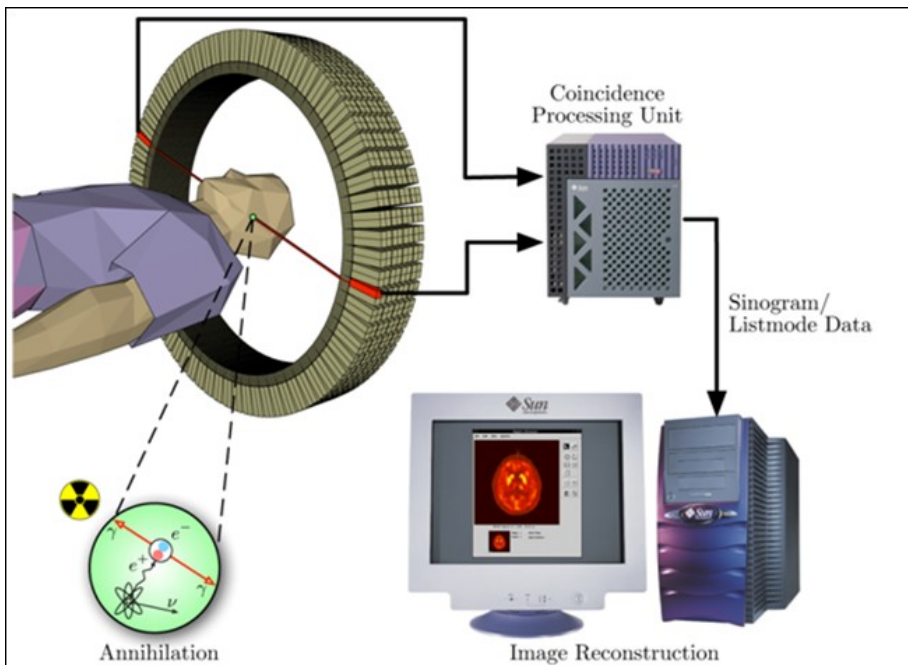
Figure 2.5: The PET imaging technique [30].

The unstable isotopes used in PET scanning are $\beta+$ emitters and have generally short lifetime, like ^{11}C (about 20 minutes), ^{13}N (about 10 minutes), ^{15}O (about 2 minutes) and ^{18}F (about 110 minutes). They are dissolved into specific drugs as carriers and injected in the patient. Rapidly the isotopes reach the right concentration inside the tissues to be analyzed and, in their decays, emit positrons[4]. The positrons suddenly annihilate with a surrounding electron, emitting two γ ray photons in opposite directions. The photon signals allow the position where the decay has occurred to be precisely reconstructed.

Moreover, different radionuclides able of inducing cell death with their disintegration emitting ionizing particles, such as α, β- and Auger electrons (see Section 4.2.2), are used as anticancer therapy and to treat pathological conditions such as rheumatoid arthritis. The final goal of these therapies is to deliver a cytotoxic level of radiation onto a disease site, without compromising the healthy tissues [31].

Finally, the "theragnostic" medical applications, that are the combination of both therapy and diagnostics for image-guided therapy and for defining the treatment outcome at an early stage, can greatly benefit from the use of radiopharmaceuticals.

2.4 The ISOLPHARM project

The radiopharmaceuticals are radio-labeled molecules, or ligands, structured in such a way as they bind to a cellular receptor and selectively accumulate within a target tissue, thus allowing precise imaging and focused therapy treatments. Therefore, researches in the radiopharmaceutical field have to be supported by both the development of ligands working for specific cellular targets, and the identification of innovative radionuclides.

In turn, the discovery of new applications for potential radiopharmaceuticals is accomplished with the actual possibility of producing them. However, the spread of novel medical radionuclides is often limited by the lack of suitable production methods able to ensure the high purity needed for the pharmaceutical preparation. Thus, along with the improvement of conventional production techniques, mostly accelerator-based or reactor-based, new approaches make use of electromagnetic mass separators to increase the radionuclide purity and its specific activity[5]. Projects such as MEDICIS at

---

[4]The positron, or anti-electron, is the antiparticle of the electron. It has the same mass and spin as an electron, but has an electric charge of $+1$.

[5]The specific activity is defined as the ratio between the activity (in terms of radioactivity) of the radioisotope and the total mass of the element considered, and it is usually

CERN [32] and ISOLPHARM ("ISOL technique for radioPHARMaceuticals") at INFN-LNL operate in this type of approach.

The ISOLPHARM project aims at the production of radiopharmaceuticals of high specific activity, exploiting the ISOL technique to selectively extract elevate purity radionuclides, in the operation framework of the SPES project at INFN-LNL.

According to the ISOL production method, a monochromatic proton beam of energy up to 70 MeV, produced by the SPES cyclotron, interacts with a primary target, inducing nuclear reactions. The reaction fragments are quickly extracted from the target thanks to its high working temperature (up to 2200-2300 °C), ionized in suitable ion sources and then extracted to form a RIB that is subsequently accelerated.

Thanks to the use of an electromagnetic mass separator, only the nuclei characterized by a given mass number are collected on a dedicated secondary deposition target. After the dissolution of the deposition target, a chemical purification step makes it possible to recover the desired isotope "carrier-free". That means that the element of interest is present only as the active radioisotope, without any isotopic contamination that decreases its specific activity. Therefore, carrier-free are those radionuclides with very high specific activity. The ISOLPHARM method is illustrated in Figure 2.6.
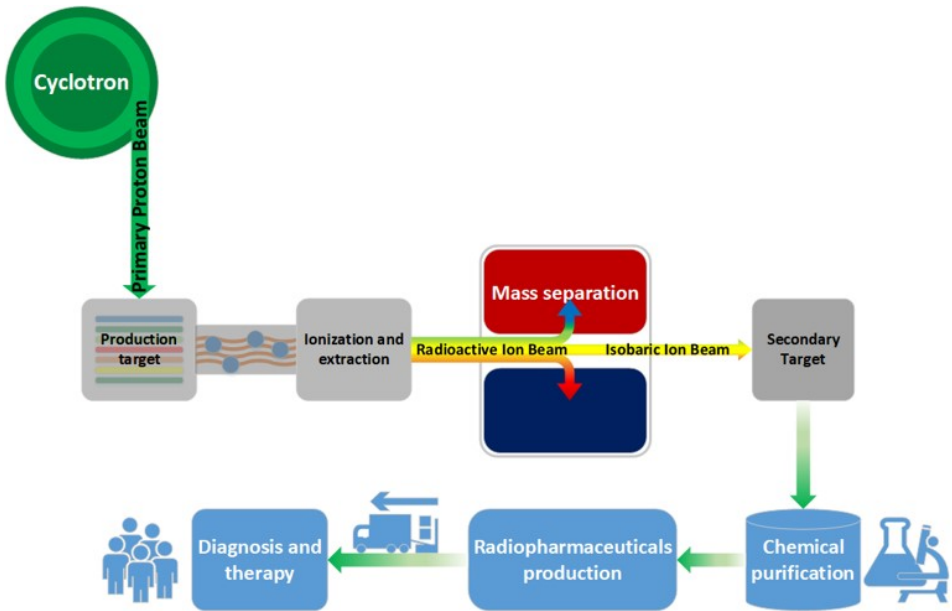
Figure 2.6: Detailed scheme of the ISOLPHARM method.

expressed in GBq/mg.

The strength points of such production method are the extremely high specific activity, close to the maximum value, and the high flexibility in the isotope production. The first point is easily achievable because the ISOL technique ensures the on-line production of high intensity and high quality RIBs. The second point derives from the fact that the same production target can be used to produce a large amount of carrier-free radioisotopes of medical interest, simply by adjusting the mass separator settings and changing the deposition target. As a proof of the proposed innovation, this production method was recognized with an international INFN patent, deposited in European Union, United States of America and Canada [33].

Initially the interest of the project was pointed towards some fission fragments produced by the SPES target, as ^{89}Sr, ^{90}Y, ^{125}I, ^{131}I and ^{133}Xe, which are isotopes already utilized in nuclear medicine. Furthermore, a theragnostic radionuclide in advanced research stage for medical application, ^{64}Cu, was soon identified as another good candidate for a feasibility study of the project.

However, it was soon realized that the ISOLPHARM method has the potentiality of going beyond the state of the art of the current radiopharmaceutical research topics. In fact, using suitable production targets, carrier-free isotopes from many different regions of the nuclide chart can be provided with the ISOL technique [34]. The availability of such isotopes, that present medically relevant decay properties in terms of half-life and radiation emission, may potentially open new research lines for the development of a new generation of radiopharmaceuticals. Some of them are based on nuclides never studied so far, because of their very limited availability in production with conventional techniques. Figure 2.7 summarizes all the isotopes selected with the ISOL technique, identifying for each one of them the possible use in producing diagnostic, therapeutic and theragnostic radiopharmaceuticals.

One of such nuclides is ^{111}Ag, which is regarded as a very promising nuclide for radiotherapy, thanks to its chemical and nuclear optimal properties [31].

Promising results on ^{111}Ag were obtained within the first two-year ISOLPHARM_Ag project, funded by INFN-Commission V. Such project aimed at studying and demonstrating, as a proof of principle, the production and use of ^{111}Ag, investigating both its ISOL production and its possible application as a radiopharmaceutical precursor [29].

A second three-year project recently approved by INFN-Commission V, ISOLPHARM_EIRA, aims at developing a prototypical therapeutic radiopharmaceutical radiolabeled with ^{111}Ag. The first step of the project con-
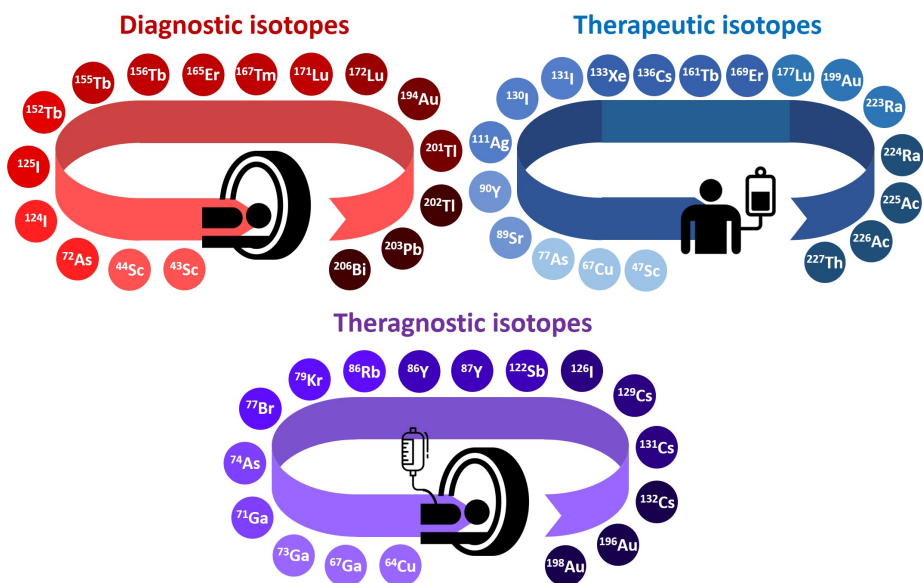
Figure 2.7: ISOL nuclides of medical interest.

sists in the production of ^{111}Ag by irradiation in a nuclear reactor and radiochemical separation. Then, the radionuclide, produced in a very pure form, is trapped inside a chelator, a chemical compound able to bind a metal ion in a stable way through a particular type of chemical bond. The chelator has a double function, because it also links the radionuclide to a appropriate targeting agent.

Therefore, new targeting agents have to be studied and synthesized. On one side, they have to be able of binding with the aforementioned bifunctional chelator, on the other side they are organic compounds capable to selectively connect with specific biological targets that are normally overexpressed in some particular cancer cells types. In this way, they make it possible to transport ^{111}Ag inside the cancer cells. In Figure 2.8 a scheme of the different parts composing the radiopharmaceutical is shown.

Once the prototypical radiopharmaceutical is developed, the first in vitro and in vivo tests with radioactive ^{111}Ag will be performed to evaluate the efficacy of the new drug and its stability in a biological environment.

Multidisciplinary competences are involved in the ISOLPHARM project, ranging from nuclear physics to engineering, from electronics to chemistry, radiochemistry and material sciences, from pharmaceutical sciences to biology and medicine [33]. Furthermore, international partners are present in the collaboration. In particular, the Polish research center POLATOM and
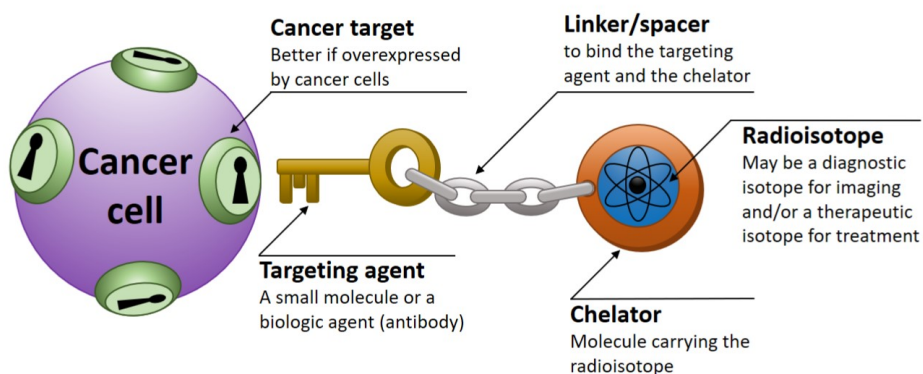
Figure 2.8: Schematic sketch of the different parts of a radiopharmaceutical.

the Greek institute N.C.S.R. DEMOKRITOS.

Finally, an added value of the project is that it contributes to lowering the global environmental and social impact, since the radionuclides produced with ISOLPHARM would otherwise be typically produced in nuclear reactors, where they may be obtained irradiating massive amount of materials, which subsequently turn into nuclear waste.

Chapter 3

The ISOL facilities

3.1   Introduction

Since the seventies, with the construction of high-energy heavy ion accelerators to study high temperature and density nuclear matter, it became clear that the same facilities could deliver big amounts of radioactive nuclei as well. In the last decades, mature techniques were developed for the production of RIBs, so allowing for a new way of investigating the isotopes with proton-to-neutron ratio very different from the one of stable isotopes [35, 36].

However, moving away from the stability region in the nuclide chart, the difficulties in the production of exotic nuclei increase. Among these, the extremely low production cross section of the reactions that produce the desired isotopes, the large contamination by unwanted species and the very short half-lives of the nuclei of interest. Two complementary techniques to produce good quality RIBs were historically developed: the "In-flight separation" and the "Isotope Separation On-Line" (ISOL).

The first technique [37] is described in Figure 3.1. It can be implemented in existing heavy ion accelerators, using a highly energetic ion source as primary beam and a thin target where beam nuclei fragment into smaller parts by retaining a part of their kinetic energy. The desired isotopes then are selected by passing through the fragment separator, in order to produce a secondary beam of radioactive ions. The range of produced nuclei is close to the projectile and target nuclei.

With this technique, intense beams can be obtained, since the chemical properties of the target and of the ion beam, as well as the half-life of the radioactive nuclei produced, don't in any way constitute a limit for final production. However, the contamination from the primary ions can be important; moreover, losses of beam intensity may occur, due to the high

dispersion in terms of fragment energy and direction.
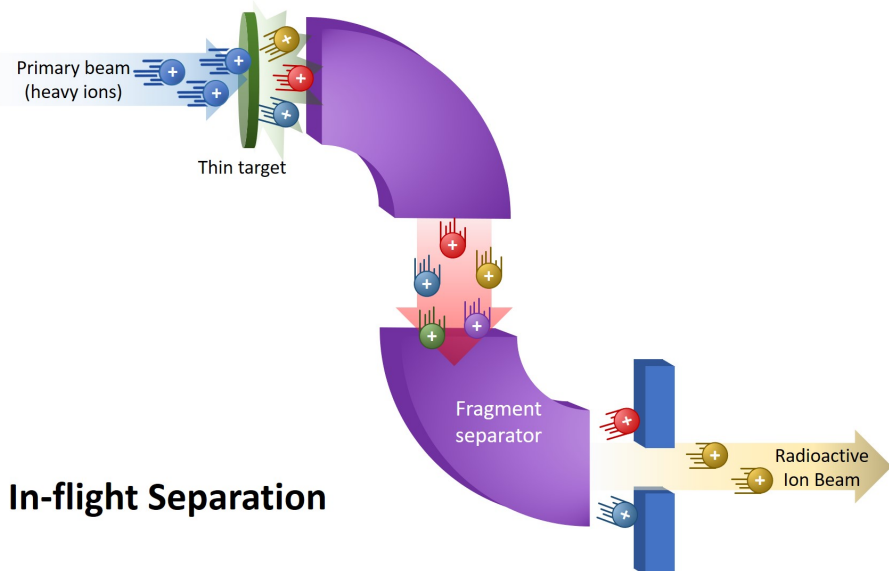
Figure 3.1: Schematic drawing of the "In-flight separation" based production method for RIBs.

Classically the ISOL technique has been associated with thick targets in which the reaction products are thermalized and diffuse towards an ion source for further acceleration and separation [38, 21].

The schema of the ISOL method is illustrated in Figure 3.2. A primary beam produced by an accelerator at the desired energy impinges on a thick target inducing nuclear reactions [1]. The produced nuclides are then thermalized at a temperature above 2000 °C and, thanks to thermal processes of diffusion and effusion, exit from the target to reach a 1+ ion source. Here they are ionized and extracted to produce a low energy beam. After a first isotopic selection and a further ionization to n+, the exotic beam is injected into a final re-accelerator phase to subsequently deliver to the experiments high intensity and high purity RIBs.

These processes depend on the physical and chemical properties of the target material where the fragment production occurs, and by the properties of the nuclides of interest, like the production cross-section, the decay half-life, the ionization potential in atomic form, the molecular formation probability, the volatility.

---

[1]In some cases the accelerated beam collides with a primary converter target that produces neutrons which, in turn, generate fission in a secondary uranium target [35].
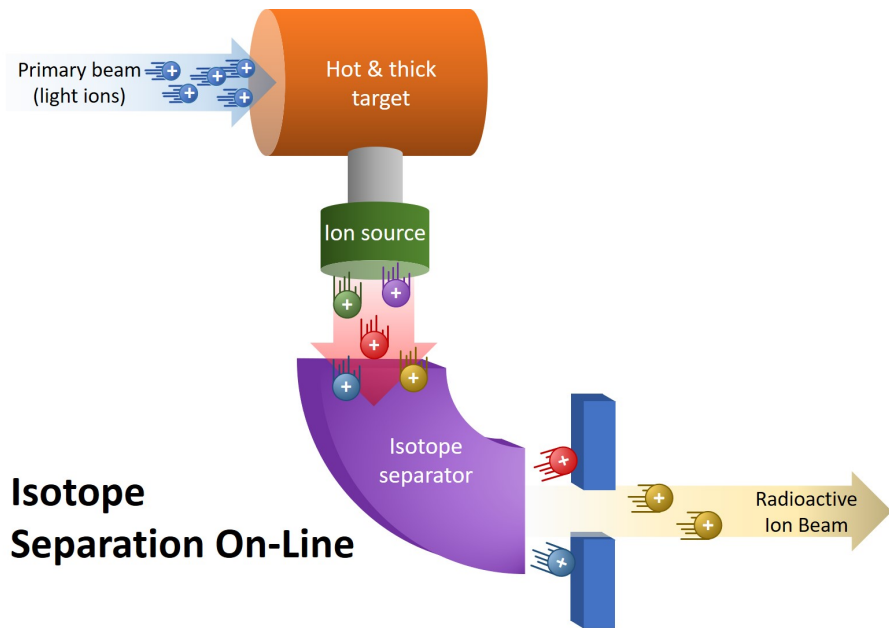
Figure 3.2: Schematic drawing of the ISOL based production method for RIBs.

Both the production methods exploit the idea to transport the nuclei of interest in a well-shielded experimental set-up away from the production target, where their nuclear properties can be explored without the huge background due to intense nuclear particle fields and to the radioactivity. Furthermore, during the transport process the beam is purified and prepared to fulfill the requirements of the experiments.

Several ISOL facilities around the world are currently producing RIBs [36], but they generally are not able to deliver very intense and pure RIBs of high energy. Therefore, second generation facilities are being built with the aim to increase the quality of the produced RIBs, in respect to the past projects [39, 40]. The experience matured with these facilities could constitute an intermediate step toward future innovative third generation projects such as the proposed "EURopean ISOL facility" (EURISOL [41]).

3.2   The ISOL technique

The main aim of the second generation ISOL facilities is the production of RIBs satisfying the requests to be intense, pure, with good timing and optical qualities and with a large range in mass. Therefore, the various processes involved in the production sequence must possess the following

properties:

1. efficiency, to prevent excessive losses of interesting isotopes during the various steps of beam manipulation;

2. speed, to reduce the losses due to radioactive decay of short half-life exotic nuclei by the production instant, until the arrival at the experimental set-up;

3. selectivity, in order to guarantee the beam purity requested by the end-users;

4. high production rate, to increase as much as possible the intensity of the secondary RIBs.

The different steps of the ISOL procedure for the production of RIBs, described in the following of the present section, highlight the above mentioned properties.

3.2.1 The isotope production

Various beams and targets can be used with the ISOL technique, according to the desired RIB to be delivered to the experiments. Usually, primary beams are composed of charged particles as protons, heavy ions or electrons, and are supplied by a particle accelerator (the beam driver).

In order to achieve the highest production rate, the beam extracted by the primary driver has to be tuned in relation to the structure of the beam line and its composing elements, like the collimators, and mostly the production target. Moreover, the size and the energy of the beam at the entrance of the target has to be such as to maximize the beam power in the target material [40].

Depending on the type of beam and target, different nuclear reactions can be induced in the target materials. They are described in the following list.

- Fission: it can occur if the target is composed of high mass actinides such as ^{238}U or ^{232}Th. The target nucleus splits into two main fragments with mass numbers generally between 70 and 160, and few neutrons.

- Spallation: a large number of protons, neutrons, and α-particles are ejected from the target nuclei. The daughter nuclei will have a mass slightly lower than the target atom and will stay in the very proton-rich side of the nuclide chart.

28

- Fragmentation: both target fragmentation, when a light ion beam impinges upon a heavy target, and primary beam fragmentation, when a heavy ion beam collides with a light target, can occur. This reaction produces a wide variety of species with masses close to those of the projectile and target nucleus.

- Light and heavy ion fusion-evaporation reactions or direct reactions: the number of produced nuclides is more limited than that generated by the three aforementioned reactions. In the case of light-ion fusion, proton-rich nuclei close to the valley of stability are produced, whereas the heavy ion fusion reaction produces very exotic proton-rich nuclei.

The production yield of a specific isotope, at a certain energy of the projectile, is determined by the reaction cross section for the production of that isotope in the target, and may be expressed with the following formula:

$$Y \ = \ \Phi \, \sigma \, N, \tag{3.1}$$

where Φ is the primary beam flux of a certain energy, σ is the microscopic cross section of the production reaction at that energy, and N is the number of target atoms per surface area. To obtain the total production yield in the target, the formula has to be integrated over the energy range of the beam impinging the target and the total cross section has to be considered.

3.2.2   The isotope release from the ISOL target

Once produced in the target, the nuclides must have enough energy to quickly exit from the target. In fact, the process of release has to be as fast as possible in order to prevent the loss of the shorter half-life isotopes.

The main release mechanisms in an ISOL target are the diffusion inside the target matrix and the effusion towards the ion source. The diffusion allows the isotopes generated inside the crystal lattice to drive to the surface of the target material. The effusion drives then the isotopes towards the ion source.

Diffusion and effusion are very complicated processes that depend on the chemical and physical properties of both the target material and the isotopes to be released, as well as on the size of the grains of the target material and on the target geometry.

In any case, one of the parameters having the largest impact on the speed of both processes is the working temperature of the target. It has to be maintained as high as possible, but below the vapour pressure of the target material to avoid the target degradation and fracture [42, 9].

Among the most common materials used as ISOL targets, there are Uranium Carbide and Silicon Carbide. These carbon-based materials resist to very high temperatures (over 2000 °C) and present high porosity and high emissivity. For this reason, diffusion through the target is favoured and, at the same time, the target system is able to dissipate the high beam power deposited [7, 9, 42, 43, 44].

3.2.3   Isotope ionization inside the ion source

Once the isotopes reach the ion source, in the form of neutral atoms, a part of them is ionized in order to be subsequently extracted. Different ionization mechanisms are generally used, in relation to the beam requested by the users. They can be associated to three main categories of ion sources: the "Surface Ion Source", the "Plasma Ion Source" and the "Resonance Ionization Laser Ion Source" [45, 46, 47].
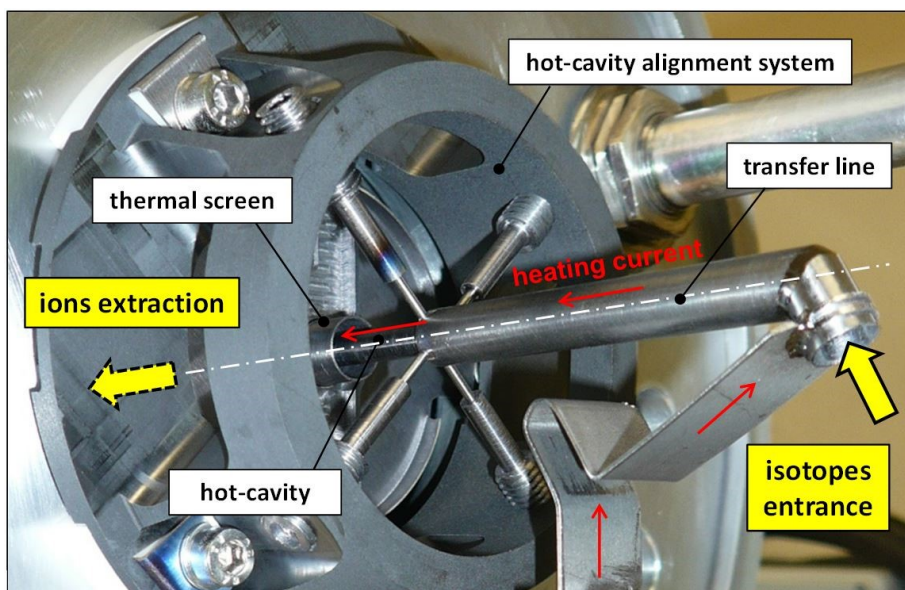
Figure 3.3: The SIS operating scheme [48].

The Surface Ion Source (SIS) is very successful for the production of singly 1+ or 1- charged isotopes thanks to its simplicity, high efficiency and selectivity. When a neutral atom interacts with the surface, it can lose an electron becoming a positive ion, if its ionization potential is smaller than 5-7 eV. This occurs for chemical elements as alkalis and some lanthanides, for which the surface ionization remains the most efficient ionization mechanism. Conversely, negative ions are produced when the electron affinity of

the atom impacting on the surface is greater than 1.5-2 eV. Negative chlorine, bromine, iodine and astatine have been efficiently produced with this method.
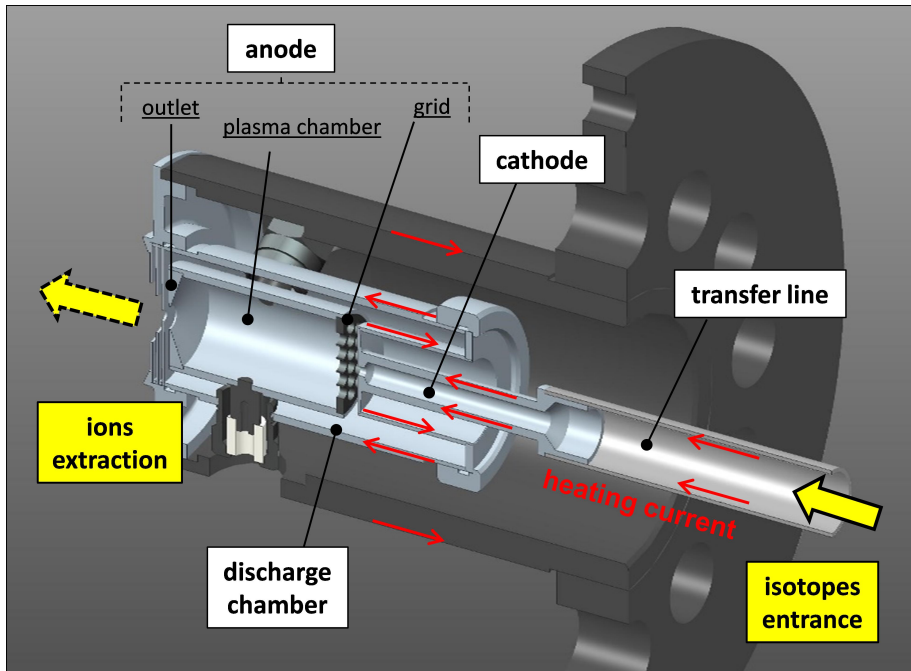
Figure 3.4: The FEBIAD operating scheme [48].

The efficiency of such processes strongly increases with the working temperature, which is about 2000 °C. Moreover, the process efficiency depends on the chemical properties of the material constituting the surface of the ion source. In particular, the work function of the surface[2] has to be higher than the ionization potential for positive ions, and lower than the electron affinity for negative ions. The operation scheme of the SIS ion source is presented in Figure 3.3.

Typical materials used for the manufacture of Surface Ion Sources are tantalum, tungsten and rhenium for positive ion beams, LaB_6 and BaO for negative ion beams.

The ionization by Plasma Ion Source (PIS), called also "Forced Electron Beam Induced Arc Discharge" (FEBIAD), takes place through the electrons emitted by thermionic effect from a cathode at high temperature and subsequently accelerated by a potential difference of one hundred volts. The

---

[2]The work function is the minimum energy needed to remove an electron from a solid to a point in the vacuum immediately outside the solid surface.
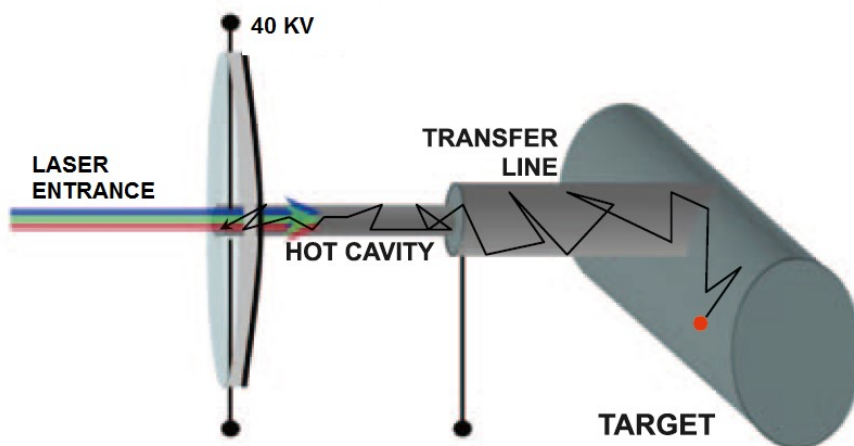
Figure 3.5: The RILIS operating scheme [49].

impact of these electrons onto a neutral atom causes the emission of an electron from the atom and the consequent ionization. Ions and electrons then create a low-density plasma that further favors the ionization process. This ion source operates steadily in conjunction with high temperature thick target materials. In order to maximize the ion source efficiency, the electron plasma energy can be tuned according to the cross section for ionization, by electron impact, of the wanted element. In Figure 3.4 the operation scheme of the PIS ion source is shown.

This type of source is very unselective but, on the other hand, it is the only method available to efficiently ionize a large number of elements. It is particularly useful for the creation of multi-charged ions or for elements with high ionization potential such as Kr and Xe noble gases and halogens.

The Resonance Ionization Laser Ion Source (RILIS) method is nowadays the most powerful tool implemented at ISOL facilities, because it provides a very selective ionization process, with inherent suppression of unwanted isobaric contamination. With this technique, the atoms traveling within the source are stepwise excited by different laser photons. Using tunable lasers it is possible to match the photon energy to the energy levels of the electronic transitions of the desired atomic species. The scheme of this ionization method is presented in Figure 3.5.

3.2.4 Secondary beam transport and re-acceleration

After the radioactive ions leave the ion source, an extraction electrode allows the beam to be shaped, performing a first acceleration step with extraction potential normally ranging between 40 and 60 kV. The properties of the beam are essentially dependent on the type of ion source used.

Such low energy beam is then forwarded to an analyzing magnet where a first mass selection is performed, obtaining thus an almost isobaric beam. When extremely pure beams are requested, a second step of beam purification is implemented using a high resolution mass spectrometer. The separation process should reduce in an effective way the contamination by unwanted ion species, taking into account that, in a nuclear reaction process, the isotopes of interest often form a minority and the unwanted isotopes, generally more stable, are produced with greater abundance.

Other optical devices may be used to increase the quality of the beam and its state of charge, in order to have a more efficient post-acceleration step to finally deliver a high energy RIB to the experiments.

3.2.5 Performance of the ISOL method

The whole production of a RIB is mainly limited by the short half-life of the radioactive isotopes produced in the target. Therefore, very crucial points for the success of an ISOL facility are both to build the target and ion source system considering with a great care the properties related to the release and the efficiency of the system, and to optimize the atom ionization and the transport of ions with the final post-acceleration step.

In Figure 3.6 a typical scheme of an ISOL system is shown, with the indication of the different production steps.

The final production yield of a specific isotope is a function of the following parameters:

$$Y \; = \; \Phi \; \sigma \; N \; \epsilon_d \; \epsilon_e \; \epsilon_i \; \epsilon_t, \tag{3.2}$$

where the first three terms are the same that in equation 3.1 and refer to the production yield, whereas Y is further attenuated by the efficiencies of diffusion (ϵ_d), effusion (ϵ_e), ionization (ϵ_i) and transport (ϵ_t) [42].

All these parameters strongly affect the final ion beam intensity, but the most critical factor is often associated with the release of the exotic atoms from the target to the ion source, that is dominated by the very complicated sequential processes of diffusion and effusion, as explained in Sect. 3.2.2.
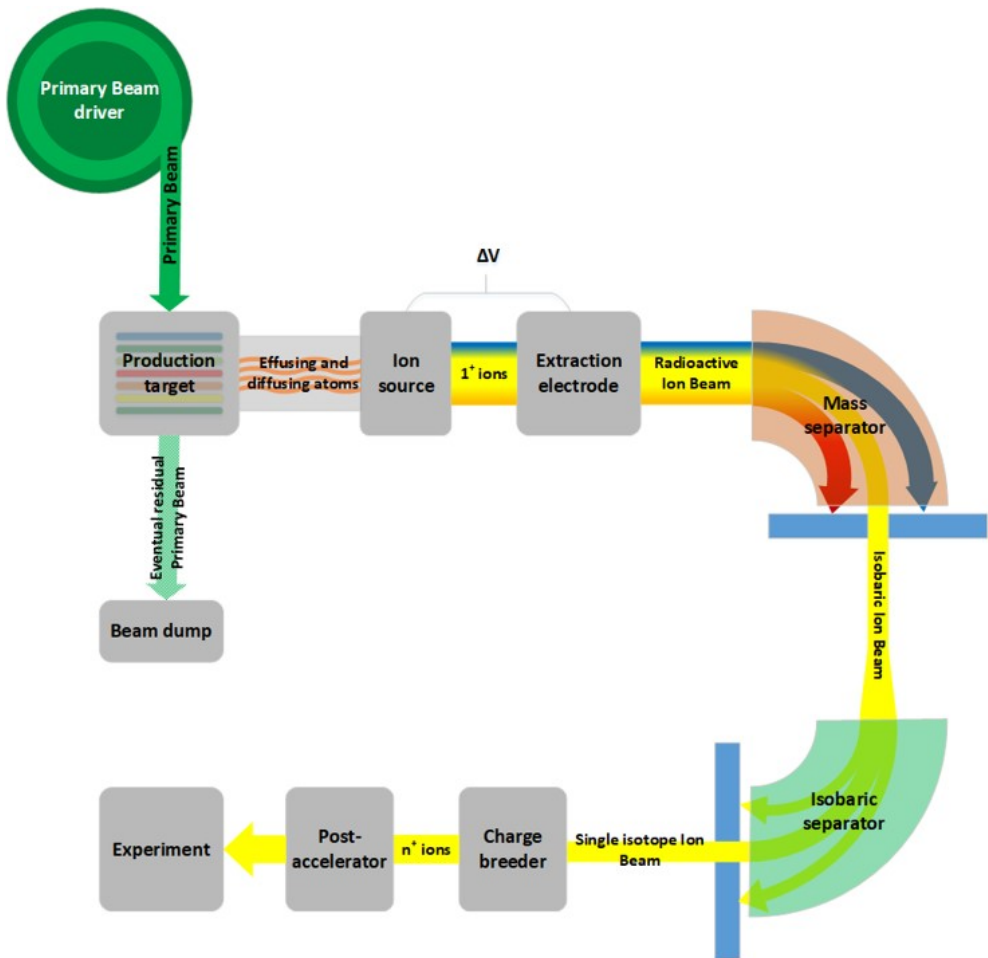
Figure 3.6: Production scheme of an ISOL system.

Anyway, the combination of all these factors makes the design of an ISOL facility a big challenge from a technological point of view.

3.3 The SPES apparatus

3.3.1 Overview

SPES is the acronym for "Selective Production of Exotic Species". It is a project devoted to design and install a second generation ISOL facility at the INFN-LNL (Istituto Nazionale di Fisica Nucleare, Laboratori Nazionali di Legnaro) in Legnaro (Padua), Italy.

Such facility has the primary goal of producing intense neutron-rich exotic beams in the mass range 80-160 u, by using a UC_x uranium carbide target, with an estimated proton induced fission rate of 10^{13} fission/s.

Figure 3.7: Cyclotron installed in the SPES building.

The primary driver, shown in Figure 3.7, is the 70p commercial cyclotron of the BEST Cyclotron Systems Inc. [50], able to provide up to two simultaneous energetic proton beams with maximum energy of 70 MeV and maximum intensity of 700 μA, corresponding to a power of 49 kW.

In the SPES full operation phase, the proton beam is expected to have 40 MeV energy and 200 μA intensity, corresponding to a power of 8 kW. It is extracted from the cyclotron, travels along a beam line and enters inside a shielded production bunker, inducing nuclear reactions in an UC_x target. The target is housed in an opportunely designed vacuum chamber installed on the SPES production apparatus, the "Front-End", that includes

all the devices necessary for the production, ionization, first acceleration and mass separation of the exotic nuclei. Figure 3.8 shows the prototype of the radioactive line of the SPES Front-End which has been developed and tested for the SPES facility, and will be soon installed in the production bunker.

Figure 3.8: SPES Front-End prototype in the off-line laboratory.

The obtained low energy beam is then delivered out of the bunker and injected into a Beam Cooler (BC), a device capable of decreasing the beam longitudinal and transversal emittance. A next High-Resolution Mass Separator (HRMS) allows the beam to be further purified from the unwanted isobaric masses. The obtained RIBs can be directly addressed to low energy experiments, or possibly be injected into a Charge Breeder (CB) to increase the beam charge state.

Another mass separation device is then able to select the most intense charge state and, finally, the beam is post-accelerated by means of the combined Radio Frequency Quadrupole (RFQ) and the already existing ALPI Linac accelerator (see Figure 3.9). The total accelerator assembly is able to deliver to the experiments isotopic pure ion beams with energies of 10 MeV/u and higher, for masses around 130 u; in the neutron-rich region, the expected rate delivered to the users is above 10^8 particles per second.

Currently, the assembly status of the SPES facility is in an advanced development stage. The LNL laboratories have dedicated a completely new building to host the plant, with the related services and infrastructures that take care of all the needs requested by the safety and radiation protection rules. The SPES building is shown in Figure 3.10.

It contains, at the underground floor, an area occupied by the cyclotron accelerator for the production of the primary proton beam, a shielded production bunker with the Front-End beam lines, a temporary storage for the exhausted targets, the Beam Cooler and High-Resolution Mass Separator areas. On the ground floor of the building, there are the laboratories for the preparation of the production targets.

Figure 3.9: On the left: a section of the ALPI Linac with the cryostats containing superconducting cavities. On the right: the inside of a cryostat with 4 copper cavities.

Figure 3.10: The SPES building at LNL.

Adjacent to the new building, an already existing building hosts the low energy experimental hall, the Charge Breeder and the beam transfer line to drive the beam in the already existing ALPI Linac post-accelerator. A general overview of the SPES facility can be seen in Figure 3.11.
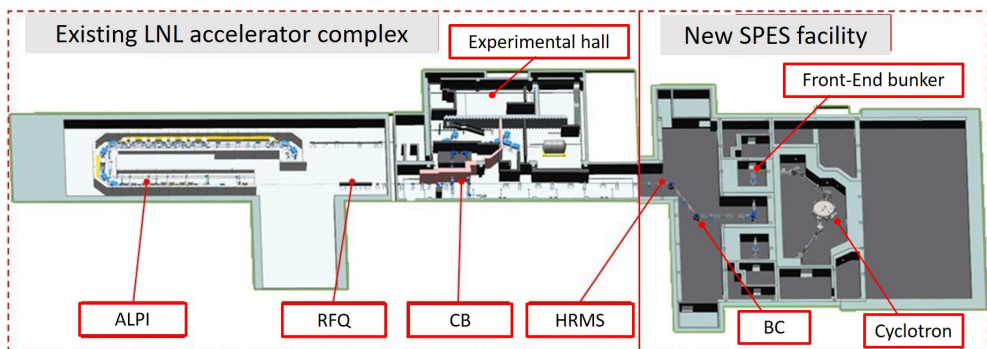
Figure 3.11: Layout of the SPES ISOL facility.

The biological hazard connected with the production and handling of radioactive ion species imposes severe radiological safety challenges to the design and operation of the SPES apparatus and, more generally, of all the ISOL facilities. Most of the safety and radiation protection issues connected to the SPES operation are related to the use of a high-intensity proton accelerator as driver for the generation of unstable species in the production target, and to the radioactivity produced in the production bunker and along the RIB line. Anyway, the target is the most critical element of the facility, so a special care is needed to handle and store the exhausted target chambers.

For this reason, in the following parts of the present thesis, the attention will be focused on the life cycle of the production target as well as on the radioactivity generated inside the SPES production bunker.

3.3.2 The SPES production bunker

The SPES production bunker is located in the new SPES building, on the underground floor. The shielding thickness of the bunker walls, required for the radiological protection of the operators in the adjacent areas, ranges from 2 m to 4 m. They were designed considering two possible different operating scenarios: the first one concerns the production of radioactive beams in standard conditions, with a 40 MeV and 200 μA proton beam; the second one, to be implemented in a successive time, foresees to use of a 70 MeV and 350 μA proton beam on a suitable UC$_x$ target. An air tight

sliding concrete door, 1 m thick, closes the bunker and makes it possible to maintain an internal depression of 40-80 Pa with respect to the adjacent external area, in order to avoid uncontrolled releases of radioactive air.

The proton beam enters in the bunker through a beam pipe directly coming from the cyclotron vault. To control the beam characteristics and avoid beam losses, several devices are placed along the primary proton beam of the Front-End system, before the target. They allow the beam to be tuned before the target irradiation.

The first elements of the proton line are four graphite beam collimators, needed to shape the beam by absorbing a certain percentage of protons in the beam external halo (about 15%, see Chapter 6). They are surrounded by a movable lead shield, which reduces the number of protons scattered on other elements downstream of the beam pipe and attenuates the secondary photons emitted by the activated graphite [51]. Then, a beam monitoring system composed of a beam profiler and a Faraday cup is installed. The first device evaluates the beam profile, whereas the second one monitors the beam intensity.

Downstream of the beam diagnostic, other structural elements complete the primary proton beam line. Among them, a gate valve mechanism seals the proton beam line during the extraction of the target and ion source system from the Front-End, scheduled after each irradiation cycle, and the proton bellow connects the proton beam line to the target and ion source system.

The radioactive line is the part of the Front-End which houses the target and ion source system and contains the electromagnetic devices needed to extract, separate and transport the RIBs out of the bunker.

Downstream of the target and ion source system (discussed in Section 3.3.3), the first structure placed on the radioactive line is the ion extraction electrode, that performs a first high voltage (40 kV) acceleration of the radioactive ions leaving the ion source.

Beyond the electrode, several electrostatic devices allow the RIBs to be shaped and transported along the radioactive ion line: the deflectors (or steerers) and the triplets. The deflectors are necessary to correct the trajectory of the beam, while the triplets control the beam size and are used to focus it. In addition, beam diagnostic devices are installed along the radioactive beam line.

Another essential element placed along the radioactive line is the Wien Filter [52, 53, 54], a velocity separator so named thanks to its inventor Wilhelm Wien in 1898. It is able to perform a first mass separation stage of the produced isotopes, in order to obtain an isobaric beam. The Wien
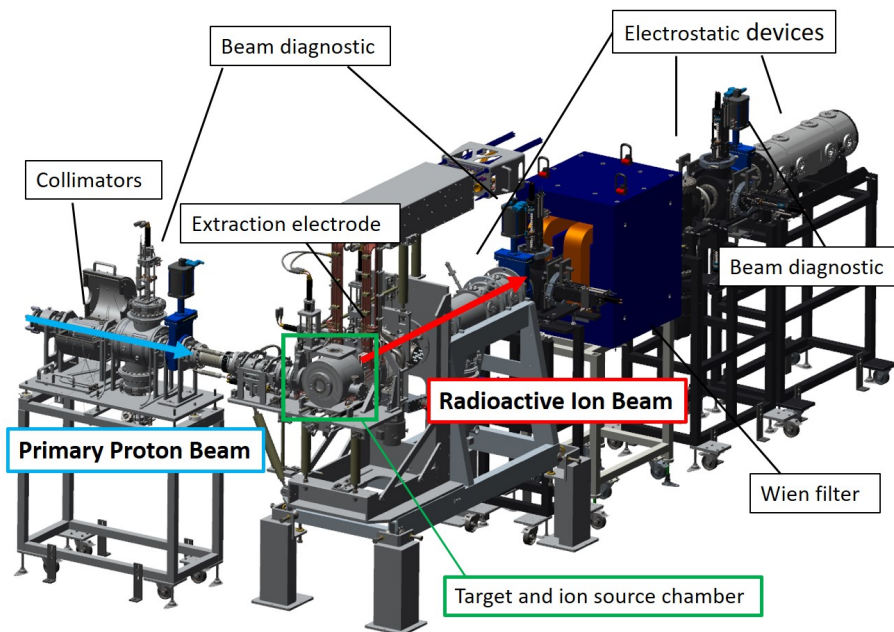
Figure 3.12: The CAD design of the SPES Front-End system.

Filter that will be mounted on the SPES Front-End is based on a first commercial version, but it was completely redesigned, manufactured and tested at LNL [55].

Finally, pneumatic motors are placed in different positions of the Front-End to operate all the diagnostics, the movable parts of the Front-End and the requested turbo-molecular vacuum pumps, necessary to maintain the appropriate vacuum conditions in the Front-End components.

In Figure 3.12, the overview of the mechanical design of the SPES Front-End system layout is shown [56]. A detailed illustration of the single elements will be given in Chapter 6.

3.3.3 The target and ion source unit

The ISOL "Target and the Ion Source" (TIS) unit of the SPES apparatus is the core of the project and, at the same time, the most critical element of the facility, due to the intense thermomechanical stresses to which it is subjected and to the large amount of radioactivity induced by the fission reactions. The TIS unit is the result of a long R&D work of the SPES ISOL community and represents a technical innovation in terms of its capability to sustain the primary beam power [9, 22, 44, 57].
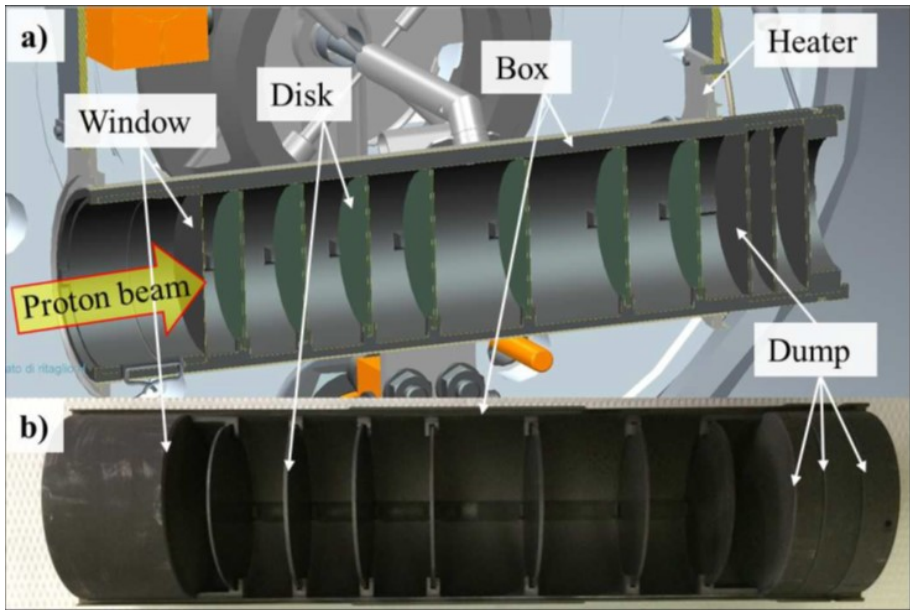
Figure 3.13: (a) The SPES production target; (b) the graphite box containing the disks and the window and dumper assemblies.

Radioactive neutron-rich isotopes with mass ranging from 70 u to 160 u are produced by nuclear fission interactions of a 40 MeV and 200 μA (8 kW) proton beam on a thin multi-foil uranium carbide target [22].

It consists of seven thin disks, characterized by a diameter of 40 mm and a thickness of 0.8 mm, with a density of about 4 g/cm^3 for a total mass of 28 g [7, 9]. The disks are opportunely spaced and positioned inside a cylindrical graphite box of 200 mm length and 45 mm diameter. The entrance extremity of the target box is closed with a thin graphite window, while on the other side three thin dumping disks are capable to completely stop the residual proton beam. A picture of the production target is shown in Figure 3.13.

This configuration guarantees a homogeneous temperature distribution in the target by efficiently dissipating the heat coming from the proton beam. Therefore, high total beam powers and, consequently, high total isotope yields are possible in principle. The proton power is absorbed by the uranium carbide disks, which are capable of reaching a temperature of about 2000 °C by maintaining their integrity. Anyway, the temperature of the disks is kept below 2300 °C, which is close to the melting point of the uranium carbide. Moreover, the multi-foil structure and the relative low density of the UC$_x$ improve the release capability of the isotopes towards
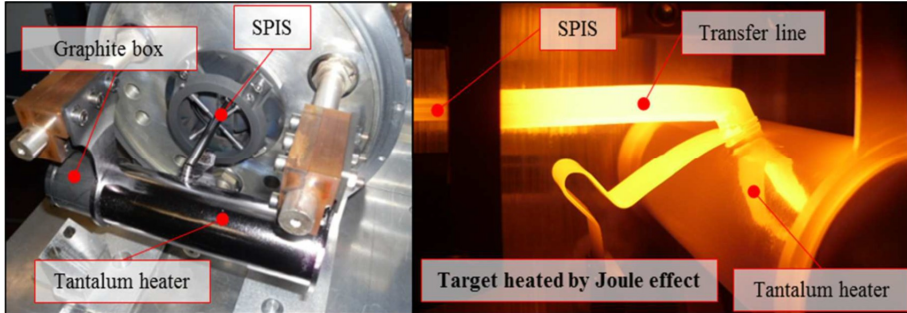
the ion source.

Figure 3.14: *Target and ion source assembled and heated by Joule effect (not at full power).*

The graphite container is inserted into a tubular tantalum heater, which can provide, by Joule effect, the amount of power required to heat the target at high temperature during the conditioning phase (before the irradiation), or in case of proton beam interruption, as can be seen in Figure 3.14. Moreover, the target is linked to the ion source by means of a tubular transfer line.

Once arrived inside the ion source, the isotopes acquire the 1+ charge state needed for their extraction. The choice of a specific ion source depends on its efficiency and capability of selective ionization.

All the ionization mechanisms discussed in Section 3.2.3 are implemented in the SPES ion source: the SPES Surface Ion Source (SSIS) [58], possibly coupled to the Resonance Ionization Laser Ion Source (RILIS), and the SPES Plasma ion source (SPIS) [59]. Once embedded in the target system, the different ion sources give rise to different TIS units.

The surface ion source (SSIS) is used to ionize the elements of the first group of the period table (i.e. Rb, Cs). The ionization efficiency is quite low (maximum 3-4%) for the elements of the second group (Sr, Ba), while it is negligible for the remaining elements. Therefore, the selectivity of this source is quite good.

The laser ionization process (RILIS) can be used to efficiently ionize most of the elements produced in the target. This ion source is very selective and only the desired element is ionized. The only inevitable contamination is constituted by the first and second group elements, since the surface ionization is always present in this source system.

The plasma ion source (SPIS) is used for the elements with high ionization energy, since it is the only source able to ionize them. As a disadvantage,

this ion source does not present any selectivity, since the efficiencies for most elements are higher for the Plasma Ion Source than for the Laser or the Surface Ion Sources. The SPIS source used in SPES is a development of the previous MK5 source used at ISOLDE (CERN).

In Figure 3.15 the elements produced with the SPES UC_x target are shown, with in evidence the preferable method used for their ionization. The elements highlighted in blue cannot be ionized since they are refractory, i.e. their evaporation temperature is too high; for this reason they are considered not extractable out of the target. However, from a theoretical point of view, they could be extracted in the form of volatile molecules. This phenomenon, and therefore the possibility to create molecular beams, is still in phase of study.

Figure 3.15: *The main elements produced with the uranium carbide SPES target, with the reference to the corresponding ionization method.*

Both the target and ion source are placed inside an aluminum water cooled vacuum chamber [57]. It is capable to dissipate the amount of power associated to both the target and the ion source, maintaining a working temperature close to 2000 °C. A complete assembly for the Target and Ion Source unit of the SPES facility and its connection to the extraction electrode of the radioactive ions are shown in Figure 3.16.

The design of the SPES production target was developed by means of Monte Carlo simulations [9, 60]. Some of these Monte Carlo tools, described

Figure 3.16: *The Target and Ion Source (TIS) unit and the RIB extraction system of the SPES facility.*

in Chapter 5, are extensively used for assessments in the field of the radiological protection, such as those to be illustrated in the last part of this thesis. Predictions on the thermal behavior of the target were performed using the Finite Element Method software ANSYS® [61]. The performance of the SPES UC$_x$ target prototype, in terms of both isotope production and thermal stability, was successfully measured during two low power irradiation tests at the HRIBF facility of the Oak Ridge National Laboratory (ORNL) [34, 42, 43].

Because of the thermomechanical stresses to which the target is subjected and the damage suffered by materials due to high temperature operating conditions, as well as to the intense proton, neutron and gamma mixed radiation fields, the TIS unit has a limited life cycle.

The exhausted TIS unit is foreseen to be removed from the Front-End after a complete irradiation cycle composed of 15 days with primary beam on, followed by a period of 15 days of cooling, with the machine turned off. This cooling period is necessary for the residual radioactivity to decrease to a level allowing the TIS unit system to be extracted from the Front-End, using a remote handling system. The TIS unit is then placed inside a lead

sarcophagus and transported in a temporary storage for a few years, until its residual radioactivity level allows disposal or recycling to be performed [11, 62, 63, 64].

After a 15 day irradiation cycle of the UC_x production target, the total number of protons incident on the target is of the order of 10^{21} and the total proton fluence is about $8 \cdot 10^{19}$ cm^{-2}. Being the proton induced fission rate of the order of 10^{13} fission/s, a large number of radionuclides, corresponding to an activity of about $4 \cdot 10^{13}$ Bq, are produced in the target at the end of the irradiation. However, around 70% of them have half-life of less than 1 hour.

Due to its radioactive impact, severe radiation protection issues and safety challenges are connected to the handling of the exhausted TIS unit during its whole life cycle, from the initial assembly until the final disposal. The different stages of the TIS life cycle will be object of the study described in Chapter 8.

Chapter 4

Brief overview on the Radiological Protection framework

4.1 Introduction

The topics discussed in the present chapter are intended only to give a taste of what the system of radiological protection does mean, and to explain how the system can be implemented in the radiation exposure situations investigated in this thesis work. The whole topic is very broad and cannot be exhausted in a few pages.

The main goal of the radiological protection is "to contribute to an appropriate level of protection for people and the environment against the detrimental effects of radiation exposure without unduly limiting the desirable human actions that may be associated with such exposure" [65].

Since the discovery of the radioactivity in 1896, radiation protection standards and the underpinning philosophy have evolved, driven by both the modification of the risk culture and the continuously updated information on the effects of the radiation on biological systems [66].

In the very early days after the discovery of the X-rays, the people didn't know that large radiation levels could cause serious biological effects. They also had no instruments to measure them. So, only immediate and visible effects of intense exposures to radiation fields were qualitatively considered to set the first limits on radiation exposure.

The "International Commission on Radiological Protection" (ICRP) was established in 1928, with the early name of "International X-ray and Radium Protection Committee" (IXRPC) [67]. It has always been and still represents

one of the main world reference organisations in the field of radiological protection.

In 1928 the IXRPC issued its first general recommendations on the protection of the medical profession, essentially based on the concept of safe radiation threshold due to the absence of observed biological harm. In 1934 it proposed the first formal standard for protecting people from radiation sources, founded on a quantitative measurement of ionizing radiation [68].

The researches on the biological effects of radiation began extensive during and immediately after World War II. In the following years, the hypothesis of the threshold was revised due to first epidemiological studies that evidenced an excess of leukaemia in the Japanese atomic-bomb survivors, and an excess of cancer incidence among American radiologists due to high-dose medical procedures [69].
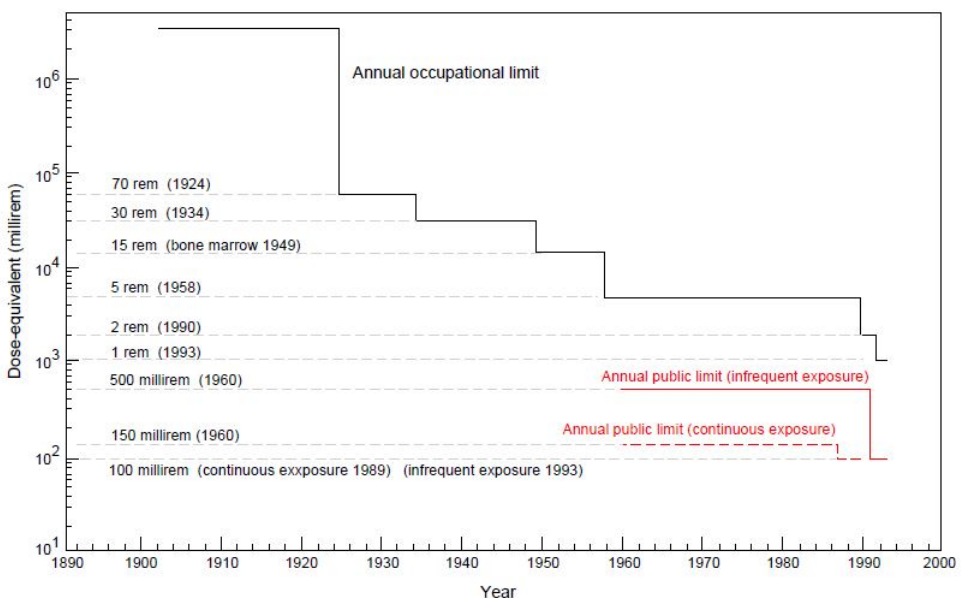
Figure 4.1: Recommended limits on occupational (black) and public (red) annual exposures to radiation over the past century [66]. Recall that 1 rem = 0.01 Sv (1 mSv is the annual dose limit recommended in ICRP-103 for the population, see Section 4.3.2).

Contextually, the development of both industrial and military employment of nuclear energy led the Commission to issue for the first time recommendations for the protection of workers and public [70].

Moreover, the growing data of malignant diseases for the atomic-bomb survivors had a profound impact on the people and also on radiation protection community. By extrapolating the high-dose data to lower doses, it

began to take shape the thought that even stochastic low levels of exposure might induce a risk, albeit small, of developing radio-induced cancer [71].

Those considerations resulted in a philosophical transition from the necessity of avoiding deterministic threshold effects to the importance of reducing low-dose stochastic effects, that were not known to have or not to have a threshold. Therefore, in the 50s the ICRP advised the first formulations of the concept of limitation of the exposure [69, 72, 73]. Later, in 1973, this concept was translated into the recommendation to maintain exposure "as low as reasonably achievable, economic and social considerations being taken into account" (ALARA) [74].

In 1977 the Commission adopted a system of risk-based control of stochastic effects of radiation, proposing three formal principles: justification, optimisation of the protection and individual dose limitation [75]. The approach required that the risk connected to activities with ionizing radiations equates to that due to other type of activities.

In the 80s, new data from epidemiology and radiobiological searches on the Hiroshima-Nagasaki survivors indicated higher estimates of risk for stochastic effects, and in 1990 the ICRP released a new set of international recommendations [76].

Figure 4.1 illustrates the behavior of the recommended radiation dose limits during the last century; the plot shows a continual decrease until 1990.

The latest recommendations of ICRP (in the following indicated as "ICRP-103" [65]) were implemented in 2007 after a long phase of public consultation involving scientists, international organisations, national authorities and users all around the world. These revised recommendations do not contain fundamental changes compared to the previous ones, but look for a new policy of stakeholder engagement, aiming to a clearer understanding and wide acceptance. Furthermore, they include societal and ethical aspects in the decision-making process concerning radiological protection issues; they also acknowledge the importance of protecting the natural environment as a whole, in all exposure situations, caused or not by human action.

The ICRP has contributed significantly to the evolution of the radiological protection system from the beginning of the last century. Today the recommendations contained in ICRP-103 constitute a reference point for decision-making processes concerning radiological protection issues.

The ICRP works closely with several organisations as the International Commission on Radiation Units and Measurements (ICRU), the United Nations Scientific Committee on the Effects of Atomic Radiation (UNSCEAR), the World Health Organization (WHO) and the International Atomic En-

ergy Agency (IAEA). It also has important relationships with the United Nations Educational, Scientific and Cultural Organization (UNESCO), the European Union (EU), the Nuclear Energy Agency of the Organization for Economic Co-operation and Development (OECD/NEA) and other international and national organisations and government bodies.

The discussion presented in the whole chapter will be based on the contents of ICRP-103.

4.2 Biological effects of ionizing radiation

4.2.1 The concept of Risk

As other fields concerning with the control of hazards, radiological protection is based on both scientific knowledge on health risks attributable to radiation exposure and value judgements.

The challenge of the ICRP-103 revision process and the philosophy unpinning the whole system of radiological protection, are to mediate between scientific knowledge of radiation-related health effects, ethical values as prudence, that is to be appropriately conservative but not excessively protective, and practical experience, that is to be easy to use in everyday circumstances by radiological protection practitioners "on the ground".

"The Commission believes that the basis for, and distinction between, scientific estimations and value judgements should be made clear whenever possible, so as to increase the transparency, and thus the understanding, of how decisions have been reached" (ICRP-103, par. 27).

In radiological protection the "Risk" is associated to the probability that a particular adverse health event will occur as the result of a particular exposure to radiation, on an individual or group of people within a particular period of time.

Taking in account that all sorts of everyday human activities carry with them some risk, and many of these activities are generally regarded as being "safe", the main question of the radiological protection is to understand what risk from a particular exposure should be considered tolerable, or acceptable, for an individual or group of people. In fact, even "unsafe" practices can likely be acceptable by virtue of their beneficial effects for society.

4.2.2 The induction of tissue reactions

The adverse health effects induced by ionizing radiation fall broadly into two general categories: *tissue reactions* and *stochastic effects*.

High doses will cause tissue reactions, as harmful tissue reactions or acute effects that surely appear if the dose exceeds a threshold value (as erythema, a typical early reaction, or deep tissue necrosis, a late effect), and increase with dose [77]. The mechanism underlying the tissue reactions is due in large part to the cell killing or malfunction caused by ionizing radiation.

Radiation is the emission and transmission of energy as electromagnetic waves or subatomic particles. Ionizing radiation can damage living things because it carries enough energy to remove electrons from atoms or molecules, leaving them electrically charged, a process called "ionization". Charged particles (e.g., electron, alpha-particle) are directly ionizing, whereas electrically neutral particles (e.g., photon, neutron) are indirectly ionizing and cause ionization through the production of charged particles in matter.

The *absorbed dose* (D) of ionizing radiation is the energy deposited per unit mass of material. The SI unit of absorbed dose is the gray (Gy): 1 Gy = 1 J/kg.
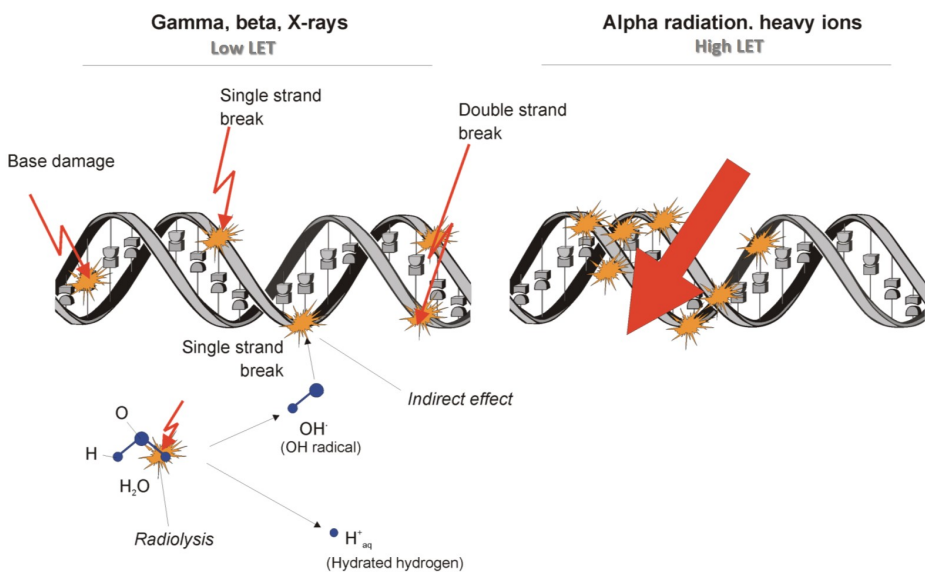

Figure 4.2: Radiation-induced DNA damage. Courtesy of A. Wojcik [78].

Although 1 J deposited in 1 kg of water will raise its temperature by only 0.24 mK, in radiological protection 1 Gy is considered a high dose. In fact, at the microscopic level the action of ionizing radiation can produce a DNA cellular damage because it causes clustered breaks in DNA strands, as shown in Figure 4.2.

Table 4.1: Absorbed dose threshold for tissue reactions [81]. See also [77].

Dose (whole-body)	Effects
<0.25 Gy	No clinically recognizable damage
0.25 Gy	Decrease in white blood cells
0.5 Gy	Increasing destruction of leukocyte-forming organs (causing decreased resistance to infections)
1 Gy	Market changes in the blood (decrease in the numbers of leukocytes and neutrophils
2 Gy	Nausea and other symptoms
5 Gy	Damage to the gastrointestinal tract causing bleeding and ∼50% death
10 Gy	Destruction of the neurological system and ∼100% death within 24 h

DNA strand breaks can lead to cell death if they cannot be repaired, but mis-repair can later contribute to the development of cancer in the exposed individual, or to hereditary disease in the individual's descendants if a germ cell is affected. Double DNA strand breaks are particularly dangerous for the natural repair mechanisms of a cell.

The potential impact of the tissue reactions, as a consequence of both the military and industrial use of radiation and radiation accidents, as well as of erroneous medical uses, was extensively studied starting from the end of the World War II, until the present days [77, 79, 80].

These studies on the biological effect of radiation allowed the ICRP to recommend a reasonable threshold (intended as a practical level to discriminate a dose below which the effect is unlikely to occur) for relevant tissue impairment around 100 mGy: "Reviews of biological and clinical data have led to further development of the Commission's judgements on the cellular and tissue mechanisms that underlie tissue reactions and the dose thresholds that apply to major organs and tissues. However, in the absorbed dose range up to around 100 mGy (low LET or high LET) no tissues are judged to express clinically relevant functional impairment." (ICRP-103, par. 60). In Table 4.1 typical values of dose threshold for tissue reactions are listed.

The dose value of 100 mGy recommended by ICRP is valid for all types of ionizing radiation, both those that spread the energy on the cellular tissue

(e.g., electron or photon) and those that release high quantities of energy locally in the cell (e.g., neutron, alpha-particle, heavy ion). This attitude of ionizing radiation is quantified by means of the concept of *Linear Energy Transfer*.

The Linear Energy Transfer (LET) is the average energy locally imparted to the medium by a charged particle of specific energy traversing a certain distance. More or less, sparsely ionizing radiation is low-LET radiation, while densely ionizing radiation is high-LET radiation. In Figure 4.3 a schematic picture of the relation between radiation types and ionization density is shown.

the average energy locally imparted to the medium by a charged particle of specific energy traversing a certain distance" [52]. Thus, stopping
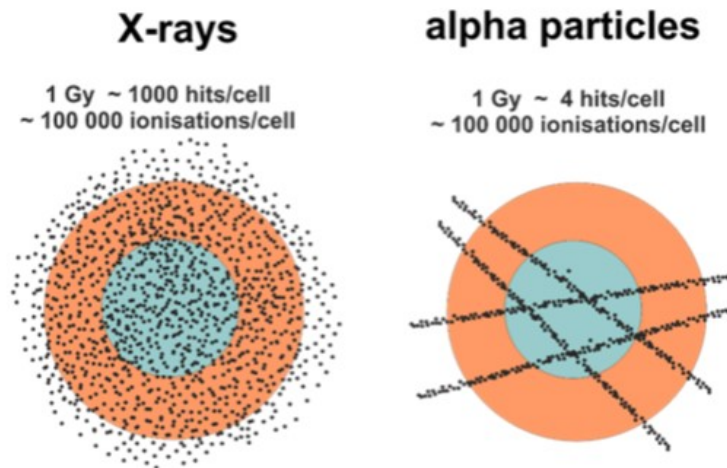
Figure 4.3: Difference in the distribution of number of hits in a cell, per unit dose, due to X-rays (low LET, on the left) and alpha particles (high LET, on the right). The number of ionizations is the same. Courtesy of A. Wojcik [78].

4.2.3 The induction of stochastic effects

Laboratory experiments have demonstrated unambiguously that both high and low quantities of ionizing radiations may cause statistically detectable stochastic effects, as cancer or heritable effects. It is assumed that the probability of incidence of these effects has no threshold dose, but increases with dose, and they can occur even after a long time from exposure. These effects depend on non-lethal cell modifications (mutation).

The level of these effects on the single person is impossible to be predicted purely from data based upon experimental studies. As an alternative, is most opportune to consider groups of humans rather than individual humans. Epidemiology is the study of the distribution of disease in human populations and the factors that determine the risk of disease in these populations.

Epidemiology uses data generated by the uncontrolled conditions of everyday life, so a reliable interpretation of epidemiological results is difficult because the radiation-induced stochastic health effect cannot be distinguished from the same effect produced by some other factors. Therefore, cancer risks must be determined from the epidemiological study of human populations exposed to ionizing radiation, as Japanese atomic-bomb survivors or radiation-exposed groups in the medical, occupational and environmental contest.

Downstream of epidemiological studies, a radiation weighting factor w_R was introduced with the aim to assess the stochastic effect induced by low-level exposure to radiation. w_R is a dimensionless factor by which the organ or tissue absorbed dose is multiplied to reflect the higher biological effectiveness of high-LET radiations compared with low-LET radiations. It is set to 1 for all low-LET radiations and to 20 for alpha-particles, fission fragments, heavy ions, while for neutrons it is a continuous function of energy, ranging from 2.5 to about 20. In Table 4.2 the values of w_R for different types of radiations are reported.

The *equivalent dose* (H_T) in an organ or tissue T is then defined as the sum of the mean absorbed doses from radiation R in that organ or tissue, each weighted by the factor w_R relevant for that radiation type. The unit of equivalent dose is joule per kilogram ($J\,kg^{-1}$) and its special name is the sievert (Sv).

However, the w_R weighting factor is not sufficient to quantify the sensitivity to radiation-induced stochastic health effects, that varies between cellular tissues. A tissue weighting factor w_T has been introduced to represent the age and population averaged contribution of that organ or tissue to the overall detriment[1], from stochastic effects following low-level exposure. Table 4.3 reports the values of w_T for different types of organs or tissues.

---

[1]The detriment is intended as the total harm to health experienced by an exposed group and its descendants as a result of the group's exposure to a radiation source. Detriment is a multidimensional concept. Its principal components are the stochastic quantities: probability of attributable fatal cancer, weighted probability of attributable non-fatal cancer, weighted probability of severe heritable effects, and length of life lost if the harm occurs (ICRP-103).

Table 4.2: Recommended radiation weighting factors (ICRP-103).

Radiation type	w_R
Photons	1
Electrons* and muons	1
Protons and charged pions	2
Alpha particles, fission fragments, heavy ions	20
Neutrons	A continuous function of neutron energy (see Table 2 of (ICRP-103))

All values relate to the radiation incident on the body or, for internal radiation sources, emitted from the incorporated radionuclide(s).
*Note the special issue of Auger electrons (see Table 2 of (ICRP-103)).

Table 4.3: Recommended tissue weighting factors (ICRP-103).

Tissue	w_T	$\sum w_T$
Bone-marrow, Colon, Lung, Stomach, Breast, Remainder Tissues* (Nominal w_T applied to the average dose to 14 tissues)	0.12	0.72
Gonads	0.08	0.08
Bladder, Oesophagus, Liver, Thyroid	0.04	0.16
Bone surface, Brain, Salivary glands, Skin	0.01	0.04

*Remainder Tissues (14 in totl): Adrenals, Extrathoracic (ET) region, Gall bladder, Heart, Kidneys, Lymphatic nodes, Muscle, Oral mucosa, Pancreas, Prostate, Small intestine, Spleen, Thymus, Uterus/cervix.

So far focus has been put only on the effects of external irradiation, coming from outside human body. However, certain short-range radiations (e.g. α particles or β particles) pose a hazard when the source enters inside the body, for example through intake. These radiations define the central difference between external and internal irradiation, and the consequent effects.

The radiological protection quantity introduced to quantify the effect on different tissues or organs of radiation doses from either external or internal sources, possibly from radiations with different w_R, is the *effective dose* (E). It is defined as:

$$E \;=\; \sum_T w_T \sum_R w_R \, D_{T,R} \quad or \quad E \;=\; \sum_T w_T \, H_T, \qquad (4.1)$$

where H_T is the equivalent dose in a tissue or organ T. The unit for the effective dose is the same as for the equivalent dose, the sievert (Sv).

Effective dose is an important radiological protection concept that permits absorbed doses received by a Reference Person[2], coming from different radiations and by different tissues, both from external and internal sources, to be weighted and added in a meaningful way. In this way the overall detriment-related value can be calculated. The effective dose and the equivalent dose are reference quantities used in the radiological protection legislation [82].

In the context of population or occupational exposure, the *collective effective dose* (S) has been introduced to quantify the exposure of all individuals in a group over a given time period or during a given operation executed by this group in a work radiation area. It is calculated as the sum of all individual effective doses over the time period or during the operation being considered. The special name used for the collective effective dose quantity is the "man sievert".

It should be emphasized that the concept of effective dose has to be used in the context of radiological protection against low-level exposure to ionizing radiation, while in some situations of higher radiation, absorbed dose or equivalent dose could be more appropriate quantities.

Equivalent dose and effective dose cannot be measured directly in body tissues. The protection system therefore developed other operational quantities that have the advantage to be measurable and from which, under

---

[2]The Reference Person is "an idealised person for whom the organ or tissue equivalent doses are calculated by averaging the corresponding doses of the Reference Male and Reference Female" (ICRP-103).

Table 4.4: *Application of operational dose quantities for monitoring of external exposures (ICRP-103).*

Task	area monitoring	individual monitoring
Control of effective dose	ambient dose equivalent, H*(10)	personal dose equivalent, $H_p(10)$
Control of doses to the skin, the hands and feet and the lens of the eye	directional dose equivalent, H'(0.07,Ω)	personal dose equivalent, $H_p(0.07)$

most irradiation conditions, the equivalent dose and the effective dose can be assessed in a conservative way.

For the case of external exposure, operational quantities for area and individual monitoring have been defined by ICRU [83, 84], to which the reader is referred for a detailed explanation. They are adopted by ICRP-103 and are summarized in Table 4.4.

These quantities are often used in practical guidance since they provide a reasonable and generally conservative estimate for the value of the protection quantities under most irradiation conditions. The operational quantity utilized in the calculations developed in the context of this thesis work, for the monitoring of external radiation exposure, is the *ambient dose equivalent*, H*(10)[3]. As it will be explained in Section 5.2.1, H*(10) represents a conservative assessment of the effective dose in the calculations performed in the following Chapters.

No operational quantities have been defined to directly assess the equivalent or effective dose for internal dosimetry. In general, these quantities are calculated by using reference dose coefficients (doses per unit intake) recommended by ICRP, and also reproduced in [85, 86].

4.2.4 The Dose-response Model

A important question for the radiological protection operators is how does the risk of stochastic health effects vary with the dose or dose-rate of ra-

---

[3]The ambient dose equivalent H*(10) is the dose equivalent at a point in a radiation field that would be produced by the corresponding expanded and aligned field in the ICRU sphere at a depth of 10 mm on the radius vector opposing the direction of the aligned field. The unit of ambient dose equivalent is the sievert (Sv) [83, 65].

diation received. Several dose-response models have been considered by extrapolating at low doses the atomic-bomb survivors data [71]. They show different behaviors with the increase of the dose, as shown in Figure 4.4.
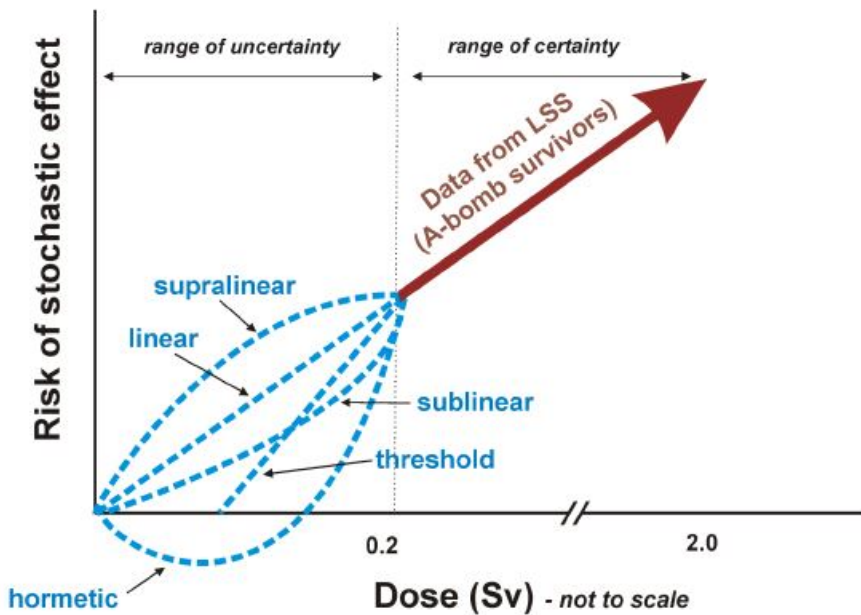
Figure 4.4: Dose-response curves describing the excess risk of stochastic health effects at low doses of radiation. Courtesy of A. Wojcik [78].

A supra-linear behavior may be associated to the "bystander effect", the phenomenon under which non-irradiated cells exhibit unwanted effects as a result of signals received from nearby irradiated cells [87]. Also the "genomic instability", referred to a high frequency of mutations within the genome of a cellular descent due to DNA damage, can give rise to a supra-linear dose-response effect.

Conversely, the "hormetic" behavior may be associated to the "adaptive response", a still little known form of direct DNA repair and protection from damage caused by external agents or by errors during replication [88].

However, due to the uncertainties on the influence of these biological mechanisms on the health at low doses, the epidemiological evidence for a possible deviation from a linear no-threshold dose-response at low doses or low dose-rates is not persuasive. Therefore, the ICRP-103 hypothesis is that, for exposure to a low dose (lower than about 100 mSv), the excess risk of cancer is taken to be directly proportional to the dose received, without

any threshold. This dose-response model is generally known as "linear no-threshold" (LNT).

"At radiation doses below around 100 mSv in a year, the increase in the incidence of stochastic effects is assumed by the Commission to occur with a small probability and in proportion to the increase in radiation dose over the background dose. Use of this so-called linear-non-threshold (LNT) model is considered by the Commission to be the best practical approach to managing risk from radiation exposure and commensurate with the precautionary principle [89]. The Commission considers that the LNT model remains a prudent basis for radiological protection at low doses and low dose rates [90]" (ICRP-103, par. 36).

4.3 The system of radiological protection

4.3.1 General assumptions

Due to the probabilistic nature of stochastic effects and the properties of the LNT model, it is clear that any dose of radiation, no matter how small, carries with it some risk. The principal objective of radiological protection is to manage and control radiation exposures to prevent tissue reactions and to limit to the extent reasonably achievable stochastic effects.

The whole of events and situations of the everyday life that contribute to the human exposure have as their common origin the presence of a radiation source, or already being in place, or introduced deliberately as a matter of choice by society, or as a result of emergencies. It may be a physical source, an installation, or a procedure involving ionizing radiation. Therefore, all the possible protection actions, with few exceptions, have to be interposed between the source and the exposed individuals.

"The Commission's system of radiological protection applies to all exposures to ionizing radiation from any source, regardless of its size and origin. However, the Recommendations can apply in their entirety only to situations in which either the source of exposure or the pathways leading to the doses received by individuals can be controlled by some reasonable means. Some exposure situations are excluded from radiological protection legislation, usually on the basis that they are unamenable to control with regulatory instruments, and some exposure situations are exempted from some or all radiological protection regulatory requirements where such controls are regarded as unwarranted" (ICRP-103). In Figure 4.5 the estimated contributions to worldwide average public exposure from different sources are mapped for two recent temporal periods.
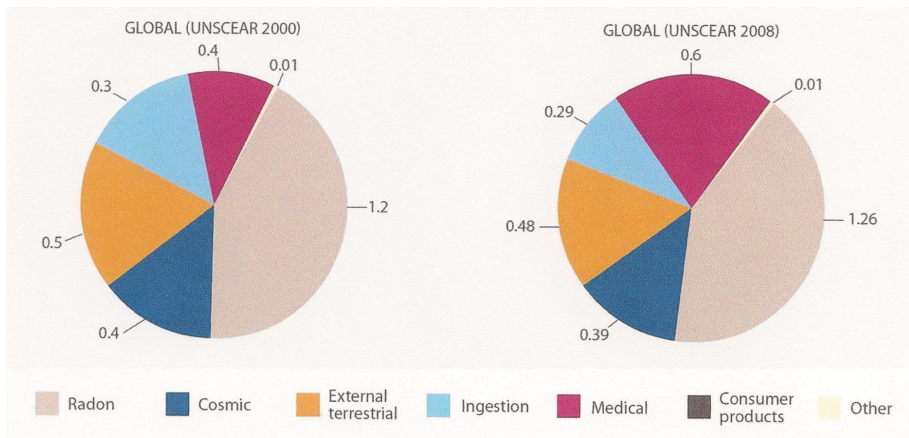
Figure 4.5: Worldwide average public radiation exposure for the years 2000 (on the left) and 2008 (on the right), in mSv [91].

The complex process that govern the ICRP building of a system of radiological protection is based on several assumptions.

- The events related to radiation exposure are distinguished in three types of exposure situations: planned, emergency, and existing exposure situations. Planned exposure situations involve the deliberate introduction and operation of sources and may give rise both to forecast (normal) exposures and to unexpected (potential) exposures. Emergency exposure situations may derive from planned or other unexpected situations, and require urgent action to avoid or reduce undesirable consequences. Existing exposure situations already exist when a decision on control has to be taken; they include prolonged exposure situations after emergencies.

- The individuals are subject to several categories of exposure, which can be treated separately: those that are certain to occur, for example in working areas, and potential exposures, for example exposure to environmental sources as members of the public or medical exposure as patients. This policy leads to the definition of three exposure categories: occupational exposure, medical exposure of patients, and public exposure (including exposure of the embryo and fetus of pregnant workers).

- Concerning the occupational exposure, on which particular attention is paid in this thesis, a mandatory function for an employer and/or

60

licensee is to control the sources of exposure and to protect the workers, mostly by defining specially designed areas of work. A *controlled area* means an area subject to special rules for the purpose of protection against ionizing radiation or preventing the spread of radioactive contamination and to which access is controlled; a *supervised area* means an area subject to supervision for the purpose of protection against ionising radiation [92]. In supervised areas special procedures are not normally needed. Conversely, "workers in controlled areas of workplaces should be well informed and specially trained, and form a readily identifiable group. Such workers are most often monitored for radiation exposures incurred in the workplace, and occasionally may receive special medical surveillance." (ICRP-103, par. 184-185).

- Each source contributes independently from the others to an individual dose, so it is generally possible to consider the exposure of all the individuals to this particular source or group of sources. This procedure is called "source-related" assessment. "For planned exposure situations, the source-related restriction to the dose that individuals may incur is the *dose constraint*. For potential exposures, the corresponding concept is the *risk constraint*. For emergency and existing exposure situations, the source-related restriction is the *reference level*." (ICRP-103, par. 198). Otherwise, in the case of planned exposure situations, separate restrictions called "individual-related" are required to address the overall (occupational and public) doses for the individual from all sources, in the form of *dose limits*. Figure 4.6 illustrates the differences between the use of individual dose limits in planned situations and constraints or reference levels in all situations.

- Three fundamental principles of protection are formulated: *justification*, *optimisation of protection*, and *dose limitation*. The first two principles are source-related and apply in all exposure situations, while the third principle is individual-related and applies in planned exposure situations. They will be discussed in the next section.

4.3.2 The principles of the radiological protection

The *principle of justification* states that "Decisions introducing a practice shall be justified in the sense that such decisions shall be taken with the intent to ensure that the individual or societal benefit resulting from the practice outweighs the health detriment that it may cause. Decisions introducing or altering an exposure pathway for existing and emergency exposure

61

Figure 4.6: Dose limits compared with constraints and reference levels for the protection of workers and members of the public (ICRP-103).

situations shall be justified in the sense that they should do more good than harm." [92].

"The responsibility for judging the justification usually falls on governments or national authorities to ensure an overall benefit in the broadest sense to society and thus not necessarily to each individual." (ICRP-103, par. 208). However, justification decisions will often be informed by a process of public consultation. They may also involve many different organisations with different responsibilities.

The *principle of optimisation of protection* states that "Radiation protection of individuals subject to public or occupational exposure shall be optimised with the aim of keeping the magnitude of individual doses, the likelihood of exposure and the number of individuals exposed as low as reasonably achievable [hence the term ALARA] taking into account the current state of technical knowledge and economic and societal factors." [92].

"Optimisation is always aimed at achieving the best level of protection under the prevailing circumstances through an ongoing, iterative process that involves: evaluation of the exposure situation, including any potential exposures (the framing of the process); selection of an appropriate value for the constraint or reference level; identification of the possible protection options; selection of the best option under the prevailing circumstances; and implementation of the selected option." (ICRP-103, par. 214).

It should be highlighted that optimisation is different from minimisation, since it carefully balances the detriment from the exposure (economic,

human, social, environmental, etc.) and the resources available for the protection of individuals. The best option is not necessarily the one with the lowest dose.

Table 4.5: Italian dose limits in planned exposure situations[a] [82].

Type of limit	Occupational	Public
Effective dose	20 mSv per year, averaged over defined periods of 5 years[d]	1 mSv in a year
Annual equivalent dose in:		
Lens of the eye[b]	20 mSv	15 mSv
Skin[c]	500 mSv	50 mSv
Extremities (hands and feet)	500 mSv	–

[a] Limits on effective dose are for the sum of the relevant effective doses from external exposure in the specific time period and the committed effective dose from intakes of radionuclides in the same period.
[b] 20 mSv in a single year or 100 mSv in any five consecutive years subject to a maximum dose of 50 mSv in a single year, as specified in national legislation.
[c] This limit applies to the dose averaged over 1 cm^2 area of skin, regardless of the area exposed.
[d] With the further provision that the effective dose should not excess 50 mSv in a single year. The occupational exposure of pregnant women is comparable with that provided for members of the public.

The *principle of dose limitation* states that "In planned exposure situations, the sum of doses to an individual shall not exceed the dose limits laid down for occupational exposure or public exposure. Dose limits shall not apply to medical exposures." [92]. The limits on effective dose apply to the sum of doses due to external exposure and committed doses from internal exposure due to intake of radionuclides.

The dose limits defined in the new Italian directive establishing relevant basic safety standards for the protection from exposure to ionizing radiation, entered into force in 2020 [82], are summarized in Table 4.5. This directive is the implementation of the European directive 2013/59/Euratom [92].

The relationship between dose limits on the one hand, and constraints and reference levels on the other hand, lies in the fact that "Dose constraints for planned situations represent a basic level of protection and will always

Dose in a y (mSv)	Examples
>20 up to 100	Reference level for evacuation in an emergency. Occupational exposures in Rescue Operations
>1 up to 20	Constraints set for occupational exposure and for comforters and carers. Reference level for radon.
1 or less	Constraints set for public exposure in Planned situations.

Figure 4.7: Exemplifying bands of constraints and reference levels. Comforters and carers refer to medical exposures of patients (ICRP-103, par. 322). Courtesy of J. Valentin [78].

be lower than the pertinent dose limit." (ICRP-103, par. 230). Conversely, "In emergency or existing controllable exposure situations, the reference levels represent the level of dose or risk, above which it is judged to be inappropriate to plan to allow exposures to occur" (ICRP-103, par. 234).

Illustrative constraints for planned exposures and reference levels in existing situations are described in Figure 4.7.

Figure 4.8 describes a possible accident scenario and the corresponding admitted dose levels. Looking at Figure 4.8, the maximum reference level value indicated on the table is 100 mSv. "Exposures above this value would be justified only under extreme circumstances, either because the exposure is unavoidable or in exceptional situations such as the saving of life or the prevention of a serious disaster. No other individual or societal benefit would compensate for such high exposures." (ICRP-103, par. 236).

In any case, "The Commission's multi-attribute approach to the selection of dose limits necessarily includes societal judgements applied to the many attributes of risk. These judgements would not necessarily be the same in all contexts and, in particular, might be different in different societies. It is for this reason that the Commission intends its guidance to be sufficiently flexible to allow for national or regional variations." (ICRP-103, par. 251).
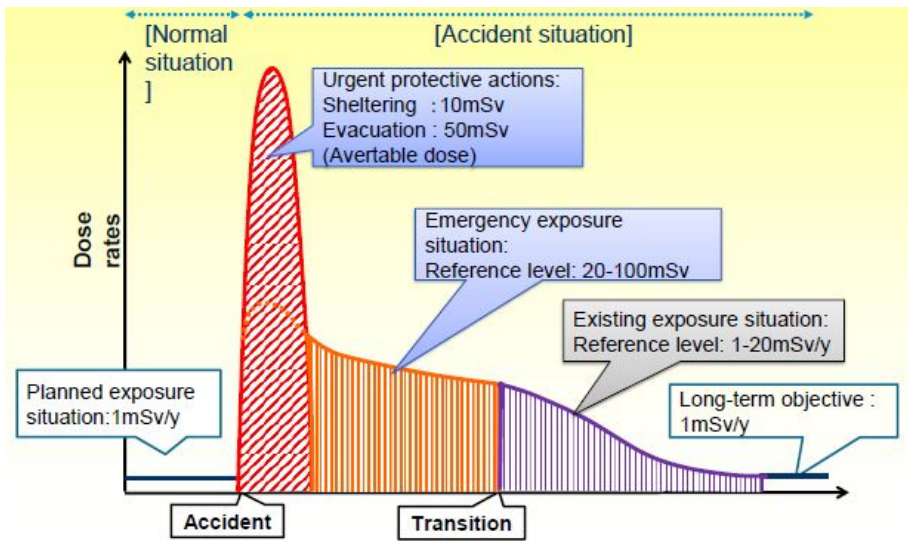
Figure 4.8: Time projection of a possible accident situation with the corresponding dose levels. Courtesy of J. Valentin [78].

4.4 Ethics and environment protection

The central question of the system of radiological protection is to understand what actions, if any, should be taken when facing with existing sources of radiation, or when considering introducing new ones. Scientific knowledge and practical experience are essential but, alone, are not enough to decide what to do. The other ingredient necessary to understand how to behave are the human and ethical aspects of exposure situations, as illustrated in Figure 4.9. These aspects sometimes are decisive, both in the decision-making process and in communication, particularly when engaging with stakeholders.

The ethical foundations of the system of radiological protection have been developed in a recent specific ICRP publication [93]. They are based on four core ethical values: beneficence/non-maleficence, prudence, justice, and dignity.

Integrated into the three overarching principles of justification, optimisation of protection and dose limitation, the core ethical values allow people to act virtuously while taking into account the radiological protection issues. This is especially true if they are effectively combined with procedural values aiding their practical implementation, as accountability, transparency, and inclusiveness.

Beneficence means promoting or doing good, and *non-maleficence* means
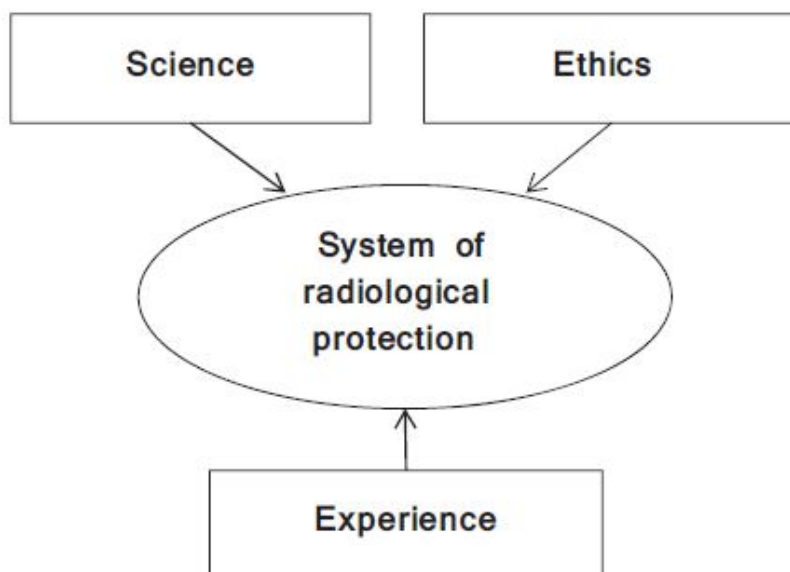
Figure 4.9: The three pillars of the system of radiological protection [93].

avoiding causation of harm [94]. Beneficence is achieved in practice by ensuring that tissue reactions are avoided and stochastic effects are reduced as far as achievable, given the prevailing circumstances. Non-maleficence is intimately connected to prevention, which aims to limit risk by eliminating or reducing the likelihood of hazards.

In evaluating potential harms and benefits of human activities involving radiation, one should also include the concern for the future generations and the environment, ensuring that the overall outcome results in more good than harm.

Nevertheless, the deliberate use of radiation may unquestionably have desirable consequence for individuals and, indirectly, for the society, such as the improvement of diagnostics or therapy in medicine, or the production of electricity. These good effects have to be weighed against the potential harmful consequences.

"*Prudence* is the ability to make informed and carefully considered choices without full knowledge of the scope and consequences of actions. It is also the ability to choose and act on what is in our power to do and not to do." [93].

In radiological protection, prudence has been constantly re-affirmed in relation to the linear no-threshold (LNT) model, considered a prudent dose-response behavior, given the lack of perfect knowledge of the level of risk

associated with very low-dose exposure.

More specifically, prudence is used in connection with the consideration for tissue reactions at threshold doses around 100 mSv, that will almost always justify the introduction of protective actions. Moreover, even in absence of direct evidence of heritable effects, prudence continues to be used in relation to the exposure of fertile woman to radiation.

In addition, prudence means implement the vigilance on the effects of radiation, that is monitoring on radiological conditions for humans and non-human biota, scientific research on unexpected findings and support to the exposed population, including diagnosis and treatment of possible pathologies induced by ionizing radiation.

"*Justice* is usually defined as fairness in the distribution of advantages and disadvantages among groups of people (distributive justice), fairness in compensation for losses (restorative justice), and fairness in the rules and procedures in the processes of decision making (procedural justice)." [93].

Justice comply with the idea of limiting individual exposures, in order to correct possible disparities in the distribution of individual radiation through the use of dose constraints and reference levels, and to ensure that exposures do not exceed the values beyond which the associated risk is considered as not tolerable given a particular context, through the application of legal dose limits.

Procedural justice is also the recognition of the right of stakeholders and citizens to participate in decision-making processes, especially concerning the environment. This was ratified in the Århus Convention on Access to Information, Public Participation in Decision-making, and Access to Justice in Environmental Matters [95].

Finally, intergenerational distributive justice is related to the sustainable development and to the responsibility towards future generations: good management of radioactive wastes, preservation of health and environment, but also transfer of knowledge and resources.

Dignity has a central place in the Universal Declaration of Human Rights: "All human beings are born free and equal in dignity and rights" [96].

The respect for human dignity in radiological protection is related to the "informed consent" in biomedical research. More in general, dignity concerns the respect of individual human rights and to the promotion of autonomy through people empowerment to make informed decisions on radiological faces of their daily live.

In the end, "Ethics cannot provide conclusive solutions, but can help to facilitate discussions among those seeking to promote the well-being of individuals, the sustainable development of society, and the protection of the

environment. A clearer understanding of the core ethical values and related principles of radiological protection will help to address issues emerging from potential conflicts in decision making." [93].

Chapter 5

Radiological protection calculations for SPES: tools and Monte Carlo methods

5.1 Introduction

In Section 4.3 the system of radiological protection built by ICRP has been described. Following those assumptions, the activities related to the SPES project have to be considered as a planned exposure situation, due to the deliberate introduction and operation of radioactive sources. Most of the issues derive by the use of a cyclotron accelerator as proton source, and by the production of RIBs.

Therefore, a deep study of the safety and reliability aspects is required to prevent hazardous situations for operators, population and the surrounding environment.

The "Quality and Safety Management System" (QSMS) is a tool that has been realized at the LNL, for handling of all the phases of the SPES project, starting from the initial design stage to the final decommissioning [97]. Within the QSMS, all aspects relevant to the safety are considered and reasonably predicted in advance, in relation to the different phases of the life cycle of the project.

The general implementation of the safety and security aspects concerning the radiation protection for the operators, population and the surrounding environment is contained in several documents of the QSMS. One of the main documents is the risk analysis of the SPES project [98]. It contains the description of activities and processes, the identification of hazards for safety and health and the assessment of the related risks, as well as the iden-

tification of the legal requirements for the operational management inherent safety and environmental aspects.

The aim of my Ph.D. thesis is to focus on the study of some "hot spots" of the SPES project, from the radiation protection point of view, with the purpose of providing useful information on the radiation hazard in different areas of the facility.

The first case study (described in Chapter 6 and Chapter 7) consists in the assessment of the radioactivity and of the external exposure to radiation inside the production bunker. The radiation dose is due to the activation of the materials of the Front-End, caused by accelerated protons in the primary beam line, and by neutrons generated by fission in the target, as well as to the deposit of radioactive ions in the RIB channel electromagnetic devices. One has also to carefully consider that, during the whole SPES life cycle, the radioactivity of the Front-End components and the consequent dose rate in the bunker progressively increase, due to the accumulation of medium-long lifetime radioisotopes.

The second case study (described in Chapter 8) regards all the radiation issues connected to the handling operations on the exhausted target and ion source unit during its life cycle, from the removal from the Front-End after irradiation, until the final dismantling and disposal after permanence in a temporary storage.

The assessment of the dose rate allows strategies to control and optimize the radiation exposure during the forecast accesses in the specially designed areas of work (for example inside the production bunker and in proximity of the temporary storage) to be developed. Maintenance interventions on the Front-End beam lines and handling operation on exhausted TIS units have to be planned in compliance with the radiation protection recommendations on source-related dose constraints and on the use of legal dose limits.

These recommendations will be necessary not only to plan inspections and maintenance work during the operation of the facility, but also to manage the waste disposal and the decommissioning phase of the installation. In fact, critical issues are also connected to the generation of radioactive waste that must be disposed of (targets, structural parts of the activated Front-End, exhausted gases, etc.).

Moreover, the methods used to assess the exposure in normal situations can be applied also to potential unexpected exposures within the project, and more generally they can be extended to other existing or future RIB facilities.

As a consequence of these studies, general considerations (described in Chapter 9) will be made on the economic, social and environmental impact

of the facility during its life cycle, and on the strategies implemented to improve the sustainable development of the project.

Later in this chapter, the calculation tools used to evaluate the induced radioactivity in the materials and the external exposure to ionizing radiation in different SPES contexts will be illustrated. Since the facility is currently at an advanced construction status, but not yet in activity, at the moment these methods represent the only possibility of quantifying the extent of biological dose hazard. Another valuable source of information is the network of collaboration of SPES with other national and international RIB facilities, as HIE-ISOLDE at CERN [13].

5.2 The Monte Carlo methods in SPES

Monte Carlo computational methods are very different from deterministic transport methods. They consists in actually describing a statistical process, by simulating sequentially the individual probabilistic events that comprise that process. The total phenomenon is then inferred by sampling the probability distributions governing these events. The sampling process is based on the generation of random numbers, similarly to throwing dice in a gambling casino, hence the name "Monte Carlo".

In the case of transport and interaction of nuclear particles with the matter, each of the many particles constituting a source is actually followed throughout its life, until its death. Probability distributions are randomly sampled using nuclear and reaction data, to determine the outcome at each step of its life. So, the Monte Carlo technique can be considered a sort of "numerical experiment".

The result of the experiment is one or more estimators of the desired quantity, which are obtained averaging over the number of primary events; for this reason, generally the results are given normalized per primary event. The higher the number of histories, the better the statistical error on the estimator:

$$\sigma \propto 1/\sqrt{N}, \tag{5.1}$$

where N is the number of full histories.

To reach a reliable estimate of the statistical precision of the quantities of interest of the user, a very large number of individual histories has therefore to be followed. For this reason, parallel running on a Cloud pc platform may be required to allocate a large amount of CPU resource to the calculations.

In the different case studies considered, to evaluate the radioactivity induced in the materials and the external exposure to ionizing radiation, with consequent biological dose hazard, two Monte Carlo radiation transport codes have been used. Namely MCNPX [99] (combined with the CINDER'90 [100] evolution code) and FLUKA [101, 102], that are commonly utilized for this type of nuclear physics applications.

5.2.1 The Monte Carlo method based on MCNPX

MCNPX is an extension of MCNP Monte Carlo program [103], developed at the Los Alamos Laboratories after the development of nuclear weapons during the World War II. MCNP is able to transport neutrons, photons and electrons in complex geometries. It includes the capability to give information on nuclear criticality, the ability to sustain a chain reaction by fission neutrons. MCNPX is designed to simulate also transport and interactions with matter of heavy charged particles and nuclei. The reference MCNPX release used for the studies reported in this thesis is the 2.7.0 version [99].

The code reads an input file created by the user, containing information about the problem: the location and characteristics of the particle source, the problem geometry description, the definition of materials and the selection of corresponding interaction cross-sections, the type of answers desired, and the possible variance-reduction techniques used to improve the statistical efficiency.

The geometry tool of MCNPX makes it possible to configure an arbitrary 3-dimensional Cartesian coordinate system building user-defined materials in geometric cells, defined by using boolean operators of intersection, union, and complement of regions bounded by surfaces. Surfaces are generally defined by supplying geometrical information, but the code also provides a "macrobody" capability for basic shapes such as spheres, boxes or cylinders. The code performs extensive geometry internal checking to find input errors and a geometry-plotting capability is implemented and helps the user to check for geometry errors.

For a given history, a new random number sequence is set up and the appropriate source routine is called. Here the source kinematic parameters are initialized and the conveniently sampled source particle is launched. Then MCNPX tracks the particle through the geometry, considering at each step of the transport the physical collisions and the intersections with each bounding surface along the trajectory, until the particle and any remaining progeny are killed and the history is terminated.

MCNPX makes use of evaluated cross-section data tables for particle

transport. However, some nuclear interactions generated by neutrons and protons are treated using external physical models, since evaluated cross-section libraries are not available for all materials, energies and reactions. Several physical models are implemented for nuclear interactions, including the Bertini intra-nuclear cascade model [104] and the ORNL fission-evaporation model [105]. They have been adopted in the present study since they are reliable in the nucleon energy ranges typical of the SPES operations [9]. The energy transition between the use of physical models and the cross-sections nuclear data libraries is set with a "mix-and-match" option, that is the libraries are used when the cross-sections are present.

MCNPX provides summary responses, called "tallies", to specify the type of information that the user asks to the Monte Carlo calculation, such as current across a surface, fluence or energy deposition averaged over a cell, residual nuclei produced by interaction of high-energy particles with target nuclei. The mesh tally method is also available to graphically displaying scored quantities on a spatial grid overlaid on top of the standard problem geometry.

The results of the MCNPX tallies represent an average of the contribution of all sampled histories. The associated statistical uncertainty depends on the number of generated histories. MCNPX contains several indicators that help the user in assessing the quality of each tally response. Variance-reduction techniques make it possible to improve the statistical convergence of results in problems with very non-uniform radiation fields, where only a very small fraction of all histories contributes to the desired response.

A fluence-to-dose conversion capability is implemented in MCNPX, making use of specific reference dose conversion coefficients [106, 107, 108, 109]. To calculate the external radiation exposure for the workers in the different SPES contexts discussed in the next chapters, the ambient dose equivalent operational quantity H*(10) for photons, as defined in Section 4.2.3, is used. This is because, in the irradiation conditions typical of the SPES activities, the H*(10) operational quantity should provide a conservative estimate of the effective dose, the reference quantity used in the radiological protection legislation [82]. In fact H*(10) overestimates the effective dose of about 15% under most irradiation geometry conditions, unless the average photon energy is extremely low, in the range of about 15-20 keV, or extremely high, above 3 MeV [106, 109].

As an example, in Figure 5.1 is reported the photon flux exiting out of the activated target, calculated 15 day cooling time after the end of a complete 15 day irradiation cycle. This time corresponds to the removal of the target chamber from the production apparatus, mandatory condition to

authorize the access to the production bunker for maintenance operations.
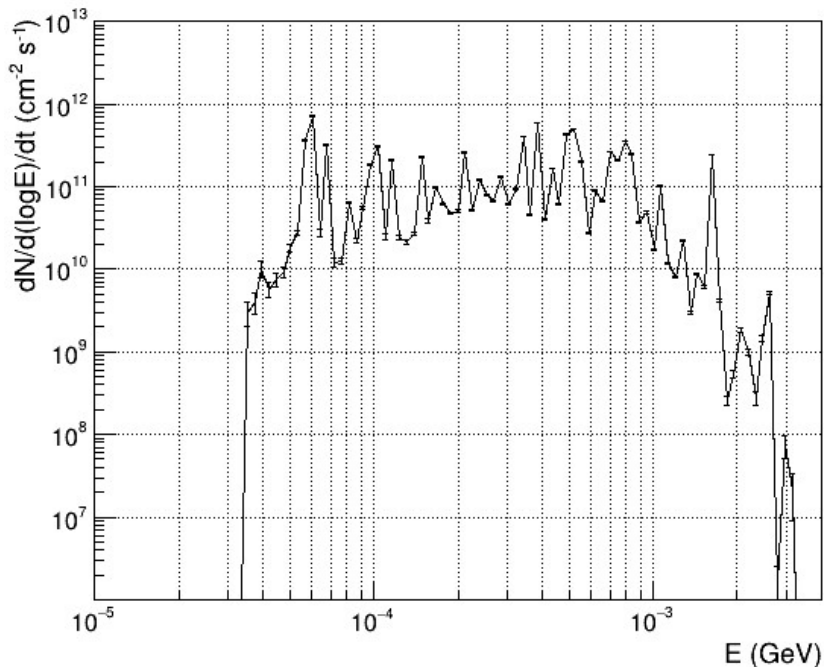
Figure 5.1: Energy flux spectrum for the photons exiting out of the target, calculated with FLUKA after 15 day from the irradiation cycle end.

The spectrum presents a sharp leading edge around a few tens of keV, due to the absorption of the low energy photons in the uranium carbide disks of the target, in the graphite closure and in the tantalum heater. The flux then decreases of three order of magnitude or more, at energy values around a few MeV. In this energy range the ratio of photon effective dose to ambient dose equivalent, calculated for mono-energetic photons, is less than one for each energy value, whatever idealised geometry conditions for whole-body irradiation[1] are considered [106, 108, 109].

The fluences are calculated by MCNPX in specific positions of interest in the modeled geometry and then converted in rate of ambient dose equivalent H*(10) as follows:

$$dH^*(10)/dt \; = \; 3.6 \cdot 10^3 \; I \int_E \; C(E) \; \phi(E) \; dE, \qquad (5.2)$$

---

[1]Antero-posterior, rotational or isotropic irradiation geometry conditions [109] can be assumed with a good approximation in the space in proximity of the SPES Front-End system and of the temporary storage system.

being ϕ(E) dE the differential particle fluence (cm^{-2}) normalized per source particle, C(E) the function interpolating the energy dependent conversion coefficients from fluence to dose (μSv cm^2) [109] and I the total source emission intensity (s^{-1}). The factor $3.6 \cdot 10^3$ is used as second to hour conversion coefficient, to give a final value for H*(10) rate in unit of μSv h^{-1}.

MCNPX is not able to calculate the activation of the nuclides present in an irradiated material at a specified time. To perform this task, a nuclide evolution program has to be interfaced with MCNPX, as CINDER'90 [100].

To determine the processes of transmutation and decay of radioactive nuclides in a complex radiation environment, this evolution code utilize Markovian chain structures consistent with the Bateman Equations [110, 111].

Let's assume a steady irradiation of a material with a spatially uniform fluence rate Φ (cm^{-2} s^{-1}), as can be roughly presumed to happen on each cell of the SPES Front-End during the proton beam irradiation. The volume density n(t) of atoms at time t for the radionuclide of interest, due both to the radionuclide build-up and to decay, according to Equation 3.1 is governed by the equation [112]:

$$\frac{dn(t)}{dt} = \lambda \ n(t) + \Phi \ \sigma \ N, \tag{5.3}$$

where λ is the decay constant of the radionuclide (s^{-1}), σ is the nuclide production cross-section (cm^2) and N is the volume density of atoms of the nuclide of interest. The solution of this equation is:

$$n(t) = \frac{\Phi \ \sigma \ N}{\lambda} \ (1 - e^{-\lambda t}). \tag{5.4}$$

For times much longer than the half-life t$_{1/2}$ of the radioisotope, Equation 5.4 gives A(t) = A$_{sat}$ = $\Phi \ \sigma$ N, being A(t) = λn(t) the specific activity during irradiation, as it can be deduced from Equation 2.1. So, at the saturation the activity equals the production rate.

In general, adding after the irradiation period t an additional cooling time t$_{cool}$, the final activity of a radionuclide can be expressed as:

$$A_{tot}(T) = A_{sat} \ (1 - e^{-t/\tau}) \ e^{-t_{cool}/\tau}, \tag{5.5}$$

being $\tau = 1/\lambda$.

In the case of more than one radionuclide, Equation 5.3 has to be written for each nuclide and the general solution is derived by the Bateman Equations [111].

CINDER'90, combined with MCNPX, has been used to calculate the residual activation of the SPES Front-End system after one or more irradiation periods, followed by a further cooling time. Moreover, the combination

of the two codes has made it possible to assess the most important quantities relevant for the radiological protection. This calculation method is discussed in Chapter 6.

5.2.2 The FLUKA Monte Carlo tool

FLUKA is a general purpose Monte Carlo program for calculations of particle transport and interaction with matter [101, 102]. FLUKA covers an extended range of applications in the field of nuclear and particle physics: particle shielding, target design, cosmic rays, neutrino physics, dosimetry, medical physics, radiotherapy.

The editing of the input file, the visualization of the geometry and of the output and the execution of the code is simplified thanks to the employment of FLAIR, an advanced user FLUKA interface [113].

The FLUKA version used for the first calculations described in this thesis is FLUKA2011.2x.2. However, all recent calculations have been performed with the FLUKA2020-0 release of the renewed INFN FLUKA team [114]. Improved features present in the new version, as the physical model describing the proton and neutron induced fission process at intermediate energies (some tens of MeV), depend also on a recent collaboration between the INFN FLUKA development team and the SPES FLUKA users. These aspects are discussed later in this chapter.

FLUKA contains features similar to the MCNPX ones, but also many different aspects, for example the way of constructing the geometry. In particular, the FLUKA geometry tool is based on the principle of Combinatorial Geometry in which basic objects called bodies (such as cylinders, spheres, parallelepipeds, etc.) are linked to form more complex objects called regions. This combination is performed using Boolean operations: union, intersection and subtraction.

It is also possible to describe any geometry in terms of "voxels", tiny parallelepipeds of equal size forming a 3-dimensional grid. Voxel geometries are especially useful to import CT scans of a human body, for example for dosimetry calculations of the planned treatments in radiotherapy.

Another difference respect to other Monte Carlo programs, including MCNPX and GEANT4 [115], a Monte Carlo program extensively used for calculations within the ISOLPHARM project [116], lies in the way of implementing physical models. FLUKA is not a "tool-kit", in the sense that the development team provides to the user the best possible physics to treat a specific problem, rather than a choice among several possible alternative models. The user has mainly to set physical thresholds and cuts, and to

activate or not few physical processes.

Several physical models are implemented in FLUKA and switched on when cross-section libraries are not available. The hadron-nucleus inelastic interactions of interest for SPES are modeled by selecting the "new evaporation model with heavy fragments'" [101], that allows accurate results for the radioactive fragment production in the target to be obtained. It is based on the PEANUT (Pre-Equilibrium Approach to NUclear Thermalization) nuclear interaction model [117, 118, 119, 120]. The Boltzmann Master Equation (BME) theory is implemented in FLUKA to describe the heavy ion interaction model in the considered energy range [121, 122].

As in MCNPX, the primary source properties are generally defined directly in the input file. However, in more complex situations, the properties of the primary particle, as space coordinates, energy, time, direction or mixture of particles, cannot be described with built-in sources. In these cases the relevant variable values have to be read from external files or generated by some sampling algorithm, or just assigned.

To handle these cases, a external source user routine can be called, overriding totally or in part the information given in input. Initialization, data reading from file, sampling and particle loading into stack for later transport can be defined in the external source, which eventually sends the information to the code routines managing the full event.

External sources have been extensively used for the several types of calculations described in Section 5.1. The sampling is generally performed from a discrete distribution (e.g. a fluence energy spectrum), through the cumulative function. The sampling method can be described as follows.

Let's suppose to have a discrete random variable x, that can assume values x_1, x_2, ..., x_n, with probabilities p_1, p_2, ..., p_n normalized to unity. Dividing the interval [0,1] in n subintervals, with limits $y_0 = 0$, $y_1 = p_1$, $y_2 = p_1 + p_2$, ..., and generating a uniform pseudo-random number ξ, the ith y-interval such that

$$y_{i-1} \leq \xi < y_i \qquad (5.6)$$

corresponds to the $X = x_i$ sampled value. In fact, since ξ is uniformly random, the following relation holds:

$$P(x_i) = P(y_{i-1} \leq \xi < y_i) = y_i - y_{i-1} = p_i. \qquad (5.7)$$

In Figure 5.2 a discrete probability distribution p_x with the associated cumulative function $\sum p_x$ is drawn.
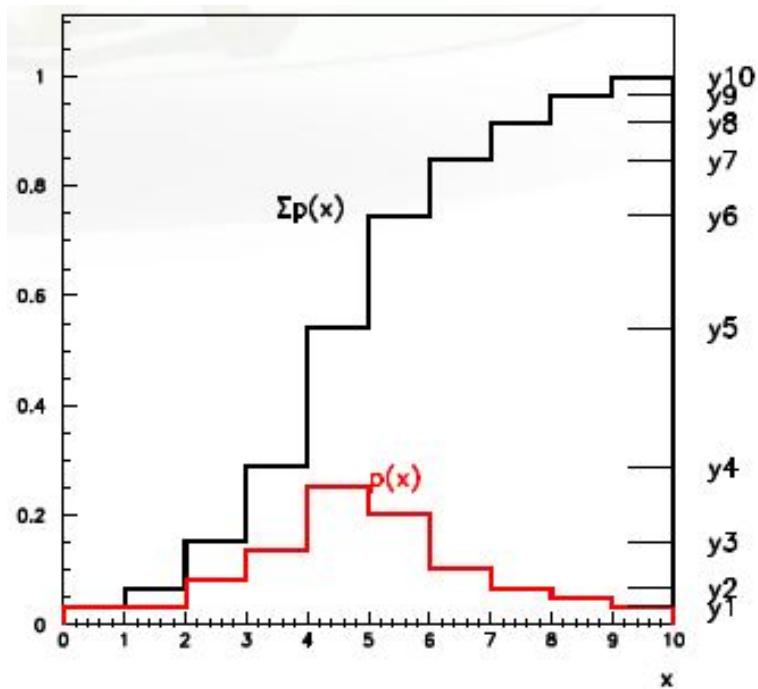
Figure 5.2: Discrete probability distribution p_x with associated cumulative function $\sum p_x$. Courtesy of P. Sala [123].

As MCNPX, FLUKA offers a number of different estimators that can be requested by the user directly from the input file, such as current on a surface, fluence or energy deposition in a region or on a spatial grid. The conversion coefficients from fluence to ambient dose equivalent H*(10) are based on ICRP values and calculations of Pelliccioni [106, 108, 109], and are implemented for different particles including protons, neutrons and photons.

Unlike MCNPX, in FLUKA the time evolution of the system (build-up of unstable radioactive nuclei during irradiation and decay during cooling) is obtained run-time for fixed cooling times during the same simulation. A dedicated database of decay emissions is used, sometimes supplemented with other data and checked for consistency. Using the Bateman Equations, FLUKA analytically calculates the daughter nuclei and the associated decay radiation, according to a user defined irradiation pattern [101].

Once the input file is ready, it is subsequently used to launch the desired simulation. In order to reduce the statistical error, FLUKA can run the same input file many times, varying automatically each time the seed random number used. Each of such runs (a "cycle") produces different output files. The final results for the simulation are obtained by merging the out-

puts from the single cycles. If necessary, variance-reduction techniques are implemented in FLUKA to estimate in the most efficient way the desired response.

5.3   The fission model

As underlined in Section 2.1.3, the process of proton induced fission at the intermediate energies typical of the SPES project, is not yet been theoretically understood. No model exists that can explain the mass dependent and excitation energy dependent transition between symmetric and asymmetric fission. Moreover, the scarcity of experimental data, sometimes decades old, and the different conditions in which the data are collected, make it difficult to compare them with theoretical models [4, 124, 125, 126, 5, 6].

Previous studies assessed the isotope yields by proton induced fission on the ^{238}U nuclei of the UC$_x$ SPES production target, by using both MCNPX and FLUKA Monte Carlo tools [9]. For MCNPX, several physical models for the intra-nuclear cascade and for evaporation-fission were considered, whereas in FLUKA, the Boltzmann master equations computational theory is embedded in the fission model. The FLUKA version used was the FLUKA2011.2x.2 release.

The results of the previous study showed a fairly good agreement (by 20%) between the two Monte Carlo codes on the fission rate value. Moreover, the fission yield spectra calculated with FLUKA at the SPES energies, showed a pronounced 3-peak shape, especially above 50 MeV, not present either in the experimental data reported in [4], or in the MCNPX calculated spectra (see Figure 5.3, on the left).
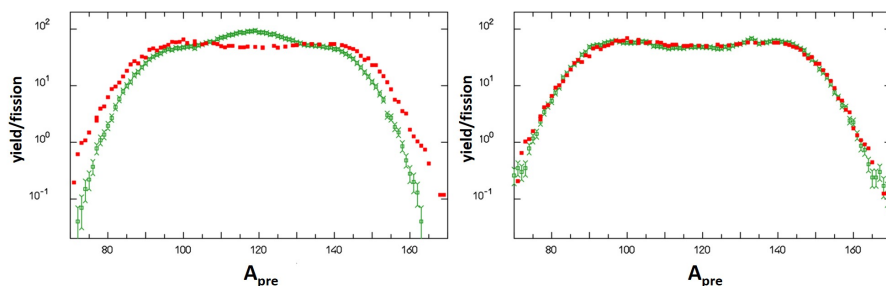
Figure 5.3: Post-fission, pre-neutron emission, fragment distribution for 60 MeV protons on ^{238}U. On the left the old FLUKA2011 version, on the right the new INFN FLUKA2020 release. In green the FLUKA results, in red the experimental data [4]. Courtesy of P. Sala [127].

In the framework of a recent collaboration between the SPES target group and the INFN FLUKA development team, the physical model simulating the fission induced by protons on ^{238}U in the range 20-60 MeV has been modified in order to better match the symmetric versus asymmetric competition and the fragment mass yield shape. The changes of the model have been includes in the FLUKA2020-0 release.

The spectra yields produced in the UC$_x$ target have been then assessed with the new FLUKA2020-0 release. The result, presented in Figure 5.3, evidences a marked improvement of the FLUKA fission model. Further improvements are expected as a result of an ongoing study, in collaboration with the INFN FLUKA team.

It is important to underline that a good knowledge on the composition of the mass spectrum of the fission fragments produced in the target is the prerequisite for the success of the SPES ISOL method; therefore, a reliable Monte Carlo response on the fission fragment distribution is crucial for the SPES project as well as for the ISOLPHARM project described in Section 2.4.

Chapter 6

Proton and neutron induced residual activation of the SPES Front-End system

6.1 Introduction

As explained in Section 3.3, the production method of SPES is based on the ISOL ("Isotope Separation On-Line") technique. A monochromatic proton beam of 40 MeV energy and 200 μA current, produced by a commercial cyclotron, enters in the production bunker along the Primary Proton Beam (PPB) line.

In order to shape the primary proton beam, four graphite collimators are placed along the PPB line to intercept a certain amount of protons in the beam eternal halo, around 15%. Moreover, all the mechanical components of the proton line can be targeted by scattered protons coming from the primary beam.

The primary protons interact with the UC_x segmented target, composed of seven disk of 40 mm diameter and 0.8 mm thickness, by inducing fission on the ^{238}U nuclei, at a rate of about 10^{13} fission/s [7, 9]. Radioactive neutron-rich isotopes produced in the target reach the ion source where they are ionized at the working temperature of about 2000 °C, before to be extracted towards the Radioactive Ion Beam (RIB) line.

Mechanical components of the Front-End system are expected to be irradiated by intense fluxes of primary protons and of neutrons originated by fission in the target. As a consequence, the materials are subjected to the nuclear activation process. In this way, a mixed radiation field composed mainly of protons, neutrons and photons is generated during the irradiation.

The neutron component is the most important secondary radiation for the evaluation of the shields and for the calculations of activation. Generally, a shield suitable for neutrons is able to shield also the other secondary radiation components produced.

The radioactive nuclei generated by nuclear activation decay according to different kinds of physical phenomena, as explained in Section 2.1.1, and many decay channels are associated with the emission of high-energy photons. These photons become therefore a relevant radiation source that is present also after the shutdown of the primary proton beam.

The SPES apparatus is expected to work with operation cycles of 30 days: the first 15 days of continuous proton beam, followed by other 15 days with proton beam switched off. Each cycle is repeated 10 times per year, while longer shutdown periods are foreseen once or twice a year [9].

As underlined in Section 3.3.3, the exhausted TIS (Target and Ion Source) unit is foreseen to be removed from the Front-End system 15 days after each shutdown of the proton beam, and replaced with a new one. Such a cooling time is needed for the activity of the UC_x target disks to decrease to a level allowing the TIS system to be extracted by the bunker. The TIS unit is then placed inside a lead sarcophagus and transported in a temporary storage by a completely automatic system. When the residual activity falls below proper safety levels, TIS disposal and recycling are performed [11, 62, 63].

Inspection and maintenance operations on the main elements of the proton beam line and of the radioactive ion beam line are planned as both ordinary and extraordinary interventions. All the human interventions are foreseen only when the access to the bunker is allowed, that is when the exhausted TIS unit has already been moved from the production bunker to the temporary storage. However, even in this situation, the residual activation of all the other elements of the Front-End needs to be carefully evaluated and all possible strategies to optimize the residual gamma dose to which the worker is exposed have to be implemented: definition of the maximum time of permanence in the bunker, of the minimum distance from the most hazardous elements, simplification of the maintenance procedure, and so on. All the plans have to be in compliance with the Italian legal dose limits and in agreement with the radiation protection recommendations.

The first case study developed in this thesis consists in the assessment of the external exposure of the personnel inside the production bunker in presence of the irradiated Front-End system. A part of the results of this first study [64] will be illustrated later in the present chapter, with a particular focus on the calculation of the gamma ambient dose equivalent rate, this quantity being a good indication of the external exposure in the production

bunker (see Section 5.2.1).

In order to increase the reliability of the results, two codes for Monte Carlo simulations, MCNPX (coupled to the CINDER'90 evolution code) and FLUKA, and two independent calculation procedures are employed in the study. Both codes make it possible to realize an "activation study" simulation to follow the time evolution of the radioactive processes.

The results obtained in the study with the two different codes are compared at each simulation step: calculation of the primary proton beam interactions in the target; simulation of the ^{238}U proton induced fission; generation of proton and neutron fluxes and material activation in some significant geometry components of the Front-End system. The calculation of the gamma ambient dose equivalent rate dH*(10)/dt inside the production bunker is then performed as a consequence of the residual activation generated by proton and neutron interactions on the materials of the Front-End system.

Since during the SPES operation the activation of the Front-End components and the dose in the bunker progressively increase, due to the accumulation of medium-long lifetime radioisotopes, the Front-End system is planned to be extracted from the bunker and to be replaced every seven years. Therefore, the residual activation and the dose rate are assessed at different times during the operation of the facility.

The contribution to dH*(10)/dt, originated by deposition of radionuclides along the RIB line devices contained inside the production bunker (e.g. the Wien Filter), is not accounted for in the study presented in this chapter. Such a contribution depends both on the selection capability of the ion source and on the particular radionuclide production program of the facility. It has been calculated separately and is discussed in detail in Chapter 7.

The procedure followed to perform the present study of the residual activation of the Front-End system, generated by primary proton beam interactions and neutron fields, and of the radiation monitoring inside the production bunker, is based on four main steps:

1. model building of the SPES Front-End system in both Monte Carlo simulation, concerning geometry, materials and primary beam source;

2. development of the calculation method, specific for each of the two codes;

3. definition of the elements of the Front-End selected for the activation analysis and of the times for the assessment of the results;

4. extraction of the results: fission yield in the target; activation of the Front-End materials; assessment of the external exposure due to the Front-End activation.

6.2 Monte Carlo models of the Front-End system

6.2.1 Geometry and media

The first complete Monte Carlo model of the structure of the SPES Front-End apparatus was built with MCNPX, based on the mechanical design of the Front-End [51]. It describes in a good detail the geometry and the materials of the primary beam line structures and of the elements of the radioactive beam line close to the target, which are generally most activated due both to primary protons and to fission neutrons. The model is shown in Figure 6.1.
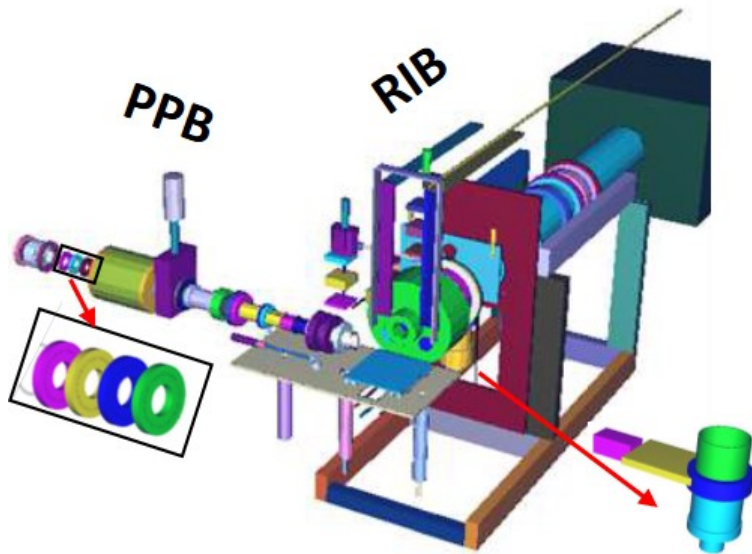
Figure 6.1: MCNPX model of the SPES Front-End ([51]). The collimators on the PPB line and the first turbo-molecular pump on the RIB line are shown on the lower side of the picture; the TIS unit is included in the model but not shown in the figure.

Based on the results of the MCNPX simulations, the mechanical design of the Front-End was then improved modifying some materials and adding shielding structures in the most critical positions, with the aim to optimize the radioactive impact due to the materials activation. The last version of the Front-End mechanical design is illustrated in Figure 6.2.

Figure 6.2: SPES Front-End system layout with indication of the main component structures (see text). The PPB line is on the left side of the picture and the RIB line on the right side, orthogonal to the former one. The last part of the RIB line is not shown in the picture. The TIS unit is located at the crossing of the two beam lines. The design is realized with 3D CAD-Creo Software [128].

It includes, on the PPB line (left side of the picture), different main components: a) the proton beam line with the graphite beam collimators and the collimator shielding structure; b) the beam monitori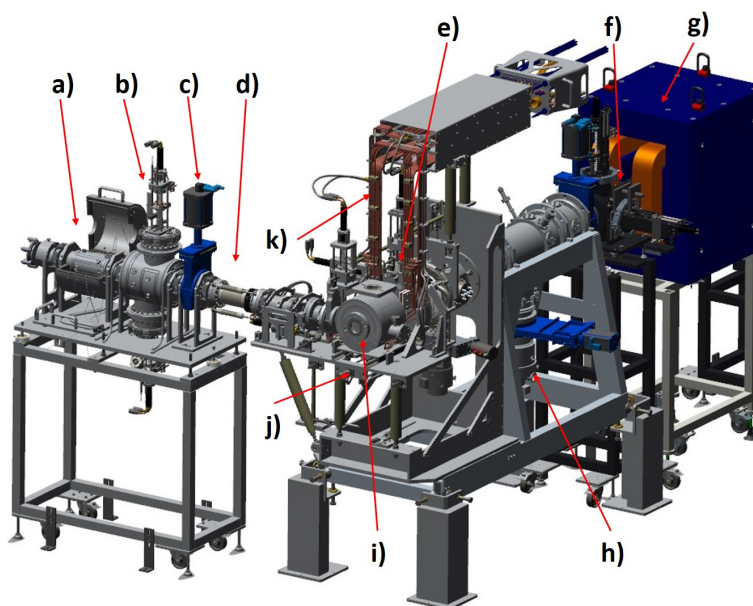ng system; c) the gate valve closing the PPB line, needed to isolate the proton beam line during the extraction of the TIS unit; d) the proton bellow connecting the proton beam line to the TIS unit, and the PPB line supporting structure.

On the first part of the RIB line (right side of the picture) the following elements can be seen: e) the first line segment containing the ion extraction electrode; f) the RIB monitoring system; g) the first mass selector (Wien Filter); h) one of the turbo-molecular vacuum pumps, and the supporting platforms.

The TIS unit is located at the crossing of the PPB and RIB beam lines. Its main components are: i) the target chamber body with the two gate valves, on the PPB line side and on the RIB line side respectively; j) the TIS unit supporting structure with the automatic sliding system; k) the current supply system for target heating.

85

The MCNPX geometrical model of the Front-End, shown in Figure 6.1, constituted the reference design for the study of the residual activation. It includes many radiation-sensitive components, for example the collimator system on the PPB line and all the elements downstream of the collimators, which can intercept the proton beam; all the steel components with mass larger than 100 g, as the vacuum pumps; the most massive Front-End system structures in aluminum and copper (cables) and the main elements on the first part of the RIB line. Due to their position on the PPB line or on the RIB line in proximity of the production target, these components represent the most critical elements for the proton beam and neutron activation.

A second model of the Front-End system was implemented using the FLUKA simulation code, by accurately checking the correspondence between the geometrical description and the component materials of the two models. With these MCNPX and FLUKA geometrical models, all the studies of residual activation of the Front-End system are performed.

More recently, the FLUKA geometry of the RIB line has been further improved and completed taking into account also the elements where the principal contribution to the Front-End activation is due to radionuclide deposition (see Chapter 7).

The layout of the RIB line of the Front-End system, and the corresponding portion of the FLUKA model, are shown in Figure 6.3. The main elements, downstream of the target and ion source system, are highlighted: a) the first triplet; b) the first series of diagnostic boxes; c) the Wien Filter mass selector, with the copper coils evidenced in orange; d) the steerers; e) the second series of diagnostic boxes; f) the second triplet; g), h) and i) the turbo-molecular vacuum pumps, and the supporting platforms.

The extension of the model to the devices actually present on the RIB line of the Front-End system has been necessary to complete the study. In fact, even if to a lesser extent than others components of the Front-End system close to the target, all the added elements undergo activation by neutron fields generated in the target during the proton irradiation. Therefore, they also contribute to the residual activation along all the RIB line and to the consequent dose rate in the surrounding areas.

6.2.2 The primary proton beam

The properties of the proton beam delivered by the SPES cyclotron were studied with particular attention within the SPES target group [9, 55]. Beam particles impinging on a material release their kinetic energy that turns into internal power generation. When this phenomenon occurs on the target,
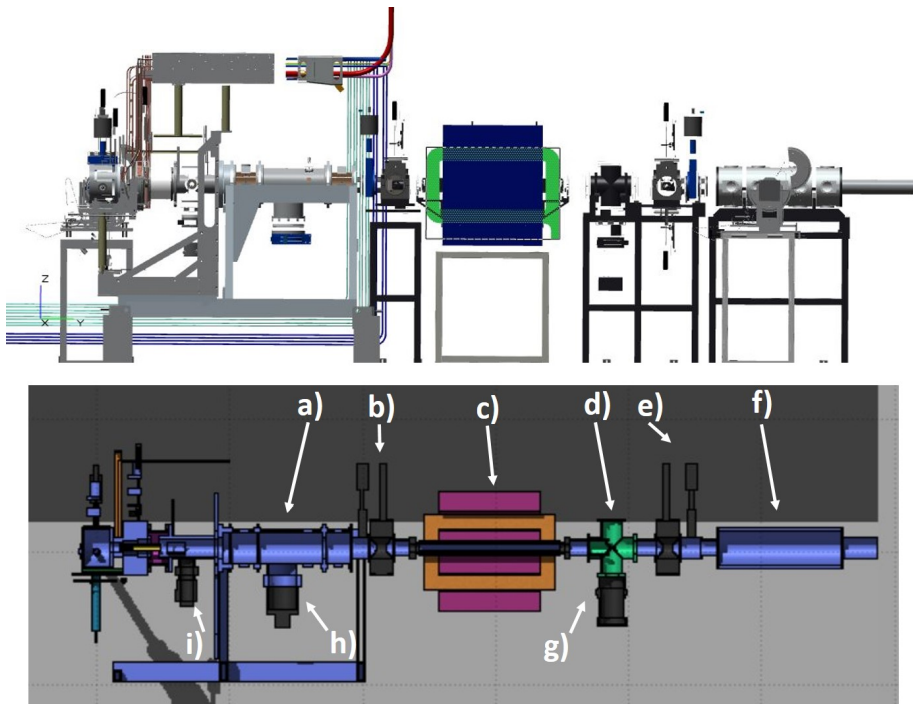
Figure 6.3: Top panel: 3D CAD-Creo layout of the RIB line of the SPES Front-End system. Bottom panel: the corresponding portion of the FLUKA model, with the indication of the principal components (see text for a detailed description).

thermal stresses could in principle cause the rupture of the disks and the consequent stop of the operations.

To spread in the most safe way the proton beam power on the target disk surfaces, a device that allows the beam to be rotated around the target disk axis, the "wobbler", is foreseen. Figure 6.4 shows two different beam profiles in the first disk of the SPES target, corresponding to the same amount of power dispersed out of the target due to the Gaussian tails. Without wobbling treatment, the power peak in the center of the disk is approximately 50% higher that at its edge. Conversely, by moving the beam, the power density is almost uniformly distributed on the disk surface. Moreover, a smaller proton beam spot focused on the disk edge allows for a lower average temperature of the disks, so reducing the thermal stress.

Furthermore, to minimize the power beam losses along the PPB line, it is essential to decrease as much as possible the sweeping radius imposed by the wobbler device. In fact, a high percentage of beam impacting on the devices along the PPB line, especially the collimators, increases the activation levels and the radiation doses.
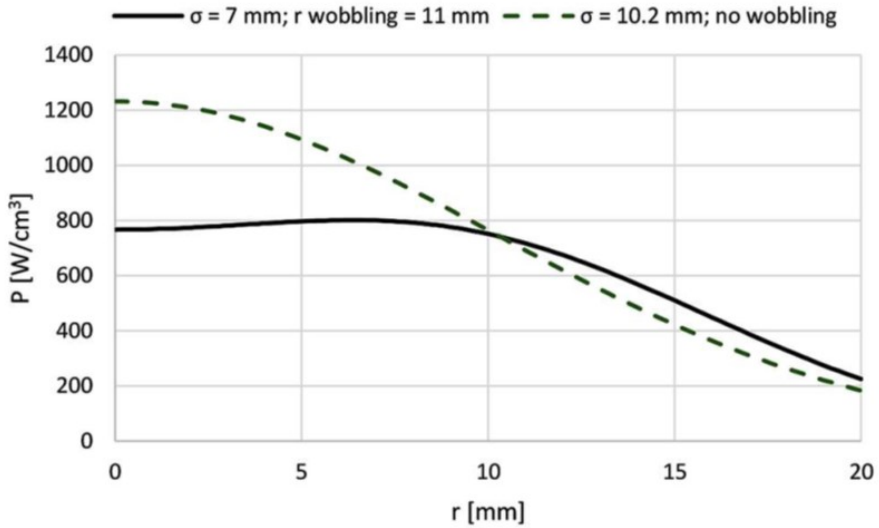
Figure 6.4: Power density in the first disk of the SPES target with and without wobbling, as a function of the distance from the center of the disk.

The shape of the proton beam is defined as a wobbled Gaussian around the target disk axis, with beam size standard deviation of 7 mm and a wobbler sweeping radius of 11 mm on the target. In this way, the beam power loss on the collimators is about 15%.

The SPES proton beam profile has been simulated with both MCNPX and FLUKA, in different ways. In MCNPX, dedicate cards are implemented to simulate a charged-particle beam produced by an accelerator, without field transport but applying the emittance factors of the beam shaped by a focusing system [99]. Eight equally probable beams have been modeled with the same Gaussian profile and with different radial positions and directions in respect to the RIB axis, according to the wobbler sweeping radius. In this way, a sort of dynamic continuous rotating beam is simulated. The model is described in Figure 6.5.

In FLUKA, an external beam source has been created, where the parameters describing the beam shape, the position and the direction on a mid-beam vertical cross-section are initialized and used in generation. Since the value of each Monte Carlo estimator is averaged on the cell where it is requested, the FLUKA generation model can be used to provide answers on physical interactions within the target, thanks to its circular symmetry.

For the study of the proton and neutron induced residual activation of the SPES Front-End system, to make easier the comparison of the results of
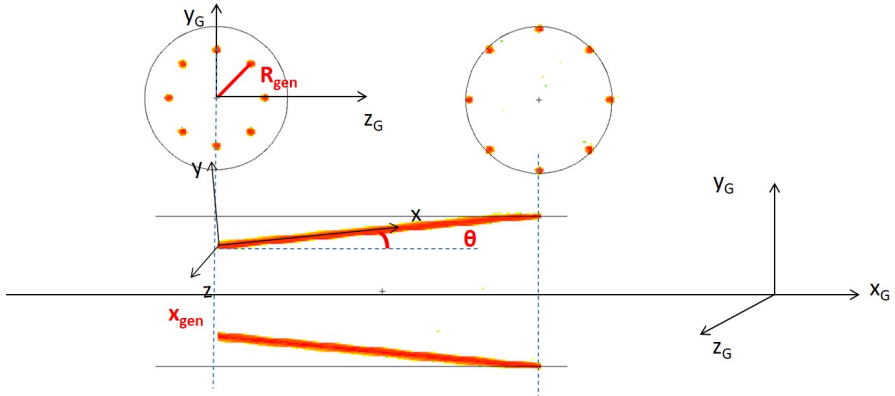
Figure 6.5: MCNPCX plot of the wobbling beam, modeled as eight equally probable Gaussian beams. The values are not in scale and have the purpose to illustrate the axial and transverse profiles of the beams. The coordinate x_G is oriented along the beam axis, the left circle corresponds at the x-coordinate of the beams at the source generation, the right circle corresponds at the x-coordinate on the target.
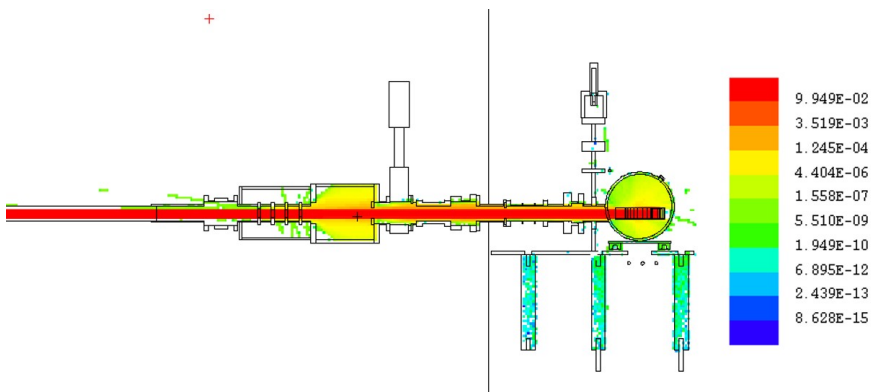
Figure 6.6: Proton flux mesh for source particle, calculated with MCNPX along the PPB line of the Front-End system, on a mid beam vertical cross-section. Units of the color scale are normalized by primary source particle.

the two Monte Carlo models, a simple proton beam profile with a flat circular distribution with radius of 18.2 mm, has been modeled with both MCNPX and FLUKA codes. This flat proton profile reproduces the same total beam loss on the collimators (about 15%) that occurs using the realistic model of the beam profile, divergence and rotation. Figure 6.6 shows a mid-beam vertical cross-section of the proton flux along the PPB line, calculated with MCNPX.

6.3   The calculation methods

As underlined in Section 5.2, the method used to calculate the activation of an irradiated material is different in the two simulation codes. In the case of MCNPX, it requires the combined use of a nuclide evolution code as CINDER'90.

6.3.1   MCNPX combined with CINDER'90

To perform the calculation of the SPES Front-End residual activation, MCNPX has been coupled with CINDER'90, an evolution code that utilizes Markovian chain structures to determine temporal densities of nuclides in a complex radiation environment, like the production bunker of SPES. The activation is assessed independently for each single nuclide in all the activated materials of the geometrical set-up.

The calculation procedure is achieved in four computational steps. At the first step, the Front-End MCNPX model is used to evaluate the interactions of the proton beam source with the materials of the PPB line and with the target. The fission induced on ^{238}U nuclei in the target produces fission fragments and neutrons. While the neutrons are free to move towards the surrounding materials, all the fragments are supposed to be retained in the TIS unit. Actually, a part of the fragments will be extracted from the ion source to form the RIB beam. The possible contamination of the RIB line due to radioactive ion deposition has to be calculated separately and is the topic of the next chapter.

MCNPX is asked to calculate the neutron and photon fluxes in all the cells of the simulated geometry of the Front-End. The neutron fluxes are calculated by library data up to 25 MeV and forwarded to CINDER'90, that evaluates the isotope production. CINDER'90 makes use of a self contained activation data library including about 3400 nuclides, with 63 energy-groups from thermal up to 25 MeV neutron energy. It is referred to as the LaBauve energy group structure [129]. Conversely, for neutrons

having energies greater than 25 MeV and for protons of all energies, the isotope production is directly estimated by MCNPX using physical models, and is forwarded to CINDER'90.

At the second step, CINDER'90 reads most of the MCNPX output information like cell geometry, material composition and low energy neutron fluxes. Then, it performs a full activation calculation in the whole energy range, from the MCNPX physics model region down to the table data region. To avoid systematic errors due to a mismatch of the energy binning between CINDER'90 neutron activation cross sections and MCNPX neutron fluxes, the neutron fluxes have to be distributed in LaBauve multi-group energy structure.

Neutron and proton induced activities are calculated on single isotopes for every cell of the designed geometry, excluding the cells constituting the TIS unit. A extensive output is produced for every cell, containing a complete information on the activity estimators of the cell at each time instant of a previously defined set of decay time intervals.

At the third step, CINDER'90 produces a 25 energy-group gamma decay spectrum for all isotopes contained in the cells where activation has been calculated. The step is performed separately for each sampled time instant. Each gamma spectrum associated to a specific decay time instant can then be used as a photon source to input in a new MCNPX run.

At the fourth step, the proton beam source used in the original MCNPX model at the first step is replaced with the new sampled photon source. The photon sampling in each cell is uniformly distributed in the specified volume. In order to simulate the TIS unit removal from the Front-End system, which is a mandatory condition for maintenance operations in the production bunker to take place, in the present step the materials of the cells constituting the TIS unit are converted into air.

Radiation monitoring is then performed throughout the production bunker, at different time instants with the corresponding sampled photon source, by calculating the rate of ambient dose equivalent dH*(10)/dt. The energy dependent photon fluences are calculated in specific positions in space and then converted in dH*(10)/dt, using the fluence-to-dose conversion coefficients [106, 107, 108, 109].

A scheme of the calculation flow described above, adapted from [100] for the SPES Front-End activation study, is presented in Figure 6.7.
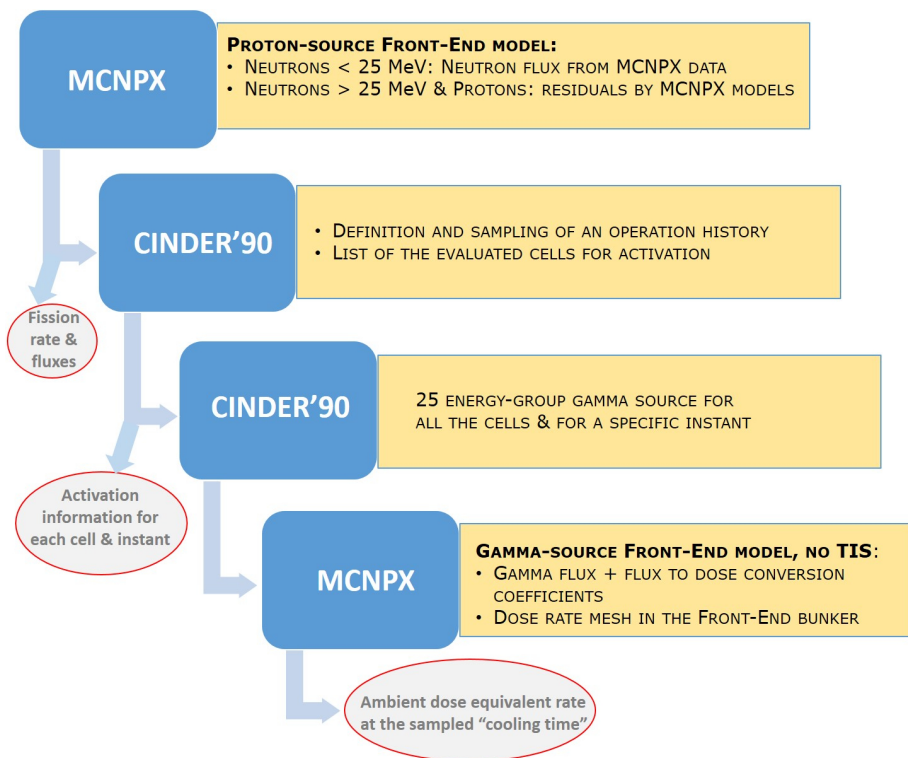
Figure 6.7: The MCNPX-CINDER'90 flow chart used for SPES calculations.

6.3.2 FLUKA

In FLUKA, both the production of unstable residual nuclei and the time evolution and tracking of the emitted radiation are performed in the same run. Implementing an "activation study case", the code is able to generate single radioactive nuclei in all the modeled materials and follow their time evolution, by analytically calculating the daughter nuclei and the associated decay radiation, according to a user defined proton irradiation profile. Irradiation profile means the definition of the number of irradiation time intervals and of the corresponding beam intensities. Implementing the FLUKA "activation study case", all quantities of interest are estimated at fixed sampling times chosen by the user. As in MCNPX, the conversion between energy dependent photon fluence and $dH^*(10)/dt$ is performed using the fluence-to-dose conversion coefficients [106, 107, 108, 109].

FLUKA allows the material of a specific geometry cell to be changed when transporting the decay radiation. In the present study, the materials of the TIS unit are selectively changed to air, to simulate the TIS unit removal from the Front-End system.

Since the whole simulation is performed in one single run, a very high number of histories is requested to reach a statistical precision comparable to that obtained by the MCNPX/CINDER'90 multistep procedure. Therefore, these simulations need cloud-based powerful computing resources, in order to maintain acceptable computing times without compromise the reliability of the results.

Indeed, the results of this study have been obtained thanks to Cloud-Veneto, a project that involves the INFN "Cloud Area Padovana", INFN-LNL and ten departments of the University of Padua [130]. CloudVeneto provides an advanced IT Platform to run in parallel codes for Monte Carlo simulation (as FLUKA and Geant4). However, differently from Geant4, the native FLUKA code doesn't provide the capability of parallel computing through to the multi-threading option. Therefore, the parallel option for FLUKA consists in simultaneously running the simulation on many cycles, repeated a user-defined amount of times. By previously forcing the assignment of different random seed numbers for each cycle, it is possible to run simultaneously all cycles in different threads. The platform is fault tolerant and automatically tries to satisfy the required parallelism degree without outage. The computation was run in parallel on 64 FLUKA instances, allocating one CPU and 2 GB of RAM to each one. With these resources, a statistical precision lower than 5% on all results was obtained in about one month of continuous run.

It must be emphasized that, although sometimes the running time factor can work against the use of FLUKA, the possibility to realize a single step simulation certainly represents one of the strong points of the FLUKA procedure, both in general and in the particular context of the SPES project. Such a procedure can, in fact, be preferred for its greater simplicity, and can be effectively used when the computing times to estimate in the most efficient way the desired response are practically affordable. This may be true when, in general, simple geometries are involved in the problem, or when most of the initial histories contribute to the desired response in the regions of interest.

Anyway, the use of FLUKA in the present study on the Front-End residual activation is highly motivated. Indeed, the comparison between MCNPX and FLUKA codes has also the purpose of testing their reliability, which is an indispensable requirement to be used successfully in this types of studies.

For example, the FLUKA code has been effectively used to design the temporary storage to house the exhausted TIS units coming from the Front-End. To characterize the photon sources emitted from the SPES target at different cooling times, specific "activation study case" simulations have

been performed with FLUKA, as explained in Chapter 8.

6.4   Selection of Front-End elements and scoring times

Although almost all structures of the Front-End system undergo activation by proton and neutron fields, only few significant geometry cells have been selected for a detailed analysis.

The most critical Front-End components along the PPB line are the four graphite beam collimators, where the remarkable residual activation produced is mainly due to the direct interactions of the proton beam impinging on the target; they are supposed to stop a fraction of 15% of the proton beam (see Section 6.2.2). To shield the resulting intense gamma radiation field, the collimators are surrounded by a lead shield 1 cm thick. Other critical elements located along the PPB line, downstream of the collimators, are the proton bellow made of a titanium-alloy and the steel and aluminum structures supporting the beam line. Being closer to the TIS unit, the activation of the latter elements is mainly due to neutron interaction.

Along the RIB line, where activation is mainly determined by neutron interactions, the most critical elements close to the TIS unit are the two turbo-molecular vacuum pumps: the one closer to the TIS unit is entirely made of steel, whereas the farther one is made of both steel and aluminum. The material composition is closely related to neutron activation; for example, steel is much more critical than aluminum at the times from irradiation foreseen for the maintenance operations.

The aim of the work on the Front-End residual activation is also to compare the results of the two codes on both interacting particles (namely protons and neutrons), at different energies, considering materials of different atomic composition and evaluating their activation at different time intervals after the irradiation. Furthermore, attention is paid on those parts of the Front-End system where specific ordinary maintenance operations are foreseen. For example in the neighborhood of the collimators, the turbo-molecular vacuum pumps, the pneumatic motors and, in general, near all the moving mechanical devices, like the gate valves and the proton bellow.

Figure 6.8 illustrates the MCNPX model of Figure 6.1 with evidenced, through red squares, the selected cells for a detailed study inside the Front-End system: 1) the graphite beam collimator closest to the TIS Unit; 2) a steel component of the PPB line gate valve; 3) the titanium bellow on the PPB line; 4) an aluminum structural element supporting the PPB line chan-

Table 6.1: Atomic compositions and densities of the materials composing the reference geometry cells. When not otherwise specified, the materials natural composition is considered.

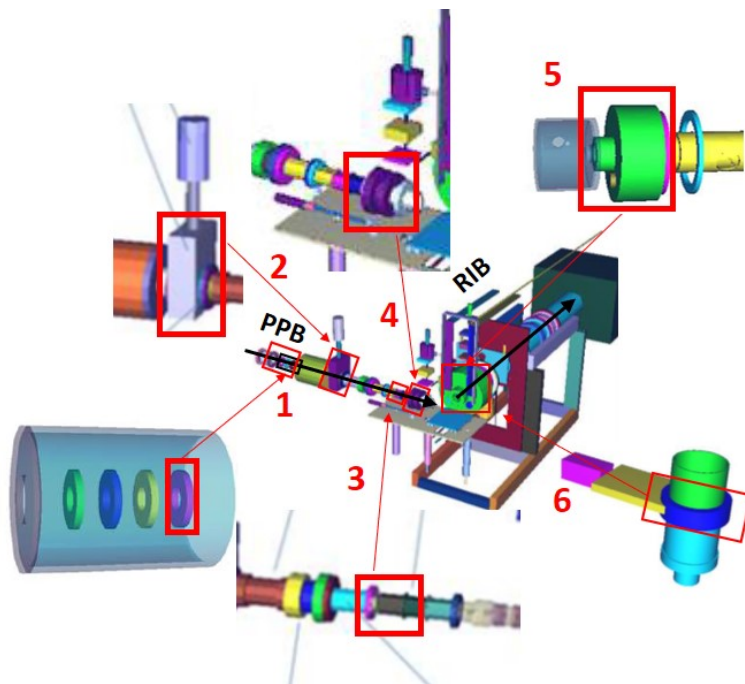| cell	description	material	weight %	density (g/cm^2)
1	collimator	graphite	^{12}C 99% ^{13}C 1%	1.76
2,6	gate valve pump	SS316L	Fe 66.137% Cr 17.250% Ni 12.000% Mo 2.500% C 0.030% Mn 1.410% Si 0.630% P 0.031% S 0.012%	8.00
3	P-bellow	Ti alloy	Al 6.000% V 4.000% C 0.080% Fe 0.300% O 0.200% N 0.700% Ti 89.350%	4.43
4,5	support cells	Al alloy	Mn 0.700% Fe 0.250% Mg 0.900% Si 1.000% Cu 0.050% Zn 0.100% Ti 0.050% Cr 0.125% Al 96.825%	2.70

Figure 6.8: MCNPX model of the SPES Front-End ([51]) with the six reference geometry cells where residual activation is evaluated: 1) the last collimator; 2) a steel element of the gate valve; 3) the proton bellow; 4), 5) aluminum components of the supporting structures; 6) a steel piece of a turbo-molecular pump.

nel and 5) another one supporting the RIB line channel; 6) a steel component of the first turbo-molecular vacuum pump. Table 6.1 shows the percentage weight compositions and the densities of the selected geometry cells.

Since the residual activation of the Front-End system structures is strongly dependent on the time elapsed from irradiation, the relevant quantities in the selected geometry cells have been sampled at different times during the foreseen operation phase of the facility.

The first time instant considered is the shutdown of the beam occurring after the very first 15 days of proton irradiation (t_0). At this moment the total number of protons incident on the target is of the order of 10^{21} and the total activity produced in the target is of the order of $4 \cdot 10^{13}$ Bq.

The second time considered is at the end of the first 15 day cooling time period and at the start of the second irradiation cycle, after the removal of the TIS unit from the Front-End system (t_1). Finally, the third time sampled is 15 days after the end of the 10th irradiation cycle: (t_{10}). Time t_{10} corresponds to a typical time scheduled for ordinary and extraor-

dinary maintenance operations inside the bunker. Therefore, at time t_{10}, the gamma ambient dose equivalent rate dH*(10)/dt is evaluated with both FLUKA and MCNPX.

6.5 The calculation results

A detailed description of the results on the residual activation of the SPES Front-End system, obtained with both MCNPX and FLUKA in the same source conditions and with the same geometrical Front-End model, is given in the present section.

One of the aims of the present work is to compare the performance of the codes on activation calculations in the SPES energy range, to provide useful inputs for the developers of the two programs. As a conclusion of the study, the global results achieved with the two codes are in a good agreement, of the order of 20-40% on average, with more important differences on some specific results. In general, the results obtained with FLUKA appear to overestimate those obtained with MCNPX, both on the activation and on the dose rate.

In the context of this thesis, greater emphasis is placed on the study of the material activation and of the dose rate inside the production bunker. The results of the study, together with the calculation of the residual activation generated by radionuclide deposition along the RIB line elements, discussed in the next chapter, are particularly relevant for planning of inspection and maintenance operations foreseen on the SPES Front-End. Furthermore, the developed computing methodology could confidently be used for the prediction of expected and unexpected exposures in different phases of the life cycle of the facility, until the final decommissioning.

6.5.1 Fission rate in the target

The starting point of all the following evaluations is the assessment of the isotope production in the SPES target. As underlined in Section 5.3, the performance of the final design of the multi-foil UC_x SPES production target was assessed in [9] for both MCNPX and FLUKA, in terms of number of fissions per second and isotope yields of the ^{238}U proton induced fission. The agreement on the fission rate value resulted about 20%.

In the present work, the same beam conditions and the same geometrical design of the target as in [9] are used. However, employing later versions of the two computational tools, a better agreement in the prediction of the total fission rate, of the order of few percent, is obtained. Moreover, recent calcu-

lations of the fission rate in the target, performed with the FLUKA2020-0 release (see Section 5.3), show a good agreement with MCNPX also on the behavior of the fission yields with the mass number, as shown in Figure 6.9.
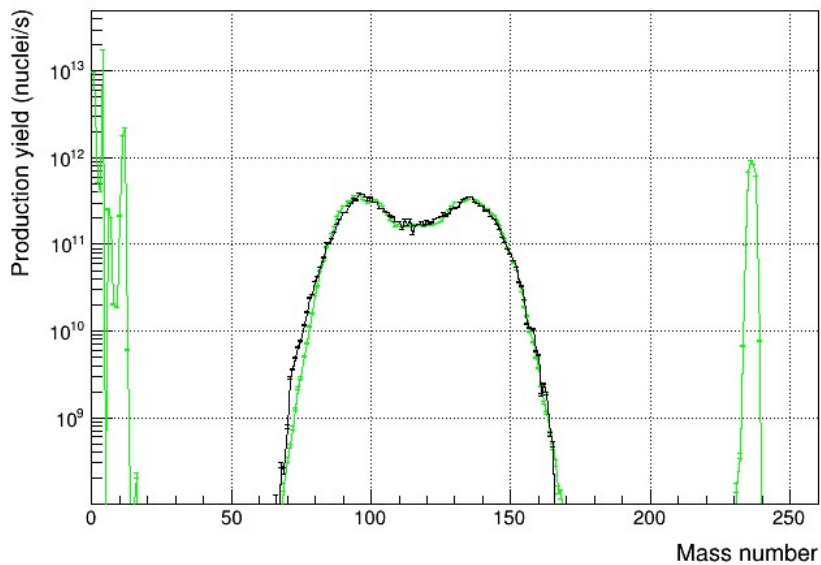
Figure 6.9: ^{238}U proton induced fission rate by mass number in the SPES UC_x production target, calculated with MCNPX (black line) and FLUKA2020-0 (green line). The FLUKA distribution shows also the contributions from fragmentation reactions induced by primary protons on carbon nuclei, at low masses, and spallation reactions induced by primary protons on ^{238}U nuclei, at high masses.

The total fission rate calculated with FLUKA2020-0 has not significantly changed, if compared with the result obtained with the previous FLUKA release. Therefore, also the flux of fission neutrons emitted by the target and their energy, that is characteristic of the fission process, should not be influenced by the changes in the fission model implemented in the last FLUKA2020-0 release. For these reason, all the results on the physical processes downstream of the fission in the target, obtained with the previous FLUKA release, should be compatible with the new results obtained for the same processes using the FLUKA2020-0 release (see discussion in Section 6.5.3).

6.5.2 Induced activation

The activation process consists in the secondary induction of radioactivity in materials due to nucleon capture by atomic nuclei (see Section 2.1.2). The nuclei increase their mass moving to compound nuclei, which de-excite through the emission of photons, nucleons, or light nuclei as α particles. The process generally results in the formation of an unstable isotope.

Charged particles can induce activation only if their kinetic energy exceeds the Coulomb barrier (a few MeV). This is the case of the SPES primary proton beam, which therefore is able to induce activation on the elements of the PPB line, mostly the collimators. On the contrary, neutrons are not affected by the Coulomb barrier of nuclei, and can thus react at any energy and produce radioactive nuclides. While for thermal neutrons the dominant process is the capture, increasing the neutron energy other nuclear reactions can occur. High-energy neutrons cause spallation reactions that can produce any nuclide lighter than the target nucleus. Electromagnetic particles may also cause activation through photonuclear interactions, although with a much lower cross-section. Thus, activation by electrons and photons is typically not a concern in facilities like SPES.

The particles produced by decay of activated nuclei interact with matter releasing part or all their energy inside of a medium, as the human body. As explained in Section 4.2.2, this fact is of particular concern for the radiological protection. Moreover, if the medium is a electronic device or a radiation sensitive material, the device can be damaged or reduce its performance. In the case of the SPES project, dedicate studies were performed to estimate the degree of modification of the physical and mechanical properties of polymeric materials and of other materials under mixed photon and neutron fields. This topic is very important because these materials are crucial for the operation of the facility [62, 131, 132].

The activation of the SPES Front-End is generated by proton and neutron interactions with the Front-End materials. It has been calculated with both MCNPX and FLUKA, for the six reference geometry cells of Table 6.1, at the two different times t_0 and t_1. At time t_0 the results are representative for the radioactive isotopes with shortest half-life. At time t_1 the contribution to the activity of the medium/long half-life nuclides, surviving after 15 day cooling time, as well as all daughter nuclides originated by secondary nuclear decays, are accounted for.

Values of the activity for the most important radioactive isotopes are calculated with the two Monte Carlo codes at the different times. They are reported in the following tables, for the most significant geometry cells

Table 6.2: Values of the activity for the most important radioactive isotopes generated in the geometry cell 1), the last graphite collimator, at the two times t_0 (upper panel) and t_1 (lower panel). The total activity of the cell is reported too. R is the ratio between the FLUKA and MCNPX results; Monte Carlo errors on R are not larger than few percent.

nuclide	half-life	FLUKA (Bq)	MCNPX (Bq)	R
time t_0				
^{7}Be	53 d	$9.6 \cdot 10^9 \pm 0.09\%$	$7.0 \cdot 10^9$	1.4
^{11}C	20 min	$3.0 \cdot 10^{11} \pm 0.04\%$	$1.4 \cdot 10^{11}$	2.1
total		$3.4 \cdot 10^{11} \pm 0.04\%$	$1.7 \cdot 10^{11}$	2.0
time t_1				
^{7}Be	53 d	$7.9 \cdot 10^9 \pm 0.09\%$	$5.7 \cdot 10^9$	1.4
total		$7.9 \cdot 10^9 \pm 0.09\%$	$5.7 \cdot 10^9$	1.4

among those analyzed: geometry cell 1), the last graphite collimator of the PPB line; geometry cell 2), a steel component of the gate valve located on the PPB line; geometry cell 5), an aluminum component of the RIB line support; geometry cell 6), a steel turbo-molecular vacuum pump located on the RIB line.

Statistical Monte Carlo errors on the activity values reported in the tables are indicated only on the FLUKA results, obtained with single step calculations. For MCNPX, the activity is analytically evaluated by CINDER'90 in the second step of the calculation procedure described in Section 6.3.1. Therefore, the statistical errors on the activity values are assumed to be of the same order of magnitude as the ones on the proton and neutron fluxes, calculated in the first step of the calculation procedure (that are not larger of few percent [64]).

In Table 6.2, the calculated activation of the geometry cell 1) is shown. Since a significant percentage of the primary proton beam is stopped in the

collimators, the resulting total activation is very high, of the order of 10^{11} Bq at time t_0 and a few 10^9 Bq at time t_1. The most significant short half-life isotope is ^{11}C, whereas the only significant isotope at time t_1 is ^{7}Be. This is the reason why a lead shield must surround the graphite collimator system. The agreement between the FLUKA and MCNPX predictions on the total activity is by a factor 2 for both the times.

The activation values reported in Table 6.3 for geometry cell 2), and in Table 6.4 for geometry cell 6), are quite high both at time t_0 and at time t_1, due to the presence of medium half-life isotopes, as ^{51}Cr and ^{58}Co, and of medium-long half-life isotopes, as ^{54}Mn, ^{55}Fe and ^{57}Co. At time t_1 the total values are still of the order of 10^8 Bq or more.

Apart from some isotope, an excellent agreement (around 10%) is obtained between the FLUKA and MCNPX predictions for the total activity. The nuclides for which a larger difference is found between the two codes are ^{52}V and ^{57}Co. The first isotope is present at time t_0 in geometry cell 2), but not in geometry cell 6). Therefore, it is not generated by neutron interactions but rather by primary proton beam interactions on elements present in the steel composition. Instead, for cell 6), that is close to the target, the contribution to the activation is mainly due to fission neutrons.

Geometry cells 4) and 5) are aluminum components of the PPB and RIB line support, respectively. In the former, activation is generated both by direct interactions of the primary proton beam and by neutron interactions, whereas in the latter activation is due mainly to interactions of neutrons generated by fissions in the target.

The total activity of both the geometry cells is rather significant at time t_0: $7.6 \cdot 10^{10} \pm 0.04\%$ is the FLUKA result for the cell 5), which is the closest to the target. This high activity value, reported in Table 6.5, is mainly due to short half-life isotopes: ^{24}Na, ^{27}Mg, ^{28}Al and ^{56}Mn. However, due to the short half-life of most aluminum isotopes, the total activity of both cells decreases rapidly with the cooling time, of about a factor 10^3 from t_0 to t_1. Therefore, at time t_1 scheduled for maintenance operation, activation of these aluminum geometry cells is less critical than that of the graphite collimators and of the steel components.

Concerning cell 3), the titanium-alloy proton bellow located on the PPB line, the total activity is due mainly to neutron interactions and its value at time t_1 is of the order of 10^7 Bq for both the codes [64].

Table 6.3: Same as Table 6.2, for the geometry cell 2), a steel component of the gate valve of the PPB line.

nuclide	half-life	FLUKA (Bq)	MCNPX (Bq)	R
time t0				
^{52}V	3.7 min	$1.7 \cdot 10^8 \pm 1\%$	$6.8 \cdot 10^7$	2.5
^{51}Cr	28 d	$5.3 \cdot 10^8 \pm 0.2\%$	$5.4 \cdot 10^8$	1.0
^{54}Mn	310 d	$1.9 \cdot 10^7 \pm 0.5\%$	$1.6 \cdot 10^7$	1.2
^{56}Mn	2.5 h	$3.0 \cdot 10^9 \pm 0.2\%$	$3.0 \cdot 10^9$	1.0
^{55}Fe	2.7 y	$2.9 \cdot 10^7 \pm 0.3\%$	$2.1 \cdot 10^7$	1.3
^{57}Co	272 d	$1.3 \cdot 10^7 \pm 0.8\%$	$6.4 \cdot 10^6$	2.0
^{58}Co	71 d	$1.7 \cdot 10^8 \pm 0.4\%$	$1.1 \cdot 10^8$	1.6
^{99}Mo	2.7 d	$1.0 \cdot 10^8 \pm 0.6\%$	$1.3 \cdot 10^8$	0.77
total		$5.1 \cdot 10^9 \pm 0.2\%$	$4.7 \cdot 10^9$	1.1
time t1				
^{51}Cr	28 d	$3.6 \cdot 10^8 \pm 0.2\%$	$3.7 \cdot 10^8$	1.0
^{54}Mn	310 d	$1.8 \cdot 10^7 \pm 0.5\%$	$1.6 \cdot 10^7$	1.2
^{55}Fe	2.7 y	$2.8 \cdot 10^7 \pm 0.3\%$	$2.1 \cdot 10^7$	1.3
^{57}Co	272 d	$1.2 \cdot 10^7 \pm 0.8\%$	$6.2 \cdot 10^6$	2.0
^{58}Co	71 d	$1.5 \cdot 10^8 \pm 0.4\%$	$9.5 \cdot 10^7$	1.6
total		$5.8 \cdot 10^8 \pm 0.2\%$	$5.2 \cdot 10^8$	1.1

Table 6.4: Same as Table 6.2, for the geometry cell 6), a steel component of the turbo-molecular vacuum pump.

nuclide	half-life	FLUKA (Bq)	MCNPX (Bq)	R
time t0				
^{51}Cr	28 d	$1.1 \cdot 10^8 \pm 0.5\%$	$1.2 \cdot 10^8$	0.94
^{54}Mn	310 d	$1.1 \cdot 10^6 \pm 2\%$	$1.1 \cdot 10^6$	1.0
^{56}Mn	2.5 h	$6.0 \cdot 10^8 \pm 0.4\%$	$6.2 \cdot 10^8$	0.97
^{55}Fe	2.7 y	$3.1 \cdot 10^6 \pm 0.3\%$	$3.0 \cdot 10^6$	1.0
^{57}Co	272 d	$2.6 \cdot 10^5 \pm 5\%$	$1.7 \cdot 10^5$	1.6
^{58}Co	71 d	$1.2 \cdot 10^7 \pm 0.9\%$	$1.0 \cdot 10^7$	1.2
^{99}Mo	2.7 d	$2.0 \cdot 10^7 \pm 1\%$	$2.7 \cdot 10^7$	0.74
total		$8.5 \cdot 10^8 \pm 0.4\%$	$9.0 \cdot 10^8$	0.94
time t1				
^{51}Cr	28 d	$7.6 \cdot 10^7 \pm 0.5\%$	$8.1 \cdot 10^7$	0.94
^{54}Mn	310 d	$1.1 \cdot 10^6 \pm 2\%$	$1.1 \cdot 10^6$	1.0
^{55}Fe	2.7 y	$3.0 \cdot 10^6 \pm 0.3\%$	$3.0 \cdot 10^6$	1.0
^{57}Co	272 d	$2.6 \cdot 10^5 \pm 5\%$	$1.6 \cdot 10^5$	1.6
^{58}Co	71 d	$1.0 \cdot 10^7 \pm 0.9\%$	$9.1 \cdot 10^6$	1.1
total		$9.3 \cdot 10^7 \pm 0.4\%$	$9.7 \cdot 10^7$	0.96

Table 6.5: Same as Table 6.2, for the geometry cell 5), an aluminum component of the supporting structure of the RIB line.

nuclide	half-life	FLUKA (Bq)	MCNPX (Bq)	R
time t0				
^{24}Na	15 h	$1.0 \cdot 10^{10} \pm 0.1\%$	$8.4 \cdot 10^9$	1.2
^{27}Mg	9.5 min	$2.3 \cdot 10^{10} \pm 0.1\%$	$1.9 \cdot 10^{10}$	1.2
^{28}Al	2.2 min	$2.6 \cdot 10^{10} \pm 0.03\%$	$2.8 \cdot 10^{10}$	0.93
^{51}Cr	28 d	$3.0 \cdot 10^7 \pm 0.8\%$	$1.7 \cdot 10^7$	1.8
^{54}Mn	310 d	$9.8 \cdot 10^6 \pm 0.6\%$	$5.7 \cdot 10^6$	1.7
^{56}Mn	2.5 h	$9.4 \cdot 10^9 \pm 0.1\%$	$5.1 \cdot 10^9$	1.8
^{55}Fe	2.7 y	$9.1 \cdot 10^5 \pm 1.0\%$	$3.7 \cdot 10^5$	2.5
^{65}Zn	244 d	$5.3 \cdot 10^6 \pm 0.4\%$	$2.8 \cdot 10^6$	1.9
total		$7.6 \cdot 10^{10} \pm 0.04\%$	$6.3 \cdot 10^{10}$	1.2
time t1				
^{51}Cr	28 d	$2.1 \cdot 10^7 \pm 0.8\%$	$1.2 \cdot 10^7$	1.8
^{54}Mn	310 d	$9.5 \cdot 10^6 \pm 0.6\%$	$5.5 \cdot 10^6$	1.7
^{55}Fe	2.7 y	$9.0 \cdot 10^5 \pm 0.9\%$	$3.6 \cdot 10^5$	2.5
^{65}Zn	244 d	$5.1 \cdot 10^6 \pm 0.4\%$	$2.7 \cdot 10^6$	1.9
total		$3.8 \cdot 10^7 \pm 0.5\%$	$2.1 \cdot 10^7$	1.8

6.5.3 External exposure assessment

The activation of the Front-End system structures, due both to proton and neutron fields, can be considered as a deliberate introduction of a radioactive source that progressively grows in intensity over the SPES operation time, due to the accumulation of medium-long lifetime radioisotopes.

The period of activity of the SPES facility, before the total or partial replacement of the Front-End system structural components, is foreseen to be of several years. Therefore, the assessment of the external exposure due to gamma radiation has to be performed at different times in the operation lifetime of the system.

Electrons and α particles generated from the decay of activated radionuclides do not play an important role in the assessment of the external exposure, being short-range radiations. However, as underlined in Section 4.2.3, they must be absolutely considered in assessing surface and internal contamination. Therefore, only the dose rate from photons has to be considered to assess the external exposure.

The gamma ambient dose equivalent rate distribution dH*(10)/dt is calculated with both the MCNPX and FLUKA codes, in the same geometrical conditions, after one year of activity in the production bunker (time t_{10}). This is the typical time in which ordinary and extraordinary maintenance operations on the main elements of the PPB line and of the RIB line need to be planned. The dose rate is calculated in several positions, corresponding to locations where the operator is supposed to stand still in order to accomplish the ordinary and extraordinary maintenance operations (for example, replacement of mechanical elements of the Front-End system). These positions are placed at the height of the beam lines and at a distance of about 40 cm from the elements of the Front-End system where maintenance operations are foreseen.

The values obtained with the two calculation tools, both on the activation and on the dose rate, are in agreement by 20-40% on average and within a factor of 2 at worst. The results obtained with FLUKA, apart from a few single cases [64], are systematically higher than those obtained with MCNPX. In particular, the differences are larger near the collimators, in the area of the production bunker close to the PPB line where activation is mainly due to protons.

New evaluations of the gamma ambient dose equivalent rate have been recently performed with the FLUKA2020-0 release, including also punctual dose rate calculations in proximity of components of the RIB line that are more distant from the TIS unit. In this regard, the whole of the results

obtained with FLUKA in the present study has been checked for consistency. The results obtained with FLUKA2020-0 show differences of less than 10% on average, and never higher of 30%, with respect to whose obtained with the previous FLUKA version. Therefore, all the results obtained with FLUKA are considered reliable for the study of the residual activation of the SPES Front-End system.
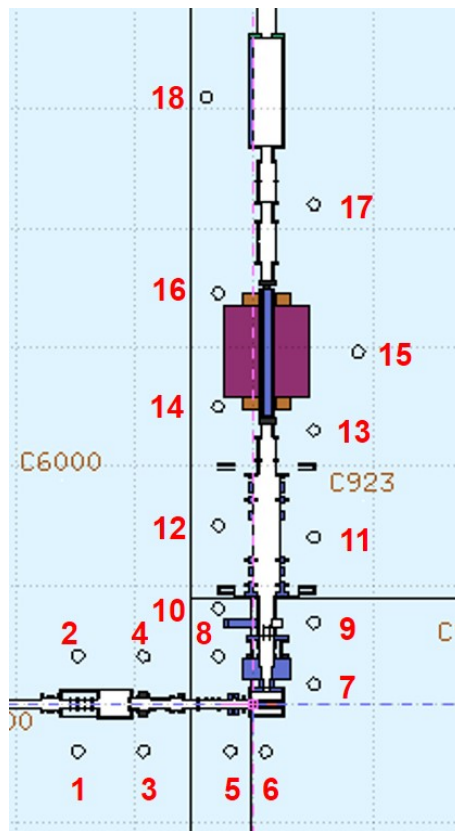

Figure 6.10: Horizontal cross-section of the FLUKA Front-End geometry at 150 cm height, with the indication of 18 positions for the dose rate sampling, located at 40 cm distance from the beam lines.

Figure 6.10 shows a horizontal cross-section of the FLUKA geometry at the axes of the Front-End beam lines (150 cm height), with superimposed a set of 18 points indicating the positions where dH*(10)/dt is specifically sampled, located at 40 cm distance from the beam lines. All these points represent typical positions for the worker, during ordinary and extraordinary maintenance operations on the main elements of the Front-End. Corresponding values of dH*(10)/dt are reported in Table 6.6; they are cal-

Table 6.6: Values of the gamma ambient dose equivalent rate dH*(10)/dt, in units of μSv/h, calculated with FLUKA in the positions shown in Figure 6.10, after 10 irradiation cycles and 60 day cooling time. The quoted errors are due to statistics in the Monte Carlo calculations.

point N.	dH*(10)/dt (μSv/h)	point N.	dH*(10)/dt (μSv/h)
1	$610 \pm 6\%$	10	$540 \pm 4\%$
2	$670 \pm 6\%$	11	$69 \pm 6\%$
3	$620 \pm 5\%$	12	$130 \pm 9\%$
4	$1.0 \cdot 10^3 \pm 4\%$	13	$94 \pm 5\%$
5	$640 \pm 4\%$	14	$97 \pm 5\%$
6	$610 \pm 4\%$	15	$55 \pm 7\%$
7	$500 \pm 3\%$	16	$62 \pm 6\%$
8	$1.3 \cdot 10^3 \pm 3\%$	17	$55 \pm 7\%$
9	$300 \pm 3\%$	18	$34 \pm 10\%$

culated after one year of activity and 60 day cooling time, which represents a typical time scheduled for ordinary maintenance operations.

In Figure 6.11 a horizontal mesh of the gamma ambient dose equivalent rate dH*(10)/dt, calculated with FLUKA in the SPES production bunker at time t_{10}, is shown. As it can be also seen from Table 6.6, the most critical positions occur along the PPB line, due to the proton activation of the graphite of the beam collimators, and in the materials near the target due to the activation by fission neutrons. Such positions are indicated on the mesh with red circles.

Finally, dH*(10)/dt has been calculated with MCNPX, at different times after the start of the facility during four years of activity, when a mid-long term extended technical stop of 6 months is planned.

Figure 6.12 shows the values of the gamma ambient dose equivalent rate at point 5 in Figure 6.11 as a function of time, until four years of SPES activity. This point is representative of the average position of an operator entering the production bunker to visually inspect the Front-End system.

Along the course of each year, dH*(10)/dt is sampled at four times: at the end of the fifth complete 30 day cycle (15 day activity plus 15 day cooling), at the end of a further 30 day cooling for maintenance at mid-year,
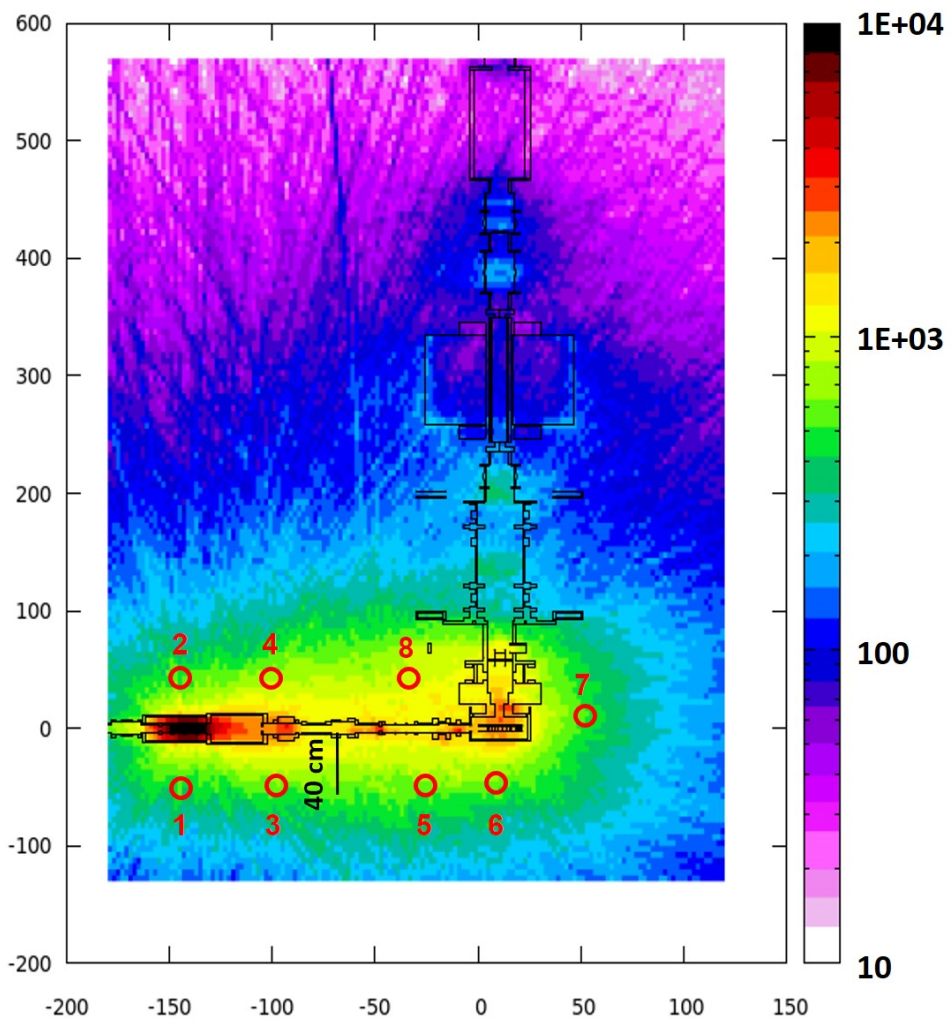
Figure 6.11: FLUKA spatial mesh of the gamma ambient dose equivalent rate dH*(10)/dt in the SPES production bunker. The mesh is calculated at time t_{10} on a horizontal plane crossing the center of the production target. The red circles represent the most critical positions where the dH*(10)/dt has been sampled (See Table 6.6). Units of the color scale are in $\mu Sv/h$.
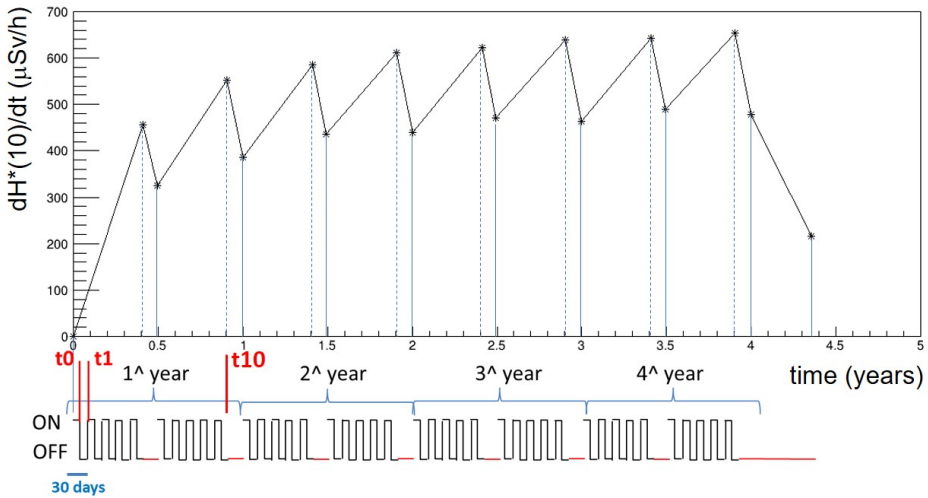
Figure 6.12: Gamma ambient dose equivalent rate at point 5 in Figure 6.11, sampled at different times during the first four years of SPES operations. The straight lines connecting the dose rate points are only guides for the eye. Calculations are performed with MCNPX + CINDER'90. The pattern in the lower part of the picture represents the alternate periods of activity (ON) and cooling time (OFF).

at the end of the tenth complete 30 day cycle and at the end of a further 35 day cooling for maintenance at the end of the year. A supplementary value of dH*(10)/dt is calculated 5 month after the last cooling period at the end of the fourth year, simulating a long stop for special maintenance operations.

Figure 6.12 shows that, after two or three years of activity of the facility, the levels of ambient dose equivalent rate in point 5 and, even more so, the activation of the Front-End system structure are saturated. It also shows that, after few months of supplementary cooling, the values of ambient dose equivalent rate can decrease very significantly. This information is crucial for the management of the final decommissioning of the facility.

As a final consideration, it is to note that the errors reported in all the calculations performed, both with MCNPX and with FLUKA, refer to the statistical precision in the result. An evaluation of the systematic uncertainty in the values obtained with the Monte Carlo tools is a more complex matter. In fact, systematic differences in the results can be the outcome of a complicated flux of operations, in which several factors play a role: physical models (the fission model included), interaction cross sections data in the materials for different incoming particles, calculation methods.

However, the fact that the global results achieved with the two Monte Carlo codes are in agreement by 40% on average, allows a systematic error of 50% to be prudently associated to all the Monte Carlo results obtained in this chapter and in the following chapters of this thesis. Once the SPES facility is commissioned, experimental validations can be performed and benchmarked against the Monte Carlo predictions.

To conclude, it is worth recalling that all the dose rate values previously calculated are due only to the activation of the materials composing the Front-End system, while the dose contributions due to radionuclide deposition along the RIB line elements are accounted for in Chapter 7. In the next chapter, also, general considerations on the strategies to adopt for the planning and organization of inspection and maintenance operations for critical components of the Front-End system are drawn.

Chapter 7

Ion deposition on the RIB line of the SPES Front-End system

7.1 Introduction

The first case study, introduced in Section 5.1, consists in the assessment of the radioactivity and of the external exposure of personnel to gamma radiation inside the production bunker. The contribution to the radioactivity due to the activation of the Front-End system by primary proton and neutron fields has been described in Chapter 6. The study has to be complemented by accounting for the radioactivity due to radionuclide deposition along the RIB channel electromagnetic elements. This work has been carried out by using the FLUKA code for Monte Carlo simulations.

The two most critical components of the RIB beam line are those where the produced radioactive isotopes others than the selected ones preferentially stop: the ion extraction electrode system and the "Wien Filter".

The ion extraction electrode is an electrostatic system present in any ISOL facility [133, 134]; its function is to perform the first acceleration of the radioactive ions after their formation in the ion source, by means of an electric field generated by a voltage difference of some tens kilovolts. The SPES extraction electrode is located on the RIB line axis, facing the ion source aperture at the exit of the TIS unit (see Figure 7.2). A fraction of the radioactive ions, as well as non-ionized radioactive atoms evaporating from the ion source, stick on the electrode tip during all the SPES operation cycles, causing a risk of voltage failure. Furthermore, the deposition of radioactive isotopes on the electrode surface grows with increasing the number

of SPES operation cycles. Therefore, the electrode tip has to be periodically replaced. The removal operation can be performed either in a semi-manual way or automatically using a remote handling system, depending on the level of ambient dose equivalent rate in proximity of the working area and on the potential surface contamination, due to the deposited radioactive isotopes.

The other critical electromagnetic element taken into account for its contamination is the "Wien Filter" (WF), a velocity selector able to perform a first mass separation stage of the produced radioactive ions with a mass resolution of about 1%. The radionuclides out of the desired mass selection window are deflected in different positions along the RIB line, depending on their mass and the selected mass window. They are deposited on the Wien Filter electrodes and on the devices of the radioactive line downstream of the Wien Filter, constituting, as a whole, a particular type of radioactive source. Maintenance operations near the Wien Filter are foreseen every one-two year period. The planning and the specific procedures to be followed for the interventions depend on the level of ambient dose equivalent rate and on the potential surface contamination in proximity of the device.

The risk of potential surface contamination outside of the Front-End system, but inside of the irradiation bunker, has to be also taken into account; the contamination could be due to fall or breakage of activated materials during maintenance operations. Moreover, potential intake of radionuclides can occur close to activated materials inside the irradiation bunker; therefore the worker entering in the bunker is provided with an adequate PPE[1]. These type of issues will be mentioned in Chapter 9, but their discussion is out of the scope of this thesis.

7.2 Radioactive contamination of the extraction electrode

The radioactive line of the Front-End consists of the target and ion source assembly, and of all those devices of the SPES apparatus having the function to extract the RIB from the ion source and to shape, control, select and transport it out of the bunker. These elements are depicted in Figure 7.1.

The extraction system is the first element of the RIB line after the TIS unit. It is composed of a titanium alloy electrode and a dedicated moving system. The tip of the electrode is located at a distance of about 60 mm from the exit hole of the ion source, as shown in Figure 7.2 illustrating the case of a Surface Ion Source.
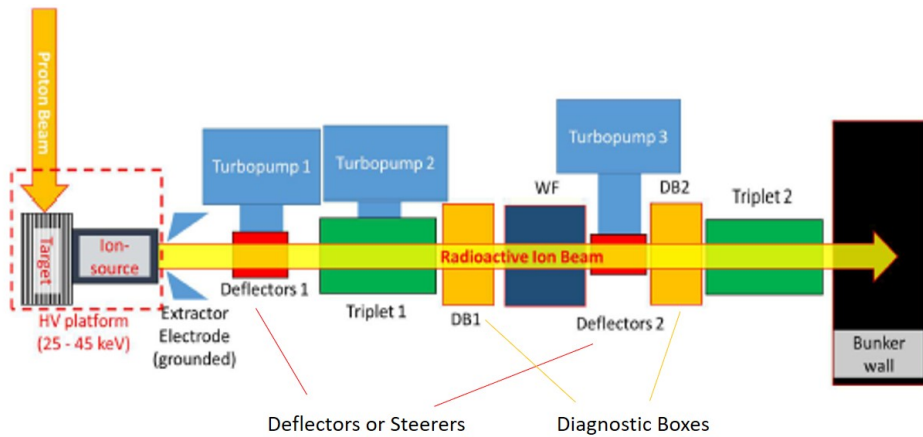
---

[1]Personal Protective Equipment.

Figure 7.1: Block diagram of the main elements of the RIB line.

The role of the electrode is to provide the first acceleration step to the RIBs. The electrical field generated by a potential difference of about 40 kV allows for the acceleration of the positive ions from the source (at high voltage) to the extraction electrode (to ground). Its extraction efficiency is a function of the electrode shape, of the distance from the ion source aperture and of the voltage difference.

The radioactive nuclei generated in the UC_x target are mainly produced by the fission induced by the 40 MeV proton beam on ^{238}U. Furthermore, spallation products including volatile α emitters are extensively produced.

Once reached the ion source, a part of these isotopes acquires a 1+ charge state before being extracted. Ionization efficiency depends strongly on the particular ion beam requested and on the selectivity of the ion source.

As explained in Section 3.2.3 concerning the ISOL technique, three types of ion sources can be used during the SPES activity: the SPES Surface Ionization Source (SSIS), the SPES Plasma Ionization Source (SPIS) and the Resonance Ionization Laser Ion Source (RILIS).

When the plasma (SPIS) source is mounted inside the TIS unit, high ionization potential elements are generally ionized in a not selective way. All the isotopes that do not compose the radioactive beam remain in the form of neutral atoms, evaporate from the ion source and can condensate on the TIS chamber walls or on the extraction electrode surface.

Conversely, the surface (SSIS) source is very effective for low ionization potential elements, while the laser-induced ionization (RILIS) is highly selective for a wide range of elements, producing isobaric and isomeric pure beams. So, in both cases, a great amount of unwanted isotopes produced in
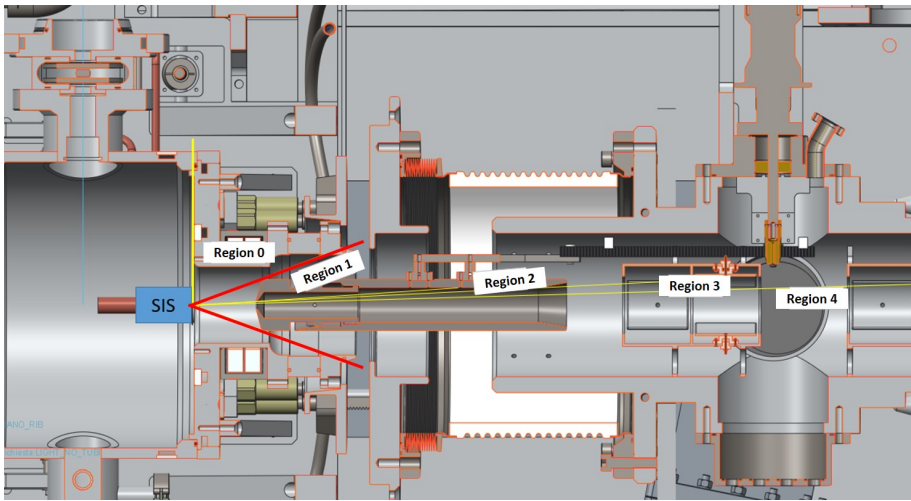
Figure 7.2: CAD image of the first part of the RIB line, with the Surface Ion Source inside the TIS unit [135]. Labelled regions are the TIS chamber (0), the mobile (1) and fixed (2) part of the electrode, the steerers (3) and the first triplet (4). The red lines delimit the solid angle covered by the electrode tip.

the target remains in the form of neutral atoms.

Anyway, a high flux of radioactive isotopes deposits on the electrode surface, that progressively increases its radioactivity with increasing the number of SPES operation cycles. It thus becomes an additional radioactive source to be carefully considered.

Moreover, there is a common finding in the RIB facility communities, that the build-up of radioisotopes and their progressive condensation on the electrode tip, set at high voltage relative to the ion source aperture, could cause extraction inefficiencies increasing the risk of high voltage discharges and failure [134].

For this reason, the periodical substitution of the ion extraction electrode must be foreseen as a regular preventive maintenance operation in the life cycle of any ISOL facility. For SPES, this operation on the Front-End radioactive line is planned once a year, during the annual shutdown period of the apparatus (1 or 2 months).

The handling of the electrode tip during the removal operation is a challenging operation, due to the high level of surface contamination of the component, that can result in possible environmental contamination and very high exposure to extremities in case of handling of the component during manual operations. The risk of spreading radioactive contamination on the close Front-End elements inside the bunker is an important issue

114

to be considered in order to develop proper strategies for the electrode tip replacement operation.

Furthermore, the resulting high levels of external exposure are hazardous not only in case of manual electrode removal operations, but also for all possible extraordinary maintenance operations on the RIB line that may be necessary and urgent even in the presence of the contaminated electrode tip.

Monte Carlo simulations have been performed to assess the external exposure for the workers during the operations of replacement of the ion extraction electrode and during possible maintenance operations in proximity of the RIB line of the SPES Front-End system.

The reference Monte Carlo model for this study contains geometry and materials composition of the whole SPES Front-End system, described in Section 6.2.1. In fact, the presence of structures and materials in the geometry model not only allows ion deposition points to be accurately located in the space, but also the radiation shielding effects in the production bunker to be taken into account. The FLUKA release utilized for all the simulations is FLUKA2020-0.

The calculation procedure consists of the following steps:

1. simulation of the isotope production in the SPES UC_x target, by using the FLUKA model in a static configuration (no time evolution);

2. selection of the fraction of the isotopes produced in the target that is supposed to stick on the extraction electrode along one year of operation, accounting for their release efficiency and decay time;

3. building of the FLUKA model for the calculation of the surface contamination of the extraction electrode, due to ion deposition, and of the ion time evolution;

4. calculation of the gamma ambient dose equivalent rate dH*(10)/dt inside the Front-End bunker, in the surrounding of the activated ion extraction electrode, at different cooling times after several irradiation cycles of the target (until one year activity).

7.2.1 The isotope deposition source on the extraction electrode

As starting point for the construction of the isotope deposition source, all radioactive isotopes produced in the first calculation step by the proton beam interactions on the UC_x target (mainly fission fragments) are considered, with the relative yields as calculated in Section 6.5.1.

Then, at the second step, the isotopes supposed to be able to reach the ion extraction electrode tip and stick upon it, after diffusion and effusion from the target and evaporation from the ion source, are selected with the following criteria adopted in a conservative approach.

- The radioactive isotopes sticking on the ion electrode tip are supposed to be deposited at the same rate as the fission yields calculated in Section 6.5.1. An unitary release efficiency for isotope diffusion and effusion up to the ion source is considered.

- The isotopes with production yields in the target less than 10^8 nuclei/s are not considered; their weight is negligible compared to the total yield, whatever the energy emitted by the associated decay photons. This threshold could seem high with respect to radioactive ion beam intensities for experiments, but is appropriate for calculating radiological dose in the considered positions inside the irradiation bunker. In fact, the gamma decay spectrum generated by the isotopes stuck to the extraction electrode tip is a subset of the total gamma energy spectrum exiting out of the activated target, shown in Figure 5.1 after 15 days from the switching off of the proton beam. Therefore, it is surely contained in the energy range between a few tens of keV and a few MeV, where the fluence-to-dose conversion coefficients for photons change by a maximum of a factor of ten [108, 109].

- All isotopes released from the target and entering inside the ion source evaporate uniformly in the external vacuum out of the ion source, through the exit aperture in front of the ion extraction electrode tip. The ionization efficiency of the ion source is set to zero, which means that all atoms exit in their neutral state. This is a plausible situation if the most selective surface (SSIS) or laser (RILIS) ion sources are mounted on the TIS unit, while it is a safe condition if the plasma (SPIS) ion source is mounted. In fact, in the latter case, the ionization efficiencies are of the order of 50% for the heavy elements close to Xe and of 36% for elements close to Kr, while for Be and the noble gases are supposed to be of the order of 5%.

- The percentage of evaporating atoms deposited on the ion extraction electrode tip is proportional to the solid angle covered by the electrode tip relative to the exit aperture of the ion source (about 6%). In fact, the isotopes outside the 6% solid angle stop on the walls of the TIS unit and are removed together with the TIS unit itself, at the end of each 30 day cycle.

- The isotopes with mass greater than M=200 u are not considered since they are refractory[2] and don't decay in non-refractory elements. Therefore they don't effuse out of the target.

- The volatile isotopes (Br, Kr, I, Xe) that transmute in non-volatile isotopes in less than 30 s are supposed to stick on the ion extraction electrode. Indeed, typical release times for isotope diffusion and effusion up to the ion source are lower than 10 s [29]. If the time for transmutation in non-volatile isotopes is larger than 30 s, the volatile isotopes are not considered, since they are likely sucked by the vacuum pumps as volatile species. However, setting the cutting time in the range between 3 s and 3 min, the composition of the isotope deposition source does not change appreciably, and the total yield changes to a maximum of 5%.

- The refractory isotopes (Y, Zr, Nb, Mo, Tc, Ru, Rh, La, Ce) that transmute in non-refractory isotopes in less than 15 days are considered. 15 days is the time available for the radioactive elements to exit from the target before the chamber is sealed at the end of the 15 day irradiation period; otherwise they don't leave the target at all.

- Concerning all the other isotopes, those that transmute in stable or volatile isotopes in more than either 10 days or 30 days or 6 months and in less than 1000 years are taken into account. Having as precautionary "thumb rule" to consider the isotopes of a decay chain until five, ten times the total half-lives for their final transmutation, the first choice represents a prudent condition if maintenance operations inside the bunker are planned not earlier than 50-100 days (let's say 2 months) cooling time after the shutdown.

Under these criteria, 78 isotopes out of the more than 600 isotopes produced in the target by ^{238}U fission are supposed to stick upon the ion extraction electrode, with the same yields as those of the fission production inside the target. Apart from ^{7}Be, they range between Z=35-62 and A=90-156. The value of the total current is $1.93 \cdot 10^{11}$ nuclei/s, calculated taking into account the solid angle covered by the electrode tip relative to the 2π half-space in front of the exit aperture of the ion source (about 6%).

The considered isotopes are highlighted in green in Figure 7.3. They are listed in the table in Figure 7.4, where isotopes that transmute in stable

---

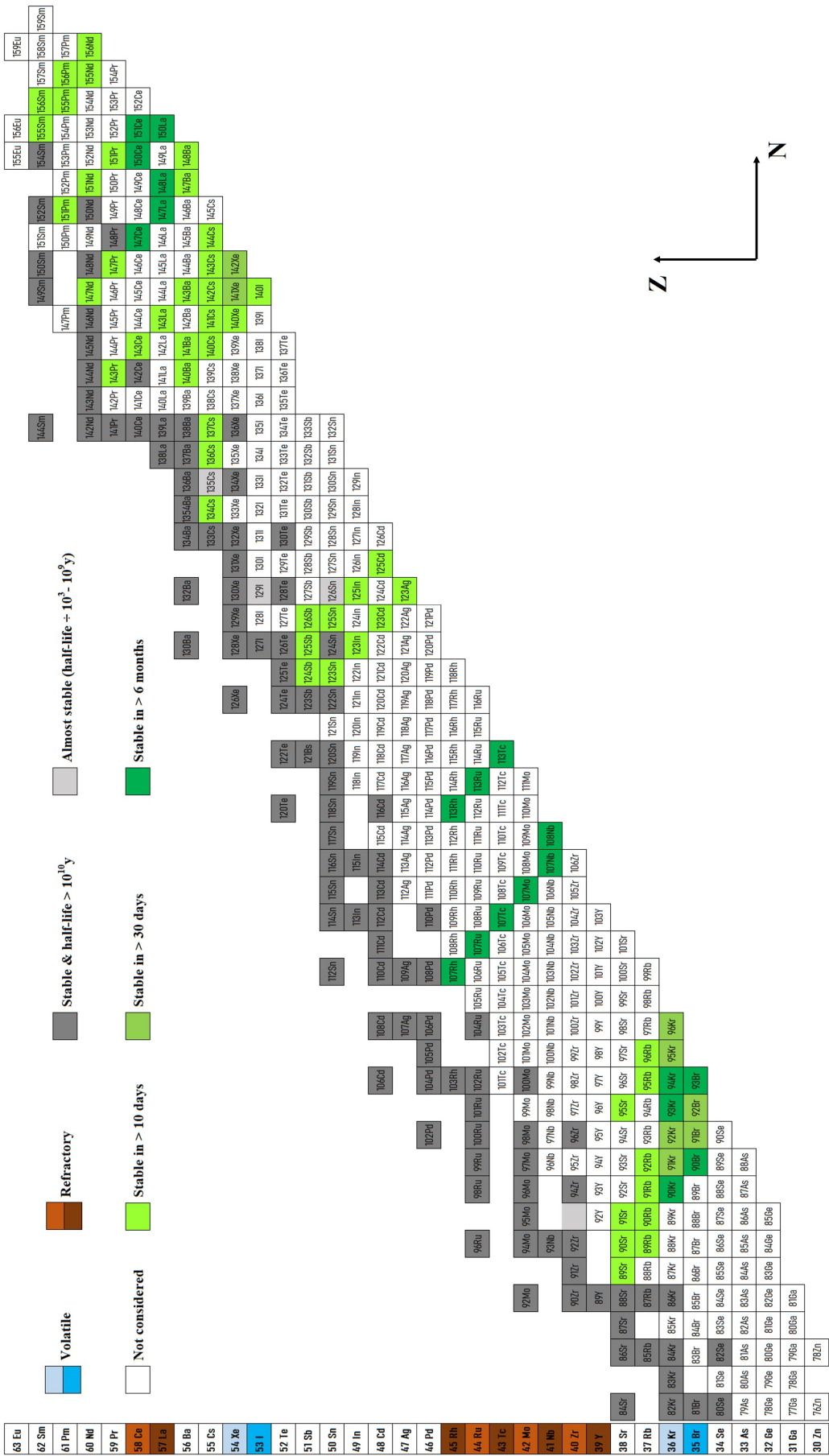[2]Elements with T_{boil} higher than about 3300 °C at standard pressure are considered refractory.

Figure 7.3: Isotopes with Z=35-62 considered for simulating the sticking upon the ion extraction electrode tip.

or volatile isotopes in more than 10 days are considered and isomer contributions are merged with the ground state of the respective isotope. The reliability of the procedure has been recently checked on data from measurements collected at CERN by HIE-ISOLDE [136, 137].

Isotope	Mass (u)	Yield (nuclei/s)	Half-life	Isotope	Mass (u)	Yield (nuclei/s)	Half-life
Be	7	1,6E+11	53,2 d	Sb	125	4,4E+10	2,76 y
Br	90	3,8E+10	1,92 s	Sb	126	6,1E+10	12,3 d
Br	91	2,8E+10	0,543 s	I	140	2,0E+09	860 ms
Br	92	8,8E+09	0,314 s	Xe	140	2,8E+10	13,6 s
Br	93	5,4E+09	102 ms	Xe	141	8,8E+09	1,73 s
Kr	90	1,4E+11	32,3 s	Xe	142	5,3E+09	1,23 s
Kr	91	7,8E+10	8.,57 s	Cs	134	1,4E+10	2,07 y
Kr	92	7,5E+10	1,84 s	Cs	136	9,3E+10	13,0 d
Kr	93	2,9E+10	1,29 s	Cs	137	1,8E+11	31,1 y
Kr	94	2,3E+10	212 ms	Cs	140	8,7E+10	63,7 s
Kr	95	6,2E+09	114 ms	Cs	141	6,8E+10	24,8 s
Kr	96	3,8E+09	80 ms	Cs	142	3,1E+10	1,68 s
Rb	89	4,9E+10	15,3 min	Cs	143	2,1E+10	1,79 s
Rb	90	8,2E+10	158 s	Cs	144	7,1E+09	1,79 s
Rb	91	1,3E+11	58,2 s	Ba	140	1,4E+11	12,8 d
Rb	92	1,3E+11	4,48 s	Ba	141	1,1E+11	18,3 min
Rb	95	6,4E+10	378 ms	Ba	143	6,4E+10	14,5 s
Rb	96	2,5E+10	203 ms	Ba	147	4,2E+09	894 ms
Sr	89	3,3E+09	50,6 d	Ba	148	2,2E+09	894 ms
Sr	90	1,6E+10	28,8 y	La	143	1,1E+11	612 ms
Sr	91	3,3E+10	9,65 h	La	147	3,3E+10	612 ms
Sr	95	1,3E+11	23,9 s	La	148	1,3E+10	14,2 min
Nb	107	8,6E+09	300 ms	La	150	1,8E+09	4,06 s
Nb	108	2,3E+09	198 ms	Ce	143	2,9E+10	1,26 s
Mo	107	3,4E+10	3,5 s	Ce	147	5,1E+10	33,0 h
Tc	107	9,7E+10	21,2 s	Ce	150	1,8E+10	56,4 s
Tc	113	2,6E+09	152 ms	Ce	151	5,9E+09	4,0 s
Ru	107	4,2E+10	3,75 min	Pr	143	2,0E+09	1,76 s
Ru	113	1,7E+10	800 ms	Pr	147	4,1E+10	13,6 d
Rh	107	4,7E+09	21,7 min	Pr	151	2,7E+10	13,4 min
Rh	113	8,0E+10	2,80 s	Nd	147	3,6E+09	18,9 s
Ag	123	4,7E+09	298 ms	Nd	151	2,1E+10	11,0 d
Cd	123	2,3E+10	2,10 s	Nd	155	4,1E+09	12,4 min
Cd	125	5,7E+09	680 ms	Nd	156	2,7E+09	8,9 s
In	123	9,0E+10	6,17 s	Pm	151	6,4E+09	5,26 s
In	125	5,3E+10	2,36 s	Pm	155	1,0E+10	28,4 h
Sn	123	4,3E+10	129 d	Pm	156	5,4E+09	41,5 s
Sn	125	7,7E+10	9,64 d	Sm	155	3,8E+09	26,7 s
Sb	124	1,3E+10	60,2 d	Sm	156	5,6E+09	22,3 min

Figure 7.4: *Isotopes considered for simulating the sticking upon the ion extraction electrode. Isomer contributions are merged with the ground state of the respective isotope.*

7.2.2 The FLUKA model of the extraction electrode surface contamination

In the third calculation step, the proton source implemented in the FLUKA model of the SPES Front-End system (see Section 6.2.1), is replaced by a

new ion source, defined starting from the isotope deposition source designed in the previous step. The FLUKA geometry includes the ion extraction electrode; it is shown in the cross section of Figure 7.5 that can be compared with the drawing reported in Figure 7.2.
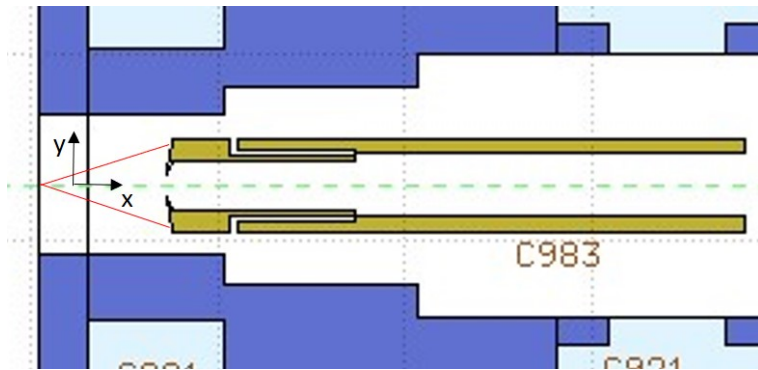

Figure 7.5: Cross section of the ion source and ion extraction electrode as modelled with FLUKA.

The selected isotopes are supposed to evaporate from the ion source exit hole with random directions, covering a forward 2π solid angle with straight trajectories. Only a fraction of them (about 6%) lies within the solid angle geometrically covered by the ion extraction electrode tip. Moreover, to stay on the safe side, the isotope flux impinging upon the ion extraction electrode is not depleted for the beam passing through its input hole.

The remaining part of the isotope evaporating flux is directed to structural components of the chamber unit where it deposits, as can be seen from the red lines of Figure 7.2. Therefore, the corresponding radioactive contamination is removed with the TIS unit, that results actually be more highly contaminated than the electrode tip. The radiation issues related to the exhausted TIS units during their life cycle are part of the second case study introduced in Section 5.1, and are discussed in the next chapter.

Under these assumptions, a FLUKA isotope source is built as a "heavy ion beam", managed by an external source routine. The 78 isotopes previously selected are sampled with the same isotope yields as the production inside the target, and are uniformly distributed inside a volume source of annular shape, with axis parallel to the ion extraction electrode (x-axis in the FLUKA reference system). The internal radius is greater than the ion extraction electrode hole shape (R_{int}=1.5 cm), while the radial extension of the source remains inside the electrode tip external area (ΔR=0.5 cm). An arbitrary cylinder height h=0.2 cm is set. The sampled isotope velocity is

directed along the x-direction, towards the extraction electrode tip.

The energy associated to the beam is of few electron volts, a typical thermal energy characterizing the non ionized isotopes. Such an energy is sufficient to allow the isotope beam to stick and stop at the surface of the ion electrode tip. In Figure 7.6 the fluence of the isotope source impinging on the ion extraction electrode tip is shown in two orthogonal views.
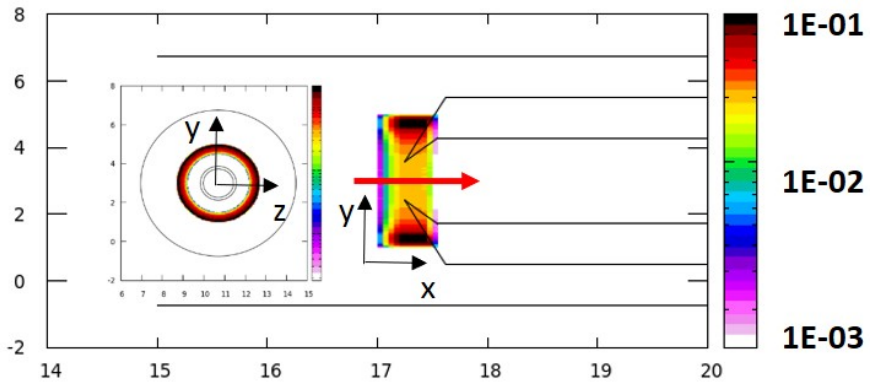

Figure 7.6: Fluence of the isotope source on the ion extraction electrode tip in two orthogonal views. Values on the horizontal and vertical axes are in centimeters, units of the color scale are normalized by primary source particle.

To simulate the build-up and decay of the deposited isotopes during the operation cycles of the SPES apparatus, a time evolution calculation is set in FLUKA. The beam intensity during the irradiation periods is calculated as the total yield of the 78 isotopes previously selected, scaled on the fraction of the solid angle covered by the ion extraction electrode tip relative to the 2π half-space solid angle in front of the ion source exit hole.

7.2.3 External exposure assessment due to the contaminated extraction electrode

The last step of the FLUKA calculation procedure consists in the assessment of the external exposure in the surrounding of the Front-End system and, in particular, of the ion extraction electrode. The ambient dose equivalent rate distribution is calculated for the gamma radiation coming from the radioactive isotope deposition on the ion extraction electrode tip, at different times during the SPES activity.

In the present calculations, the irradiation periods defined for the isotope

source are those foreseen during one year of operation of the SPES facility (10 irradiation cycles). The assessments are performed at different cooling times after the conclusion of the irradiation periods: 15, 30, 45 and 60 days after the turning off of the proton beam. These cooling times match with possible scenarios of maintenance interventions inside the production bunker and with the planned replacement of the exhausted ion extraction electrode, that has to be performed during the annual shutdown period of 1-2 months. Periods of six months and one year of cooling time are considered too; they are related to possible maintenance activities in medium-long term shutdown periods. For all considered times it is supposed that the exhausted TIS unit containing the irradiated target has already been removed from its location on the Front-End lines. On the contrary, no human intervention inside the bunker would be possible.

Figure 7.7 shows a horizontal mesh of dH*(10)/dt in the SPES production bunker, calculated at the vertical height of the axes of the Front-End beam lines (150 cm height). The mesh refers to 15 days of cooling time following the conclusion of the annual ten SPES operation cycles. The red circles on the mesh corresponding to the points from 5 to 8 represent the positions closest to the extraction electrode, among those introduced in Figure 6.10. Moreover, the point labeled with "H", in correspondence to the RIB axis of the mesh, 2 m away from the ion extraction electrode, represents a hypothetical position of an operator during the handling operation of the ion extraction electrode tip, in the case of semi-manual extraction. The dose rate values corresponding to these positions are reported in Table 7.1 for all cooling times considered.

For these most critical positions, the values of dH*(10)/dt shown in Table 7.1 are above 1 mSv/h even after 45 days of cooling time at the conclusion of the annual SPES activity period. Moreover, it is worth remarking that, after 45 days of cooling, the value of dH*(10)/dt at point H is still about 500 μSv/h. This fact suggest the need for an automatic equipment for the ion extraction electrode tip replacement in ordinary conditions.

Finally, Figure 7.8 shows the behavior of the dose rate for the points from 5 to 8, as a function of the number of irradiation cycles and with 45 days of cooling time. Intermediate operation conditions as two or five cycles of irradiation, represent a possible scenario in which extraordinary maintenance operations are necessary inside the Front-End bunker before the scheduled annual stop. In the event that this happens, it is important to know whether it is possible to operate even in presence of the contaminated electrode, or if an early electrode tip replacement is necessary before carrying out maintenance interventions.
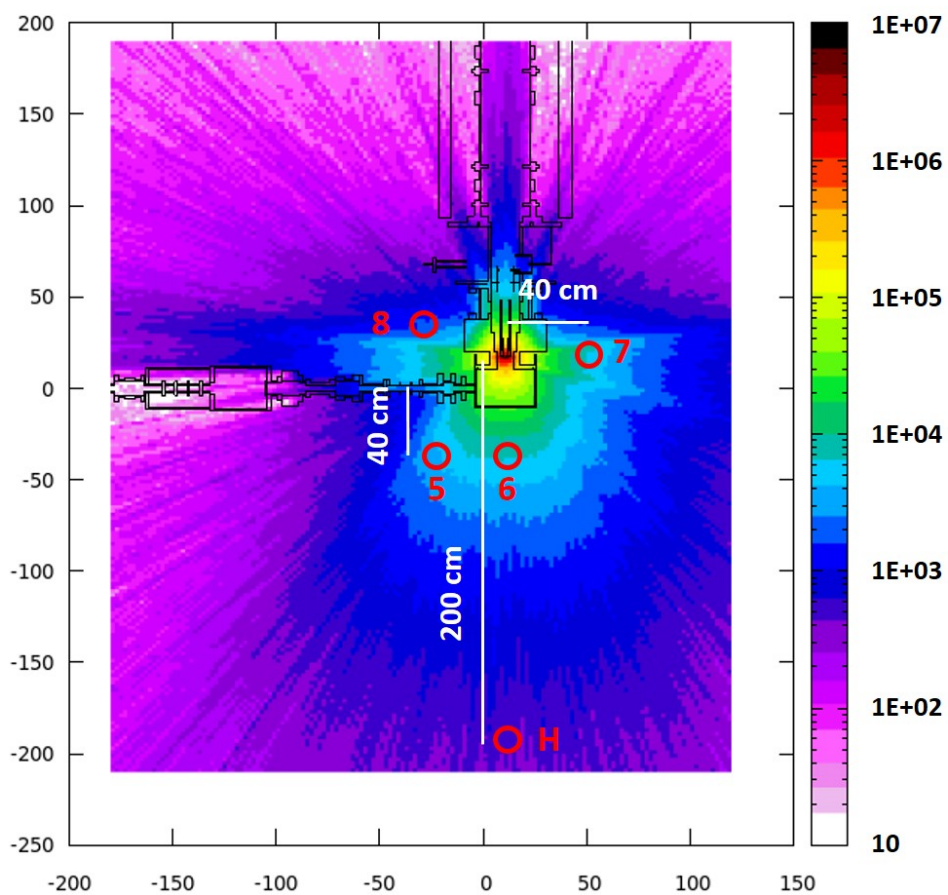
Figure 7.7: Horizontal mesh of dH*(10)/dt in the SPES production bunker, due to the isotope deposition upon the ion extraction electrode tip after 15 days of cooling time following the conclusion of the annual SPES activity period. Red circles represent few sampled positions on the mesh plane (150 cm). Units of the color scale are in $\mu Sv/h$.

Table 7.1: *Values of the ambient dose equivalent rate dH*(10)/dt, due to the ion deposition on the electrode tip inside the SPES bunker. The values, expressed in μSv/h, are calculated with FLUKA at different cooling times after 10 complete irradiation cycles, in the positions shown in Figure 7.7. Monte Carlo errors are less than 1%.*

point N.	$t_c = 15\ d$ (μSv/h)	$t_c = 30\ d$ (μSv/h)	$t_c = 45\ d$ (μSv/h)	$t_c = 60\ d$ (μSv/h)	$t_c = 180\ d$ (μSv/h)	$t_c = 1\ y$ (μSv/h)
5	$8.8 \cdot 10^3$	$5.2 \cdot 10^3$	$3.5 \cdot 10^3$	$2.6 \cdot 10^3$	$7.6 \cdot 10^2$	$2.3 \cdot 10^2$
6	$1.3 \cdot 10^4$	$8.1 \cdot 10^3$	$5.5 \cdot 10^3$	$4.1 \cdot 10^3$	$1.3 \cdot 10^3$	$4.0 \cdot 10^2$
7	$1.7 \cdot 10^4$	$9.9 \cdot 10^3$	$6.5 \cdot 10^3$	$4.8 \cdot 10^3$	$1.4 \cdot 10^3$	$4.5 \cdot 10^2$
8	$3.4 \cdot 10^3$	$2.0 \cdot 10^3$	$1.3 \cdot 10^3$	$9.0 \cdot 10^2$	$2.5 \cdot 10^2$	78
H	$1.2 \cdot 10^3$	$7.1 \cdot 10^2$	$5.0 \cdot 10^2$	$3.7 \cdot 10^2$	98	34

Figure 7.8 shows that, passing from two to five irradiation cycles, the dose rate increases of about 30%, while after five irradiation cycles it reaches a plateau, presenting a further increment of only 10% from five to ten irradiation cycles.

Most likely, the dose levels at the points closest to the exhausted ion extraction electrode are principally due to the isotope deposition on the electrode tip. However, as underlined in Section 5.1, the total external exposure during the permanence inside the production bunker near the Front-End elements, is due to the sum of the contributions from all the radioactive sources that build-up over time on the Front-End structure.

Global considerations on the implementation of the procedures of optimization for maintenance and inspection operations inside the front-End bunker have to take into account the relative importance of all the radiation "hot spots". They will be discussed in Section 7.4, after the section devoted to the ion deposition on the Wien Filter and its downstream components.

7.3 Radioactive contamination due to Wien Filter mass separation

Downstream of the extraction electrode, the radioactive line of the SPES Front-End includes several elements necessary to shape and transport the RIBs out of the bunker. As explained in Section 3.3.2, most of them are
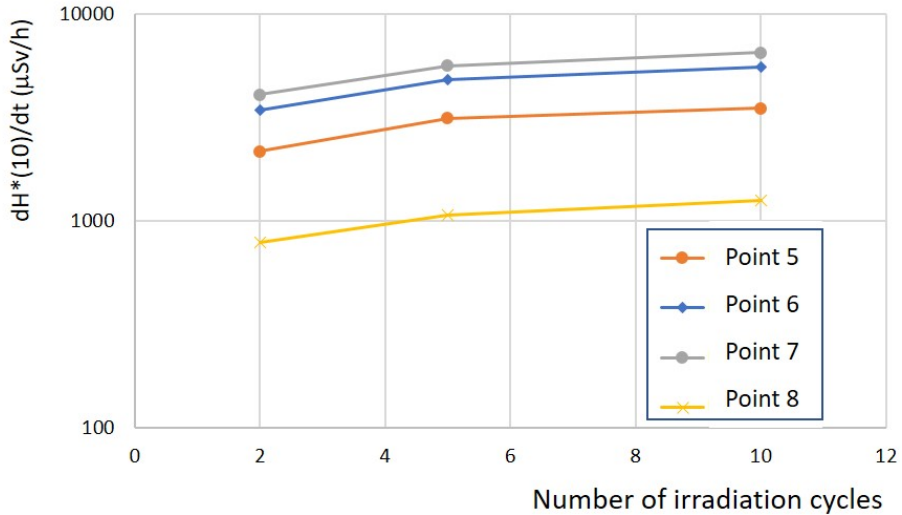
Figure 7.8: Behavior of dH*(10)/dt calculated for the points from 5 to 8, as a function of the number of irradiation cycles and after 45 days of cooling time.

electrostatic devices: the steerers, able to correct the trajectory of the beam and align it to the beam axis centre, and the triplets, that control the beam size and focus it through the beam pipe.

In addition, beam diagnostic devices are installed along the radioactive Front-End beam line to monitor the beam current and profile. They are housed in vacuum chambers, closed by stainless steel flanges. The vacuum condition also prevents any spread of radioactive material out of the lines. Turbo-molecular vacuum pumps allow the appropriate vacuum conditions along the beam pipes to be maintained and, at the same time, act as filter device for the volatile isotopes, holding back significant amounts of radioactivity. For this reason they require periodic maintenance (see Section 9.2.4). All the moving parts of the Front-End, the diagnostics and the turbo-molecular vacuum pumps, are connected to special pneumatic motors, needed to provide their handling.

The Wien Filter is a device which uses perpendicular electric and magnetic fields to select particles with a given velocity. It is able to perform a first mass separation of the mono-energetic ion beam coming from the extraction electrode, in order to obtain a quite isobaric beam, with a mass resolution of around 1/100.

The ions which are not comprised in the selected mass window are deflected away from the RIB axis and are deposited on the radioactive beam line elements both inside and downstream of the Wien Filter. The radioactive isotopes spread mostly on the Wien Filter electrodes, but also on the deflectors after the Wien Filter and on the separation slits of the second diagnostic box. These slits are used as a mechanical barrier to stop the unwanted deflected beam. In the diagnostic box, a Faraday cup measures the beam that eventually exits from the bunker, towards the subsequent selection and acceleration phases.

The Wien Filter contamination depends on the specific ion beam required by the users and on the procedure adopted to extract and separate it. Anyway, the continuous build-up of the radioactive isotopes sticking on the RIB line elements constitutes a new radioactive source that becomes more and more critical with the accumulation of active periods of the SPES facility. This fact has to be taken into account for the maintenance operations in proximity of the Wien Filter, foreseen every one-two year period.

A previous study on the radiation protection constraints related to the transport of the radioactive ions along the SPES RIB line, and in particular on the Wien Filter, was performed using the FLUKA code for Monte Carlo simulation [138]. As a result of this work, contributions to the ambient dose equivalent rate were assessed, considering both the activation of the materials of the Wien Filter due to the intense neutron fields in the bunker, and the radionuclides stopped by the Wien Filter during the selection of the beam of interest.

The first contribution to the dose rate was calculated by FLUKA at 1 m distance from the Wien Filter surface, considering only one irradiation cycle, and resulted to be about 100 μSv/h. The second contribution was evaluated after two years of extraction of the ^{132}Sn beam and some months of cooling time. Separate calculations for the build-up and decay of each stopped radionuclide were performed using simplified Bateman equations, then the contribution from all the sources were summed up to give the final result of about 3 mSv/h at 1 m distance from the Wien Filter.

In this thesis work, a more complete and general calculation method is followed. The FLUKA Monte Carlo code is employed to simultaneously evaluate the build-up and decay of all radioisotopes deflected by the Wien Filter during the selection of different beams, chosen on the basis of the main user requests.

Depending on the produced beam, different positions of deposition of the isotopes are calculated and the corresponding radioactive source sampled accordingly. The dose rate is then calculated in the whole volume of the

production bunker and especially in proximity of the devices located on the RIB line. Several positions are chosen for the dose rate calculation, on the basis of the planned maintenance operations.

As for the electrode, the calculation procedure is achieved in few steps:

1. simulation of the isotope production in the target (the same calculated in Section 6.5.1), which is used as first step in the ion extraction electrode procedure;

2. selection of the isotope deposition source, supposing selection criteria similar to those used in Section 7.2.1, but taking into account the ionization process as well as the sticking properties of the volatile ions;

3. building of the FLUKA model, implementing the isotope deposition source and proper sampling points and directions of the ions. The specific model obtained depends on the selected ion mass;

4. calculation of the gamma ambient dose equivalent rate inside the Front-End bunker and its time evolution, for some isobaric beams requested by users to be produced in the first year of operation of the facility.

7.3.1 The source of ions deflected by the Wien Filter

The ion deposition source to input to FLUKA is constituted by that portion of the 40 kV radioactive beam exiting out of the extraction electrode, which is not selected by the Wien Filter and, therefore, is deflected and deposits along the RIB line. As for the extraction electrode, the starting point to build the FLUKA source are the radioactive isotopes produced in the UC_x target.

A MatLab code has been specifically realized to automatically generate and implement in FLUKA such an ion deposition source, taking into account the decay chains of the radioactive isotopes. The code predicts how many of the isotopes produced in the target are available at the ion source [9]. Depending on the particular ionization method, the code then calculates the relative yields of the isotopes that reach and leave the ion extraction electrode. These isotopes have to pass a series of selection criteria, in a similar way to how it has been seen in Section 7.2.1 for the extraction electrode contamination. The adopted criteria are described in the following.

- Zero release time and unitary release efficiency are supposed. For each isotope the fission yield calculated in the target in Section 6.5.1 is

127

Isotope	Mass (u)	Yield (nuclei/s)	Half-life	Isotope	Mass (u)	Yield (nuclei/s)	Half-life	Isotope	Mass (u)	Yield (nuclei/s)	Half-life
Be	7	7,21E+09	53,2 d	Cd	115	3,21E+08	53,5 h	—	137	1,71E+10	24,5 s
Se	89	3,93E+09	0,43 s	Cd	117	1,08E+10	2,49 h	—	138	7,61E+09	6,26 s
Se	90	2,52E+09	195 ms	Cd	119	2,40E+10	2,69 min	—	139	4,18E+09	2,28 s
Se	91	5,91E+08	0,27 s	Cd	121	2,26E+10	13,5 s	—	140	1,32E+09	860 ms
Br	89	2,61E+10	4,36 s	Cd	123	9,59E+09	2,10 s	—	141	5,75E+08	430 ms
Br	90	1,33E+10	1,92 s	Cd	125	2,29E+09	680 ms	—	142	1,20E+08	222 ms
Br	91	9,83E+09	0,543 s	Cd	126	1,41E+09	0,515 s	Xe	137	5,01E+10	3,82 min
Br	93	1,88E+09	102 ms	Cd	127	3,93E+08	0,37 s	Xe	140	1,57E+10	13,6 s
Br	94	4,36E+08	70 ms	In	117	1,01E+09	43,2 min	Xe	141	4,89E+09	1,73 s
Kr	89	3,36E+10	3,15 min	In	119	1,03E+10	2,4 min	Xe	142	2,96E+09	1,23 s
Kr	90	4,67E+10	32,3 s	In	121	3,17E+10	23,1 s	Xe	143	6,65E+08	511 ms
Kr	91	2,69E+10	8,57 s	In	123	2,13E+10	6,17 s	Xe	144	3,55E+08	1,15 s
Kr	93	1,02E+10	1,29 s	In	125	2,41E+10	2,36 s	Cs	134	5,92E+09	2,07 y
Kr	94	7,97E+09	212 ms	In	126	1,08E+10	1,53 s	Cs	136	4,02E+10	13,0 d
Kr	95	2,35E+09	114 ms	In	127	5,63E+09	1,09 s	Cs	137	7,95E+10	31,1 y
Rb	86	4,69E+08	18,6 d	In	129	1,31E+09	611 ms	Cs	140	3,76E+10	63,7 s
Rb	89	2,65E+10	15,3 min	In	130	4,97E+08	0,29 s	Cs	141	2,94E+10	24,8 s
Rb	90	4,49E+10	158 s	In	131	1,39E+08	0,28 s	Cs	142	1,35E+10	1,68 s
Rb	91	7,18E+10	58,2 s	Sn	121	2,50E+09	27,0 h	Cs	143	8,90E+09	1,79 s
Rb	93	7,57E+10	5,84 s	Sn	123	1,11E+10	129 d	Cs	144	3,06E+09	994 ms
Rb	94	4,35E+10	2,70 s	Sn	125	4,09E+10	9,64 d	Cs	145	1,63E+09	587 ms
Rb	95	3,49E+10	378 ms	Sn	127	3,32E+10	2,10 h	Cs	146	4,31E+08	322 ms
Sr	89	1,49E+09	50,6 d	Sn	129	1,34E+10	2,23 min	Cs	147	1,47E+08	230 ms
Sr	90	7,25E+09	28,8 y	Sn	131	3,00E+09	56,0 s	Ba	140	8,15E+10	12,8 d
Sr	91	1,49E+10	9,65 h	Sb	124	2,99E+09	60,2 d	Ba	141	6,24E+10	18,3 min
Sr	93	5,34E+10	7,43 min	Sb	125	2,20E+10	2,76 y	Ba	143	3,75E+10	14,5 s
Sr	95	5,81E+10	23,9 s	Sb	126	3,07E+10	12,3 d	Ba	144	3,22E+10	11,5 s
Y	95	1,38E+08	10,3 min	Sb	127	5,99E+10	3,85 d	Ba	147	2,45E+09	894 ms
Ag	113	5,66E+09	5,37 h	Sb	129	6,46E+10	4,37 h	Ba	148	1,28E+09	612 ms
Ag	115	2,71E+10	20,0 min	Sb	131	2,98E+10	23,0 min	Ba	149	2,34E+08	344 ms
Ag	117	4,61E+10	72,8 s	Te	127	2,27E+09	9,35 h	Sm	151	1,05E+08	90 y
Ag	119	3,28E+10	2,1 s	Te	129	8,85E+09	69,6 min	Sm	155	1,92E+09	22,3 min
Ag	121	1,13E+10	0,78 s	Te	131	6,25E+10	25,0 min	Sm	156	2,78E+09	9,4 h
Ag	123	2,36E+09	298 ms	Te	137	1,09E+09	2,49 s	Eu	155	1,79E+08	4,75 y
Ag	124	6,05E+08	191 ms	Te	138	5,92E+08	1,4 s	Eu	156	3,29E+08	15,2 d
Ag	125	2,68E+08	159 ms	I	131	6,18E+10	20,8 h				

Figure 7.9: Ions exiting out of the extraction electrode, able to be deflected by the Wien Filter and deposited along the RIB line. Isomer contributions are merged with the ground state of the respective isotope.

multiplied by proper ionization efficiency values. These values have been obtained by measurements performed at HIE-ISOLDE [13] with the plasma ion source (conservative hypothesis). For noble gases, the ionization efficiency found in this way is very likely while, for others isotopes, it is based on values found in literature or it is the result of extrapolations. Anyway, these values of ionization efficiency provide sufficiently precise estimates for the purposes of the work [135].

- The isotopes with production yields in the target less than 10^8 nuclei/s are not considered (same criterion as in Section 7.2.1).

- The isotopes with mass greater than M=200 u are not considered since they are refractory (same criterion as in Section 7.2.1).

- The refractory isotopes that transmute in non-refractory isotopes in less than 15 days are considered (same criterion as in Section 7.2.1).

- Based on several works [139, 140, 141, 142], it seems that, at the SPES extraction energies (about 40 kV), all volatile ions hitting metal materials inside and downstream of the Wien Filter, penetrate and remain trapped in the metal lattice for a certain time, depending on the specific volatile. In a conservative hypothesis, this time interval, called "saturation time", is assumed to be of about one year for all the volatiles, even if it has been evaluated in some days for the noble gases at the SPES isotope fluxes. Therefore, if the time for transmutation in non-volatile isotopes is smaller than one year, the volatile isotopes are considered, since they cannot be released as volatile species and likely sucked by the vacuum pumps.

- Concerning all the other isotopes, those that transmute in stable or volatile isotopes in more than 10 days and less than 1000 years are taken into account (same criterion as in Section 7.2.1).

The ion source created with these criteria contains 107 isotopes, for a total current of $1.93 \cdot 10^{12}$ nuclei/s. They are listed in the table in Figure 7.9. Apart from ^{7}Be, they range between Z=34-63 and A=89-156. Isomer contributions are merged with the ground state of the respective isotope.

7.3.2 Position and direction of the deflected ions

The correspondence between the mass of the ion deflected by the Wien Filter and its position and direction when it deposits along the RIB line, inside

129

or downstream of the Wien Filter, is calculated for each deflected ion, and passed as input to FLUKA.
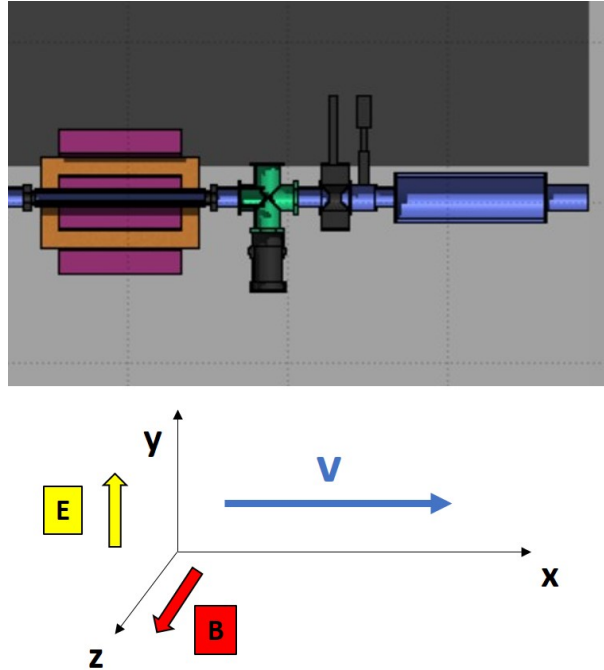

Figure 7.10: The RIB line modelled with FLUKA: the Wien Filter and its downstream elements. On the bottom panel the direction of the electric and magnetic fields acting on the ion beam travelling inside the beam pipe is indicated.

The mass selection capability of the Wien Filter is based on the simultaneous presence of an electric field **E** and a magnetic field **B**, both uniformly distributed in the space and perpendicular to each other and to the ion beam line axis.

When a ion beam crosses the Wien Filter electrodes with direction normal to both electric and magnetic fields, as shown in Figure 7.10, it is subjected to the force

$$\boldsymbol{F} \ = q \ \boldsymbol{E} \ + \ q \ \boldsymbol{v} \ \times \ \boldsymbol{B}, \tag{7.1}$$

where **v** is the particle velocity and **F** represents the Lorentz force.

If **F** is equal to zero, the particle travels undeflected in the space along the beam line axis. In this case, writing equation 7.1 in scalar form:

$$v \ = \frac{E}{B}. \tag{7.2}$$

If the ion beam of a fixed energy is composed of ions of different masses, the ion velocity depends on its mass and the Wien Filter can be used as a mass separator. The ability of separation of the Wien Filter can be defined as:

$$ott = \frac{s}{d},\tag{7.3}$$

where s is the distance between the centers of two consecutive mass peaks and d is the diameter of the beam, as shown in Figure 7.11. If ott is greater than one, the beam can be completely separated because the distance between the passing mass peak and the consecutive one is greater than the diameter of each of the two mass beams.
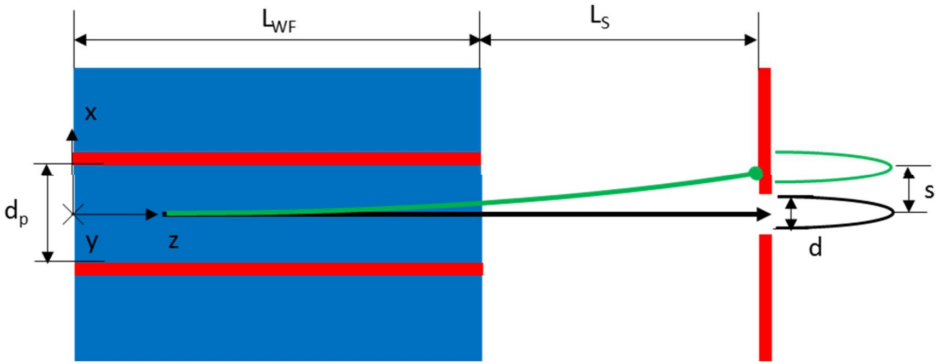
Figure 7.11: Schematic view of the SPES Wien Filter, with the indication of the most relevant geometrical parameters (see text). The beam profiles relative to two consecutive mass values are drawn on the picture.

The Wien Filter designed for the SPES Front-End was developed in [55], where the analytic procedure to obtain the expression of the s mass separation it described in detail. For the purpose of the present work, it is enough to know the relation that expresses the separation s of a certain mass $\Delta M + M$ of the ion beam, with respect to the mass M. Considering a beam perfectly aligned with the axis, and of negligible dimensions, if ΔM is small, of the order of a few units, the following relation is a good approximation of the general expression. It can be written as:

$$s = \frac{L_{WF}(L_s + L_{WF}/2)}{2\,d_p}\frac{V_p}{V_e}\frac{\Delta M}{M},\tag{7.4}$$

where L_{WF}=874 mm and d_p=50 mm are the Wien Filter effective length and distance between the electrodes providing the electric field, L_s is the dis-

tance from the Wien Filter exit aperture at which the separation is calculated, $V_p = 4.65$ kV is the potential difference on the Wien Filter electrodes and $V_e = 42$ kV is the potential difference between the ion source and the ion extraction electrode (see Section 7.2).

In Figure 7.12 a scheme of the masses stopping inside and downstream of the Wien Filter is shown for a desired mass M=120 u. The masses lower than M=112 u and greater than M=128 u stop inside the Wien Filter, while the masses between M=113 u and M=127 u are deposited on the structures between the output hole of the Wien Filter and the separation slits.
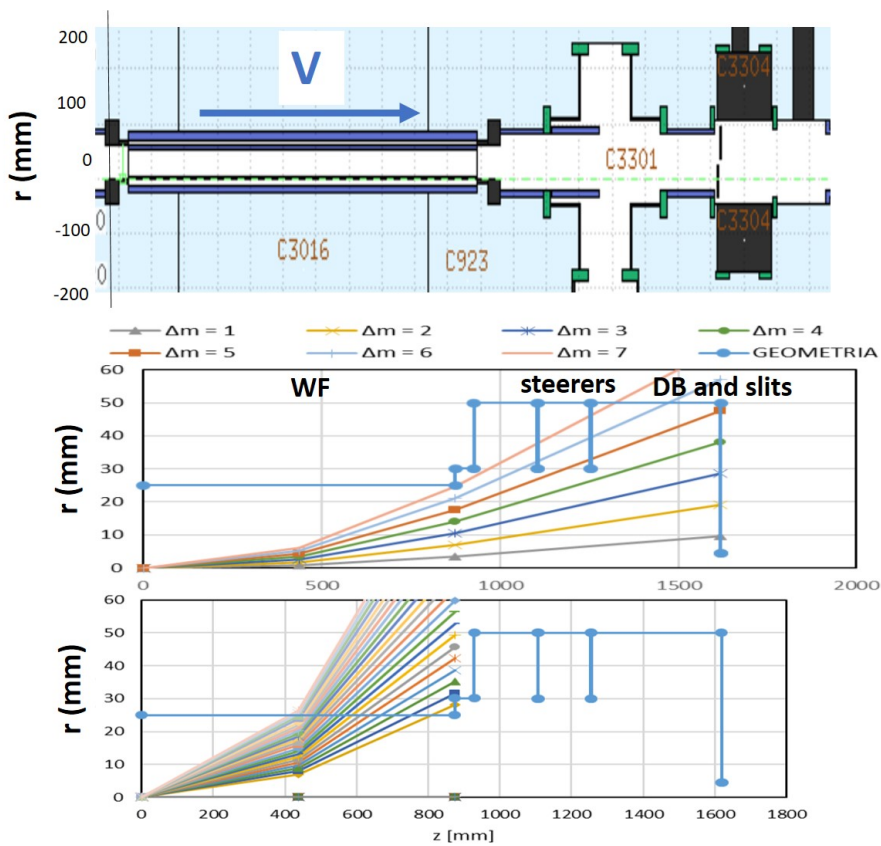
Figure 7.12: The top panel shows a vertical cross-section of the FLUKA geometry of the RIB beam line, between the Wien Filter and the separation slits mounted in correspondence of the diagnostic box; the medium panel shows, for the desired mass M=120 u, the schematic trajectories of the masses deflected away from the WF ($\Delta M \leq 7$ u), while the bottom panel shows the masses deflected inside the WF ($7 < \Delta M \leq 30$ u).

7.3.3   The FLUKA model of the Wien Filter contamination

The isotope deposition source and the information on the correlation between mass and kinematic parameters of the ions that are deflected away from the RIB axis, are implemented in the FLUKA geometry model of the Front-End system developed in Section 6.2.1.

As for the extraction electrode study, an external FLUKA source routine is built, associated to a "heavy ion beam" source.

The external source routine performs the following operations:

1. it loads the file containing the ion deposition source composed of the 107 isotopes with the corresponding intensities, as defined in Section 7.3.1;

2. it loads the file containing the information on the position and velocity of the ions, in the FLUKA reference system, for the desired mass, as defined in Section 7.3.2;

3. it samples on the ion intensities to choose the ion that is actually generated;

4. it associates to the sampled ion mass the corresponding kinematic information (point and velocity of generation).

So, each ion generated by the external source routine is directed towards a RIB structure, depending on its mass, and sticks on its surface, as indicated in Figure 7.12 for a desired mass M=120 u.

The setting of the evolution time, that is of the build-up and decay times for the generated ion beam, depends on the particular selected mass. The list of experiments sought for the first year of the SPES facility activity is based on the number of "Letter Of Intent" (LOI) for the production of a certain selected mass, and is also related to the source that will be used.

For the assessment of the external exposure on the Wien Filter, it is assumed that all the masses are produced with the plasma source. This is a conservative hypothesis from the radiation protection point of view, because the SPIS-produced beam exiting from the electrode is less selective and therefore richer in radioactive isotopes.

In Figure 7.13 the number of LOI for each sought mass is reported. It results that the most requested masses are around M=81 u, 95 u and 132 u. On the basis of Figure 7.13, the isotope masses M and the corresponding number of devoted operation cycles likely foreseen for the first year of SPES activity can be:
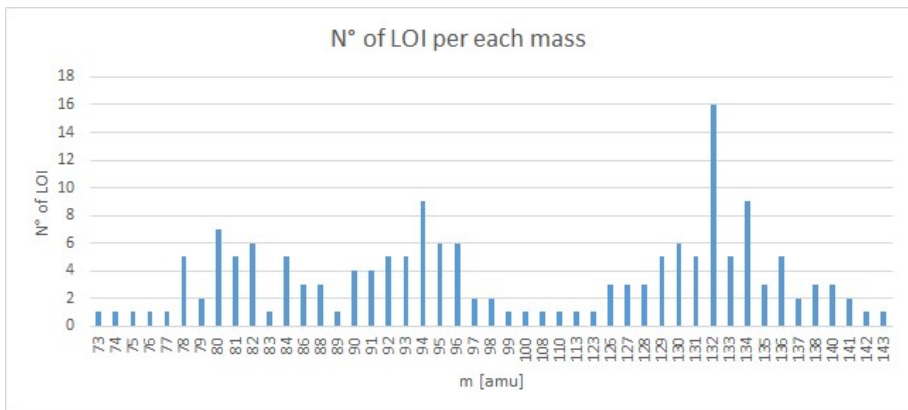
Figure 7.13: Number of LOI's for the production of a certain mass.

- mass M=82 u: 3 complete irradiation cycles;

- mass M=95 u: 3 complete irradiation cycles;

- mass M=132 u: 4 complete irradiation cycles;

for a total number of 10 cycles.

7.3.4 External exposure assessment due to the Wien Filter deflection

The ambient dose equivalent rate dH*(10)/dt, due to the ions deflected by the Wien Filter and deposited on the RIB line structures, is calculated in proximity of the RIB line of the SPES Front-End, at different times during the SPES activity.

The ions deposit on the Wien Filter electrodes and on the elements of the RIB line such as the steerers and the separation slits located before the second diagnostic box. Their deposition position depends on the sought mass of the ion to be produced. Therefore, the dose rate calculated in the same points of the bunker, in proximity of the RIB line, is expected to be different for each isobaric beam produced. Furthermore, also the temporal evolution of the dose rate changes with the deposition position, since different isotopes means different half-lives and different gamma energies.

The calculation of the dose rate has to be performed in the hypothesis of one year SPES activity, taking into account the LOI's requests from the users on the RIBs to produce. However, according to the criteria set out in Section 7.3.1, the lower mass in the deposition ion source of Figure 7.9 is M=89 u (excluding ^{7}Be). This means that masses lower than M=89 u have

point N.	$t_c = 15\ d$ (μSv/h) M=95 u	$t_c = 60\ d$ (μSv/h) M=95 u	$t_c = 1\ y$ (μSv/h) M=95 u	$t_c = 15\ d$ (μSv/h) M=132 u	$t_c = 60\ d$ (μSv/h) M=132 u	$t_c = 1\ y$ (μSv/h) M=132 u
15	$1.6 \cdot 10^3$	$1.3 \cdot 10^3$	68	$4.6 \cdot 10^3$	$4.0 \cdot 10^2$	38
16	$3.1 \cdot 10^3$	$2.4 \cdot 10^3$	$1.3 \cdot 10^2$	$1.8 \cdot 10^4$	$1.6 \cdot 10^3$	$1.2 \cdot 10^2$
17	$3.4 \cdot 10^4$	$2.7 \cdot 10^4$	$1.4 \cdot 10^3$	$6.7 \cdot 10^4$	$5.9 \cdot 10^3$	$7.2 \cdot 10^2$
18	$3.9 \cdot 10^3$	$2.9 \cdot 10^3$	$1.5 \cdot 10^2$	$7.2 \cdot 10^3$	$6.5 \cdot 10^2$	72

little effect on the dose assessment, compared to higher masses. Therefore, the dose rate assessment has been performed only for two sought masses: M=95 u and M=132 u.

Figure 7.14 and Figure 7.15 show two horizontal meshes of ambient dose equivalent rate, calculated for the masses M=95 u and M=132 u respectively. The dose rate is calculated in the SPES production bunker, after 15 days of cooling time following 3 irradiation cycles for the mass M=95 u, and 4 irradiation cycles for the mass M=132 u. The red circles evidenced in the figures represent the most extreme positions of Figure 6.10 along the RIB line, those furthest away from the TIS unit, where larger contributions to the dose rate are expected. In Figure 7.16 the corresponding vertical meshes crossing the RIB line are shown.

Table 7.2 shows the values of dH*(10)/dt in the positions evidenced in Figure 7.14 and Figure 7.15. They are calculated at different cooling times following 3 irradiation cycles for the mass M=95 u and 4 irradiation cycles for the mass M=132 u.

Looking at the dH*(10)/dt meshes of Figure 7.14 and Figure 7.15, one can see that, for both sought masses, the highest dose values correspond to the deposition positions, according to Figure 7.12. For the mass M=95 u the isotopes deposit mostly on the electrodes of the Wien Filter and on the
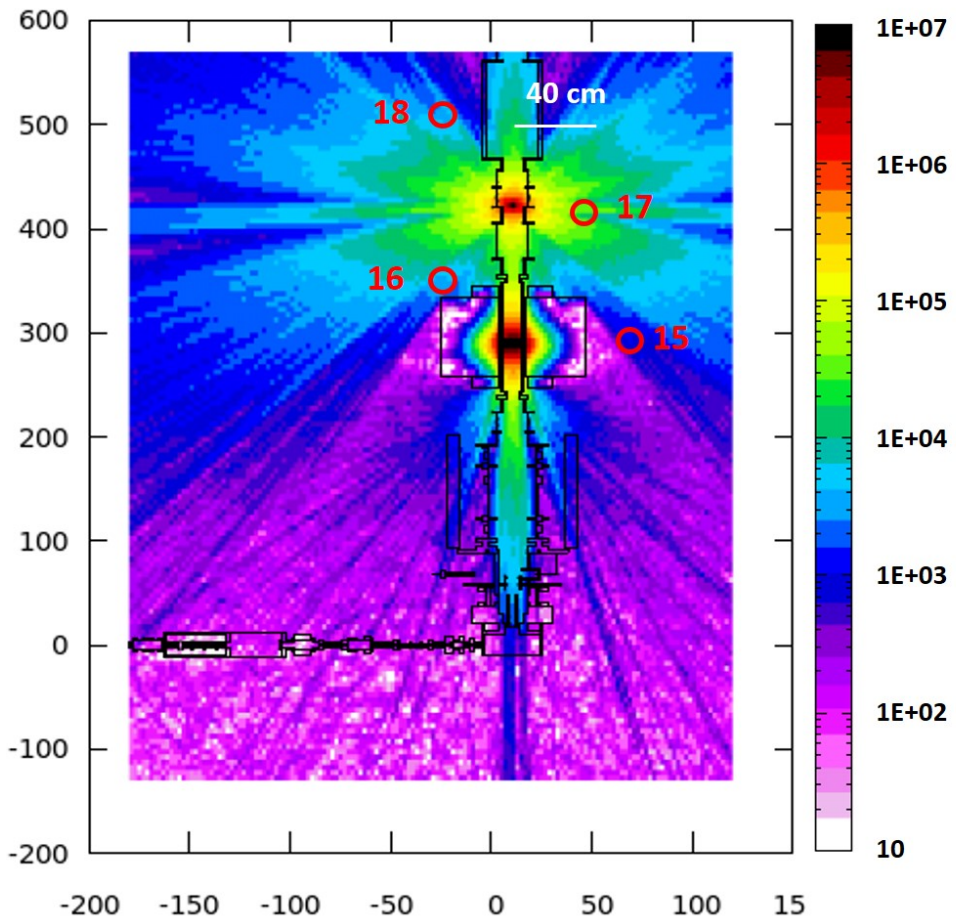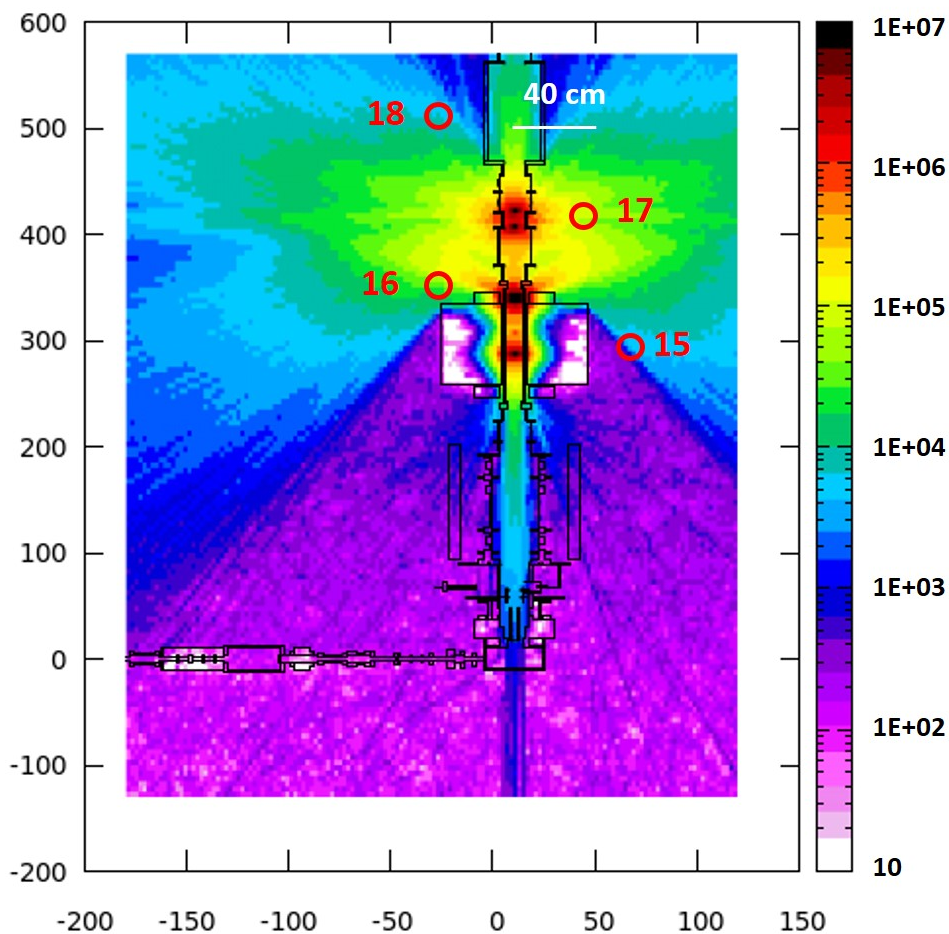
Figure 7.14: *Horizontal mesh of dH*(10)/dt in the SPES production bunker due to isotope deflection away from the RIB line, calculated for the mass M=95 u passing the selection of the Wien Filter. The mesh is calculated after 15 days of cooling time following 3 irradiation cycles. Red circles represent sampled positions on the mesh plane (150 cm). Units of the color scale are in μSv/h.*

Figure 7.15: Horizontal mesh of dH*(10)/dt in the SPES production bunker due to isotope deflection away from the RIB line, calculated for the mass M=132 u passing the selection of the Wien Filter. The mesh is calculated after 15 days of cooling time following 4 irradiation cycles. Red circles represent sampled positions on the mesh plane (150 cm). Units of the color scale are in μSv/h.
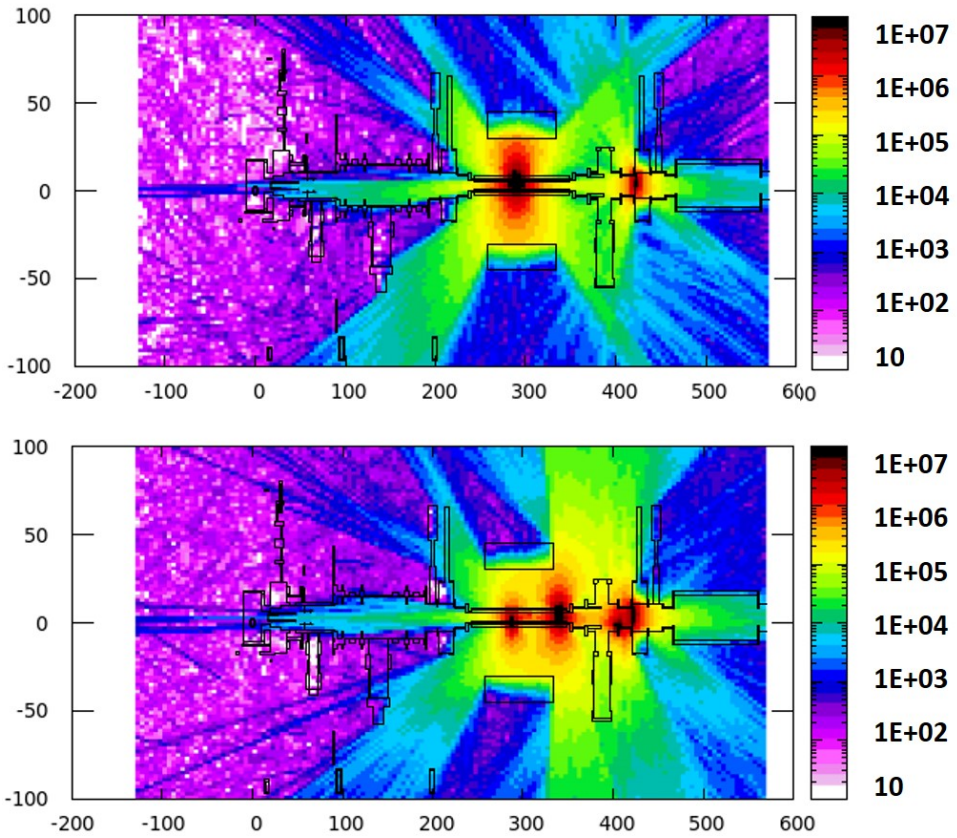
Figure 7.16: Meshes as in Figure 7.14 (top) and Figure 7.15 (bottom), but calculated on a vertical section crossing the production target along the RIB line.

slits of the second diagnostic box, while for the mass M=132 u they deposit also on the coupling flanges at the exit of the Wien Filter and of the steeres.

The most critical position for both masses is in point 17, near the slits. It presents a dose rate level about 10 times higher than the values of the other points, and maintains abundantly above 1 mSv/h until long cooling times (60 days or more). The same thing happens for the mass M=132 u in point 16, near the exit flange of the Wien Filter.

Furthermore, both meshes show that the Wien Filter constitutes a good shield for the gamma radiation, thanks to the high density of the iron and copper components. In fact, in point 15, the closest to the Wien Filter, the dose rate level at all cooling times is lower by more than a factor of 10 compared to that of point 17. A similar behavior is found in point 18, close to the second triplet, further away from the main structures of the RIB line where the ion deposition occurs.
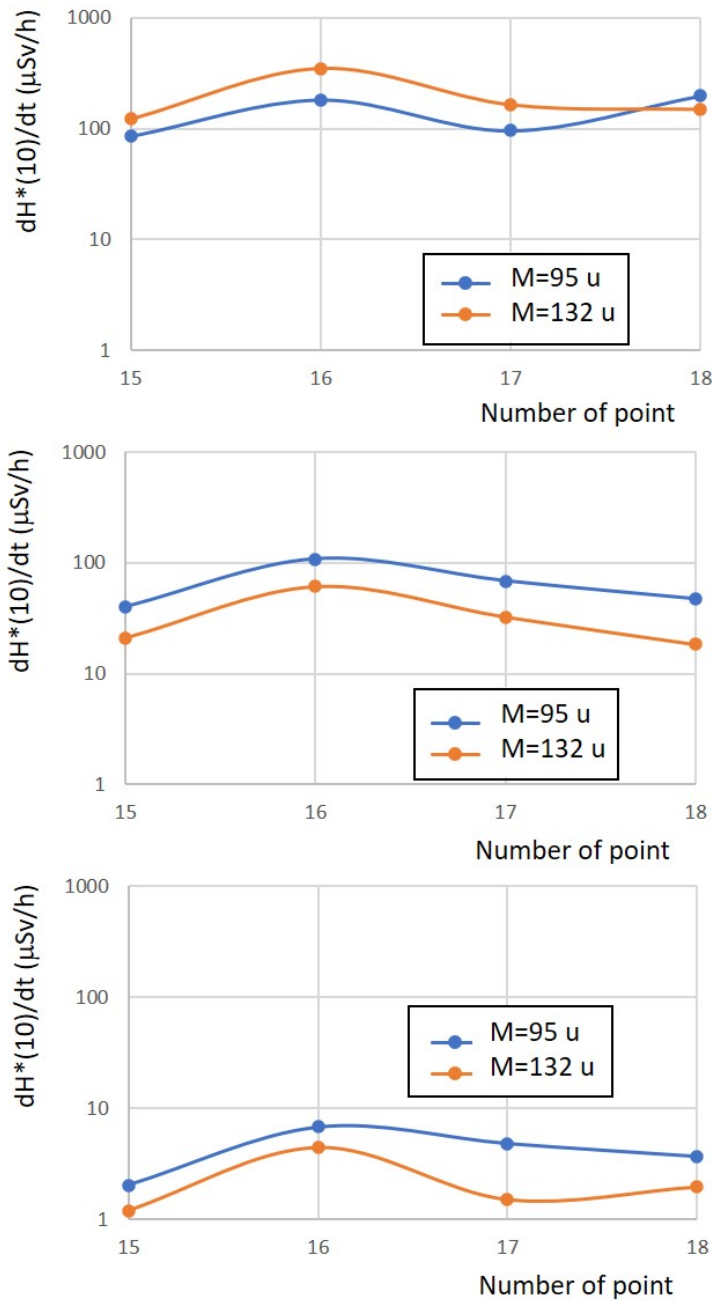
Figure 7.17: Values of dH*(10)/dt calculated as in Table 7.2: after 15 days (top panel), 60 days (medium panel) and 1 year (bottom panel) cooling time. In blue the values for the mass M=95 u, in red the ones for the mass M=132 u.

Figure 7.17 shows the values reported in Table 7.2 for the positions close and beyond the Wien Filter. At 15 days cooling time the dose rate values for the mass M=132 u (red curve) are higher in average than those for the mass M=95 u, probably due to the higher number of operation cycles for the mass M=132 u, with respect to the mass M=95 u. However, at longer cooling times the situation is reversed, in fact the dose rate values are higher for the mass M=95 u. This difference in the time evolution of the dose rate is due to the different half-lives of the isotopes stopped on the RIB line structures, for each desired mass.

To assess the dose rate until one complete year of SPES activity, that is 12 months from the start of the first irradiation cycle, and to stay on the safe side, an additional group of 3 complete irradiation cycles has been considered for the mass M=95 u. Therefore, the total operation time set in FLUKA for 10 operation cycles is: 6 consecutive irradiation cycles for the mass M=95 u, followed by 4 complete irradiation cycles for the mass M=132 u. The cooling times considered for the two sought masses are 6 months for M=95 u and 2 months (=60 days) for M=132 u, the last produced.

The contributions to the dose rate are calculated separately for each sought mass, and then added together to assess the whole dose rate caused by all isotopes deposited on the RIB line due to the Wien Filter deflection in one year activity. The result of this procedure is presented in Table 7.3 for the same positions of Table 7.2. These values of the ambient dose equivalent rate dH*(10)/dt, calculated for a period of one year of SPES activity are comparable, as order of magnitude, with the value of 3 mSv/h found in [138] for radionuclide stopping at 1 m distance from the Wien Filter, after two years of extraction of the beam of ^{132}Sn.

7.4 Global exposure assessment due to the irradiated Front-End system

7.4.1 Preliminary considerations

According to the ICRP recommendations (see Section 4.3), the assessment of the dose rate for occupational exposure allows strategies to plan and optimize maintenance interventions on the Front-End structures to be implemented. Such operations can be, for example, the removal of an exhausted electrode or of the Wien Filter at the end of their continuous permanence on the Front-End, but also ordinary inspections in proximity of the beam lines or maintenance of critical structures of the Front-End.

The global gamma dose rate is assessed after one year irradiation in

140

Table 7.3: Values of the ambient dose equivalent rate dH*(10)/dt, due to the iso-
topes deflected by the Wien Filter and deposited on the RIB line structures. They are
calculated after 6 consecutive irradiation cycles for the mass M=95 u, followed by 4
complete irradiation cycles for the mass M=132 u. The sum of the two contributions
is reported too. The cooling times considered for the two desired masses are 6 months
for M=95 u and 2 months for M=132 u. Units of dH*(10)/dt are μSv/h. Monte Carlo
errors are less than 1%.

point N.	$t_c = 180\ d$ (μSv/h) M=95 u	$t_c = 60\ d$ (μSv/h) M=132 u	(μSv/h) Sum
15	$6.4 \cdot 10^2$	$4.0 \cdot 10^2$	$1.0 \cdot 10^3$
16	$1.4 \cdot 10^3$	$1.6 \cdot 10^3$	$3.0 \cdot 10^3$
17	$1.3 \cdot 10^4$	$5.9 \cdot 10^3$	$1.9 \cdot 10^4$
18	$1.4 \cdot 10^3$	$6.5 \cdot 10^2$	$2.0 \cdot 10^3$

the SPES production bunker. One year is a typical time-line of activity of
the facility, before the ordinary annual technical stop, where maintenance
operations on the Front-End system structural components are foreseen.

High values of dose rate are the consequence of the presence of sev-
eral radiation "hot spots" inside the bunker; in this thesis the activation of
the structures of the Front-End system, induced by interactions of primary
protons with the Front-End elements and by fission neutrons produced in
the production target, as well as by the deposit of ions in the RIB channel
devices, have been considered.

In a "source-related" approach applied to planned exposure situations, as
the SPES project, each of these radiation sources contributes independently
the ones from the others to the individual dose. Therefore, the worker that
enters in the bunker for ordinary (end extraordinary) maintenance opera-
tions is exposed to the sum of doses coming from all these radiation sources,
calculated separately.

The first contribution to the gamma dose rate, due to the proton and
neutron induced residual activation of the Front-End materials, has been
discussed in Chapter 6. Different times during the life cycle of the facility
have been considered for the dose rate calculation, initially performed using

both MCNPX and FLUKA tools for Monte Carlo simulations, with the same geometry model. More recent calculations have been then performed with FLUKA, including the positions close to the component structures of the RIB line more distant from the TIS unit (see Figure 6.10).

The second and third contributions, discussed in the present chapter, have been calculated for all positions of Figure 6.10, and are reported for the most critical positions in Section 7.2.3 and Section 7.3.4, for the case of the ion extraction electrode and of the Wien Filter respectively.

For planned exposure situations, the ICRP "source-related" restrictions to the doses that all individuals may tolerate, coming from a particular group of sources, are the "dose constraints". Otherwise, separate restrictions to the overall doses from all sources, called "individual-related", are applied to several categories of exposure, for example occupational and public, in the form of "dose limits". The dose constraint prevents possible iniquities in the protection process to occur, for example the possibility that some individuals are subject to much more exposure than the average. Therefore, it has always to be lower than the pertinent dose limit.

The dose limits at the LNL laboratories depend on the Italian law on the radiation protection [82], that limits the effective dose to 1 mSv/year for unexposed workers, the same as for the public, and to 20 mSv/year for exposed workers (see Table 4.5). Moreover, the internal regulation of the laboratories has assumed, as main radiation protection objective on all SPES activities, the limitation of the effective dose to 0.5 mSv/year for unexposed workers and to 5 mSv/year for exposed workers [143, 144].

For individual practices, conservative dose rate constraints must be adopted with respect to legal limits. There is no absolute value for the maximum acceptable dose rate during the maintenance operation. It depends on the need for intervention (indispensable, urgent, desirable, delayed, etc.), on the protocol adopted for the specific operation (maximum time of permanence in the bunker, minimum distance from the most critical elements, use of PPE, presence of protection shields, etc.), on the frequency in one year (times for each maintenance intervention, possible splitting of the interventions over several workers).

Reasonable dose rate constraint values can be deduced starting from those adopted at other RIB facilities, as for example HIE-ISOLDE at CERN. Dose limits, in terms of effective dose, and dose rate constraints are shown for CERN in Figure 7.18, for each specific area of work (controlled, supervised and non-designated).

As underlined in Section 4.2.3, the observance of the limit to exposure from external radiation, in terms of effective dose, is ensured by limiting

Figure 7.18: Summary of the classification of non-designated areas and radiation areas at CERN, with relative dose limit and dose rate constraints [81].

the ambient dose equivalent H*(10). For example, the access to areas with dH*(10)/dt values higher than 100 mSv/h is never allowed, apart from exceptional situations (not related to the SPES project) such as the saving of life or the prevention of a serious disaster.

The dose rate constraints for each maintenance intervention in the SPES production bunker are decided by the radiation protection expert, with the involvement of the operating management and of the workers. At the underground level of the SPES building, the production bunker, as well as the areas connected to the handling and storage of the exhausted targets (see Chapter 8), are classified as a controlled area. Criteria for the access for the personnel in controlled area, in presence of gamma radiation fields, are indicated in [144] for the different types of SPES interventions.

In general, a dose rate of a few hundred μSv per single ordinary intervention is judged reasonable, supposed that the intervention is necessary, infrequent and of limited duration. Otherwise, if maintenance interventions that incur higher doses, up to 1 mSv and above, are necessary, the subdivision of the exposure over several individuals can be considered with the purpose of optimizing the radiation protection. In these cases, in addition to the constraints on the individual dose rate, also the constraints on the collective dose rate for all workers during the given operation have to be taken into account.

7.4.2 Final results

In Figure 7.19 the single contributions to the ambient dose equivalent rate dH*(10)/dt in the production bunker and their sum, calculated on all the positions of Figure 6.10, are shown for a typical scenario of one year of SPES activity in the production bunker (10 cycles and 60 day cooling time after last irradiation). The overall contribution to the ambient dose equivalent rate dH*(10)/dt after one year irradiation is always abundantly less than 100 mSv/h. However, to optimize the protection of the worker during different maintenance operations, the reduction of the doses and of the dose rates to levels as low as reasonably achievable (ALARA) would be ensured.
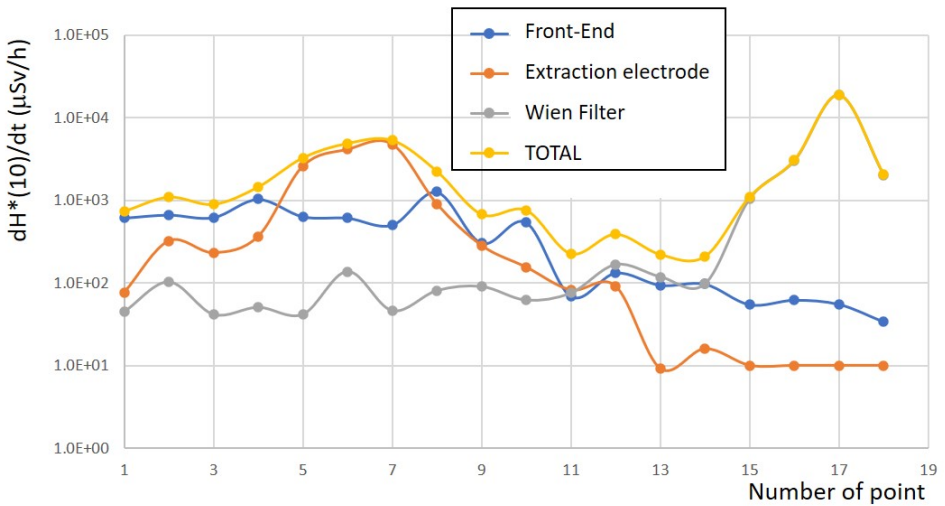
Figure 7.19: Contributions to the ambient dose equivalent rate dH(10)/dt from the Front-End residual activation (in blue), from the ion deposition on the extraction electrode (in red) and on the Wien Filter (in gray), and their sum (in yellow). The values are calculated on all positions of Figure 6.10, after 10 irradiation cycles and 60 day cooling time.*

The dose rates due to Front-End residual activation are generally less than about 1 mSv/h; they present the highest values near the PPB line, due to proton activation of the graphite of the collimators, as well as in proximity of the TIS unit and of the first part of the RIB line, due to neutron activation of the surrounding structures. In points 1-4 this contribution is predominant.

In points 5, 6 and 7, close to the TIS unit and to the extraction electrode, the contribution to the dose rate due to the ion deposition on the electrode

predominates. It is higher by a factor of 10 than the one due to the Front-End residual activation, and by a factor of 100 than the one due to the ion deposition on the Wien Filter and on the RIB line elements downstream of it. For these positions, the values of dH*(10)/dt are a few mSv/h. In the worst case, in point 7, the dose rate value due to the extraction electrode is 4.8 mSv/h (see Table 7.1).

The dose rate due to the isotopes deflected by the Wien Filter and deposited along the RIB line is generally not much above 100 μSv/h. However, in points 16 and 18 located in proximity of the Wien Filter and downstream of it, the dose rate values are above 1 mSv/h and their contribution predominates. Furthermore, the last column of Table 7.3 shows that in point 17, near the separation slits of the diagnostic box, the dose rate is about 20 mSv/h. For the CERN radiation protection policy, this is a value associated to a "high radiation" dose rate for a controlled area (see Figure 7.18).

Due to the high levels of gamma radiations, maintenance interventions close the Front-End system, both ordinary and extraordinary, are in general critical. The presence of lead shields near the beam collimators (see Chapter 6) allows the surrounding dose levels to be kept lower than 1 mSv/h. However, the dose rate levels are still high enough to request a careful planning of the interventions along the PPB line.

The times requested for the ordinary interventions near the extraction electrode have also to be carefully planned. For an access around point 7 close the ion extraction electrode, the exposure level is superior to the dose rate indicated in Figure 7.18 for a "limited stay" in controlled area (2 mSv/h). After 10 irradiation cycles and 60 day cooling time, a permanence of 10 min close to the ion extraction electrode causes to the operator a dose of about 800 μSv, a value considered too high for a single intervention. For this reason, the replacement of the extraction electrode may be required before carrying interventions in the surrounding areas. Moreover, Figure 7.8 shows a tendency towards the saturation of the dose rate after five irradiation cycles. This is an important information to plan possible early extraordinary intervention near the extraction electrode, especially if they occur in the first months of the annual production.

The possibility of a manual or semi-manual handling for the extraction electrode depends also on the distance of the operator from the electrode during the removal operation. For example, for an ordinary removal operation, after 10 cycles of operation and 60 days of cooling, the value of dH*(10)/dt in point H at 2 m distance from the electrode is about 370 μSv/h. Prudently assuming to add another 100 μSv/h, due to the residual activation of the Front-End, the dose rate results still lower than 500 μSv/h. Therefore, even

if the use of a remote handling system for the removal of the extraction electrode is highly recommended, the design should include the capability for manual intervention or assistance in case of problems with the system, as long as the extraction operation lasts less than 20 min and the operator stays at least two meters away from the electrode tip.

Finally, extreme caution has to be used in planning maintenance operations in the last part of the RIB line, downstream of the Wien Filter and especially in areas close to the second diagnostic box. All possible strategies to reduce the residual dose to which the worker is exposed have to be adopted.

In conclusion, it is worth emphasizing that all the calculated values of the ambient dose equivalent rate are overestimated for the sake of prudence. For example, in the building of both isotope deposition sources, unitary release efficiency is set. Furthermore, all the refractory isotopes that transmute in non-refractory isotopes in less than 15 days are considered, as if they are generated in the target at the beginning of the irradiation period.

For the isotope deposition source on the extraction electrode, the ionization efficiency of the ion source is set to zero (no atom is ionized). Furthermore, the fraction of isotopes that are considered to enter in the solid angle covered by the electrode tip (about 6%) contains also the beam passing through the input hole of the electrode.

The deposition source constituted by the ions deflected by the Wien Filter and deposited along the RIB line is built considering an ionization efficiency evaluated with the SPIS ion source, that is the least selective. Moreover, volatile isotopes are assumed to remain trapped in the RIB line metal structures for about one year before being released. By simulating the annual exposure due to the ion deposition on the RIB line devices downstream of the Wien Filter, the masses selected by the Wien Filter (M=95 u and M=132 u) and the times of production are set to produce the highest dose values.

For all these reasons, it is reasonable to assume that the calculated values of ambient dose equivalent rate are overestimated of at least a factor two. Anyway, the ALARA approach has to be used to decide the strategy to adopt for the maintenance interventions in the different areas of the production bunker.

Chapter 8

The life cycle of the Target and Ion Source system

8.1   Introduction

In Chapter 6 and Chapter 7 the study of the residual radioactivity in the SPES production bunker has been illustrated. The radioactivity is due to the activation of the Front-End system structures due to the proton and neutron fields and to the radionuclide deposition along the RIB line.

During the facility operation period, the activation of the Front-End components and the consequent ambient dose equivalent rate progressively increase, due to the accumulation of medium-long lifetime radioisotopes, as shown in Figure 6.12. Some components, such as the ion extraction electrode, are periodically replaced due to their intense radioactivity accumulation and to the growing risks of failure of performance. More in general, the total or partial replacement of the Front-End system is planned after several years of activity of the SPES facility, also to ensure the full efficiency of the system and to limit the damage due to wear on the mobile mechanical components.

Conversely, the target chamber has a much more limited life cycle and must be replaced after each irradiation cycle, due to the thermomechanical stresses and to the intense mixed neutron and photon radiation fields present during the activity periods of the facility. The exhausted Target and Ion Source system (TIS unit) is foreseen to be removed from the Front-End every 30 day operation cycle: 15 days of irradiation and other 15 days of cooling down, necessary for the residual radioactivity of the target to decrease enough to allow for its extraction. After removal out of the Front-End, the TIS unit is stored in a temporary storage for a few years, until the

final disposal.

The handling operations on TIS unit during its life cycle, from the Front-End removal after irradiation until the final disposal, is the second case study addressed in the present thesis, with particular emphasis on the concerns of radiation protection.

Figure 8.1 illustrates the area of the underground floor of the SPES building at LNL, where the production of RIBs takes place. The areas in which the handling operations of the TIS unit are foreseen are the following: the production bunker A6, the area containing the Front-End system; the pre-bunker A7 that isolates the other areas from the radiation area A6; the external corridor A8b and the temporary storage of the exhausted target units A8a. All production, handling and storage areas are classified as controlled areas.
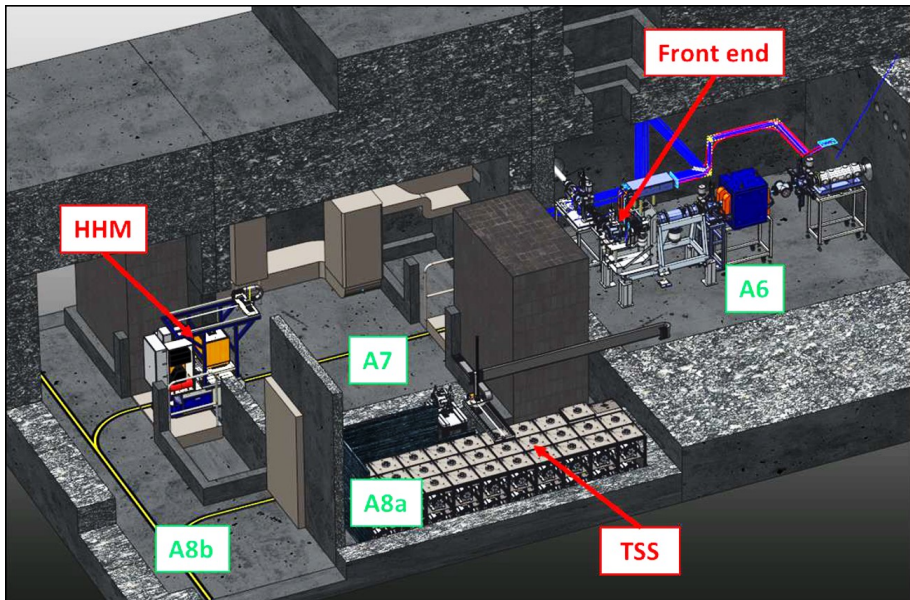
Figure 8.1: Underground floor of the SPES building, with evidenced the areas involved in the TIS unit handling operations.

The life cycle of the TIS unit consists of several steps, the last of which differs according to the final treatment to be performed on the TIS unit [145]. The cycle starts from the preparation of the target material and from the target chamber assembly, performed in dedicated laboratories on the ground floor of the SPES building. The transport of the TIS unit from the laboratories to the bunker A6 at the underground floor follows. Then it is installed on the Front-End system to be irradiated. After the irradiation, the TIS

unit is pulled out from the Front-End system and it is transferred to the temporary storage A8a, for a long cooling down period. Finally, the TIS unit is extracted from the storage system and can undergo different treatments:

- it may be reused for a second irradiation;

- it may be reassembled on the Front-End and heated by joule effect to extract long-lived radioisotopes;

- it may be disassembled in a hot cell, with separation of the various parts for possible reuse of some of them. In particular, the target material can be radiochemically treated to extract useful radioactive isotopes still present. The materials that can no longer be used are then sent to specialized companies for subsequent treatments.

In Figure 8.2 the scheme of the life cycle of the TIS unit is illustrated.
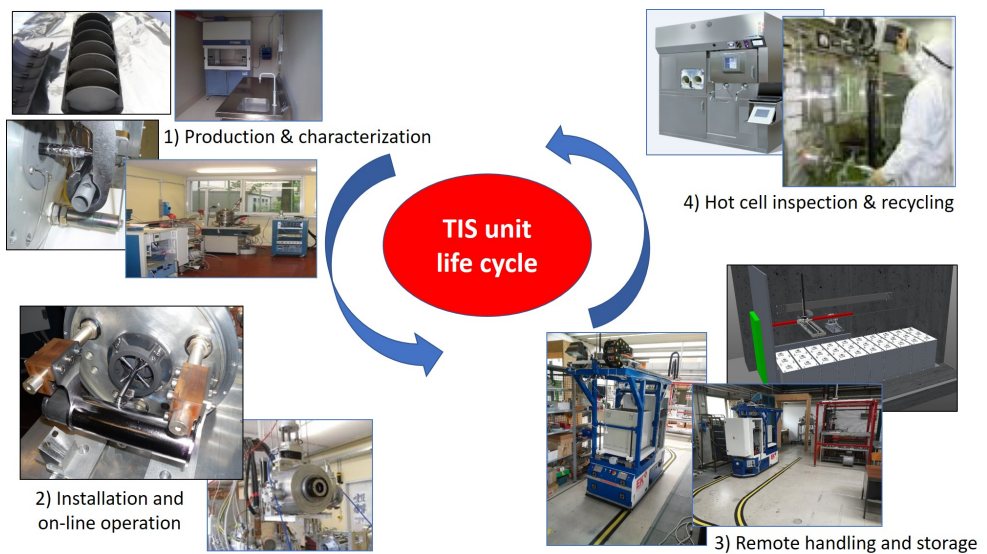
Figure 8.2: Scheme of the TIS unit life cycle.

In the ICRP source-related approach, all the radiation "hot spots", throughout the main handling operations of the TIS unit during its life cycle, have to be considered.

The first step of the TIS unit life cycle consists in preparing the target to be subsequently irradiated. In the case of non fissile targets, this step doesn't represent a problem from the radiation protection point of view. On the other hand, all assembly operations of uranium carbide targets must be

carried out with great caution to avoid the risk of surface contamination by uranium oxide powders [143]. It is for this reason that the laboratory for the preparation of the TIS units is defined as a controlled area. However, this issue will not be investigated because it is out of the scope of the present thesis.

All the next steps of the TIS unit life cycle can concern radiation exposure for the personnel during the handling operations. The radiation "hot spots" are located in different working areas of the SPES building.

The most critical area is the production bunker A6, for the presence of the activated Front-End system. However, the positioning and removal of the TIS unit in the bunker are performed by an automatic system without any human intervention. Only in the first phase of the activity of the apparatus and in some particular irradiation conditions, manual handling operations of the irradiated target can be allowed (see Section 8.3).

The other very critical area is the temporary storage A8a, due to the presence of a large number of activated TIS units for long cooling periods. The TIS unit is transported here after the irradiation, always in an automatic way. However, in the corridor A8b external to the storage A8a, passage of unexposed workers is allowed when no TIS unit is in transit. Moreover, periodical operations (see Section 8.5) and potential maintenance interventions are carried out inside the area A8a.

The final transportation from the temporary storage to the hot cell, or to the other areas for a subsequent treatment, can take place manually with the use of a trans-pallet and of a trolley equipped with a lead sarcophagus. The TIS unit is placed inside the sarcophagus after being extracted from the temporary storage area with the trans-pallet. The sarcophagus is positioned using the trolley in the access area of the hot cell, for the subsequent operations. Mobile hot spots accompany the path travelled by the operator during the handling sequences in presence of a shielded TIS unit, after the extraction from the A8a room.

For all cases considered, a dose assessment has been performed with FLUKA Monte Carlo code, to develop proper strategies for the radiation protection of the workers, depending on the type of exposure situation and in relation to the different SPES production phases. FLUKA has been also used to design the shielding structures for the exhausted TIS unit handling operations. All these calculations are discussed in detail in the next sections.

8.2   The target chamber handling systems

Several handling systems have been designed for the TIS unit during the different steps of its life cycle [11]. They are used to transport the TIS unit inside and outside the irradiation bunker, to couple and to uncouple it to and from the Front-End system, then to place it in the temporary storage and, finally, to extract and move it towards the hot cell laboratory. In order to increase their reliability, the various systems are designed in such a way as to have redundancy in case of failure of one of them. Some of these systems are shown in Figure 8.1.

The primary handling device of the TIS unit is the "Horizontal Handling Machine" (HHM). It is formed by an Automatic Guide Vehicle (AGV) to move the TIS unit to and from the handling area, and by a cartesian system to interface it with the hosting structure, for example the Front-End system, once the AGV is in position. The cartesian system makes it also possible to lift and lower the chamber, to extract it from or insert it into a shielded 2.5 cm lead sarcophagus. The HHM vehicle is shown in Figure 8.3.
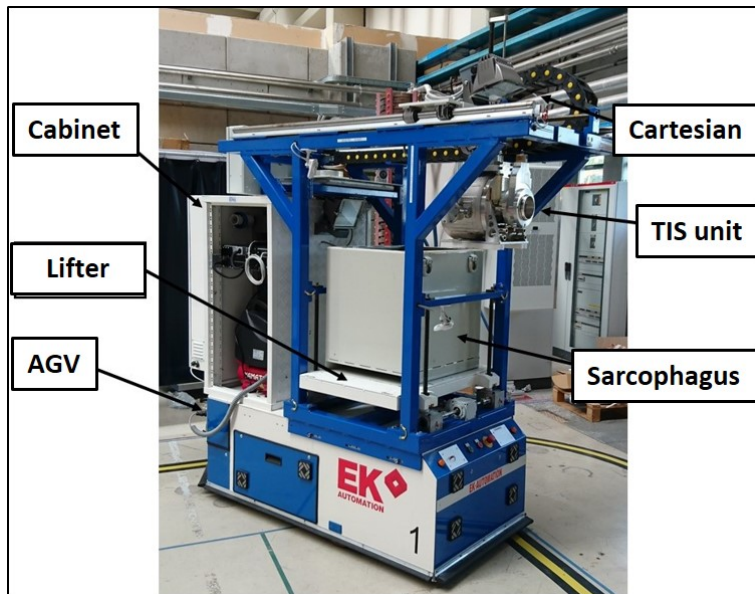

Figure 8.3: The Horizontal Handling Machine.

The HHM operates on batteries and communicates with a user interface by wireless communication. This makes it possible to reach various destinations in a completely automated way, from the bunker during the TIS unit positioning to the temporary storage during the insertion of the TIS unit.

Since the HHM is a complex vehicle that works in hostile environment, possible damage of the main control elements and of the cartesian system has to be taken into account. The primary cause of failure is attributable to the exposure of the main HHM elements to the gamma radiation coming from the irradiated TIS unit and from the activated structures of the Front-End system.

Therefore, in case of emergency or failure of the automatic HHM system, a "Manual Handling Machine" (MHM) driven by manual operation, could be considered as a backup solution, depending on the specific irradiation conditions. The MHM can be used both inside the bunker and near the temporary storage; it is furnished with an emergency sarcophagus for the transport of the exhausted TIS unit. The MHM is described in Section 8.3.

8.3   Handling of the TIS unit in the production bunker

In ordinary SPES activities, the human interventions inside the bunker in presence of the exhausted TIS unit are excluded, due the high radioactivity of the target elements (mostly the UC_x disks). Therefore, the handling systems used in the A6 bunker, as the HHM machine, are totally automatized.

However, in the first SPES production phases, low energy and low intensity ion beams are planned to be produced using a proton beam of 40 MeV energy but with a reduced beam intensity of 34 μA. Silicon carbide (SiC) and uranium carbide targets having a reduced size (disk diameter 13 mm) will be used. Due to the reduced radioactivity of the production target, in these first production phases the MHM could to be utilized for the TIS positioning inside the bunker [63].

The machine may be provided with a lead shield with three leaded glass windows, which insure both the shielding from direct radiation and the visibility needed to complete the positioning operations during the TIS handling and extraction.

The upper windows allow the operator to drive the machine inside the A6 bunker, while the lower window, smaller and located about 1 m above the floor, is used to align and center the machine. The worker operates behind the shielding panel, at a minimum distance of 2 m from the TIS unit. The MHM is shown in Figure 8.4, upper panel [146].

To evaluate the possibility to use the MHM in the first operation phases, several FLUKA simulations have been performed. The Front-End model described in Section 6.2 constitutes the starting point for the simulation.
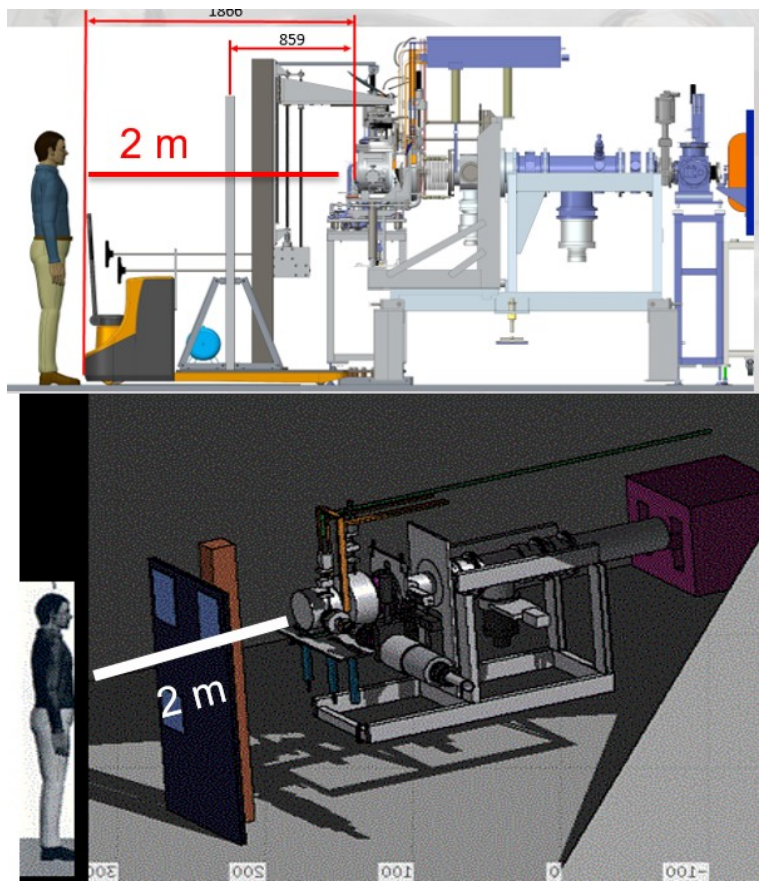
Figure 8.4: The Manual Handling system in the Front-End layout: CAD design (upper panel) and FLUKA model (bottom panel).

The proton source parameters are modified to match with the first phase requests: 40 MeV proton energy and 34 μA beam intensity. The target disks are brought closer to each other and their diameter is reduced to 13 mm. The materials considered for the target disks are silicon carbide and uranium carbide. A schematic design of MHM, supplied of the lead shielding panel, is added to the geometry model of the bunker. The FLUKA model of the MHM is shown in Figure 8.4, bottom panel.

An activation study has been set up to calculate the rate of H*(10) at the time of the TIS unit extraction from the Front-End, after 15 day of cooling after the end of the 15 day irradiation period. Different values of thickness of the shielding panel and size of the leaded glass windows have been tested in the code, with the criterion to optimize the design of the shielding panel, in terms of radiological protection and mechanical properties. Obviously, the calculation of the dose rate takes in account both direct and scattered radiation in the scored point.

In this first SPES production phase, the manual TIS removal operation inside the production bunker is allowed as long as the constraint of 150 μSv/h on the dose rate is respected. This dose rate constraint takes into account the frequency and the duration of the planned operation. In fact, the maximum annual dose received by a worker which carries out ten accesses of 15 min each, would be about 400 μSv. Such a value is less than 0.5 mSv, the annual value of effective dose assumed, for unexposed workers, by the internal regulation of the laboratories.

The first simulation set refers to a SiC target. Being the SiC not fissile, the radioactive impact of the target is expected to be much lower than the one foreseen with the UC_x target. In the former case, the possibility of a direct manual replacement of the target is considered. Therefore, the dose rate is calculated at different distances from the TIS unit, at contact (point 0), at 1 m (point 1) and at 2 m (point 2) from the TIS unit. Furthermore, the shielding panel is not introduced in the geometrical set-up of the bunker.

Figure 8.5 represents the behavior of dH*(10)/dt versus the cooling time, calculated for the three mentioned distances between the operator and the SiC target. The plot shows that the manual extraction of the TIS unit is not possible since, even after 15 day cooling time, the contact dose rates are higher than 900 μSv/h and decrease slowly. Conversely, at distances of one meter or more, the values of dH*(10)/dt after 15 day cooling time are lower than the dose rate constraint and at 2 m distance are less than 25 μSv/h. Therefore, the MHM can be used in this production phase, without any necessity to install a lead panel on the machine to shield the direct radiation.

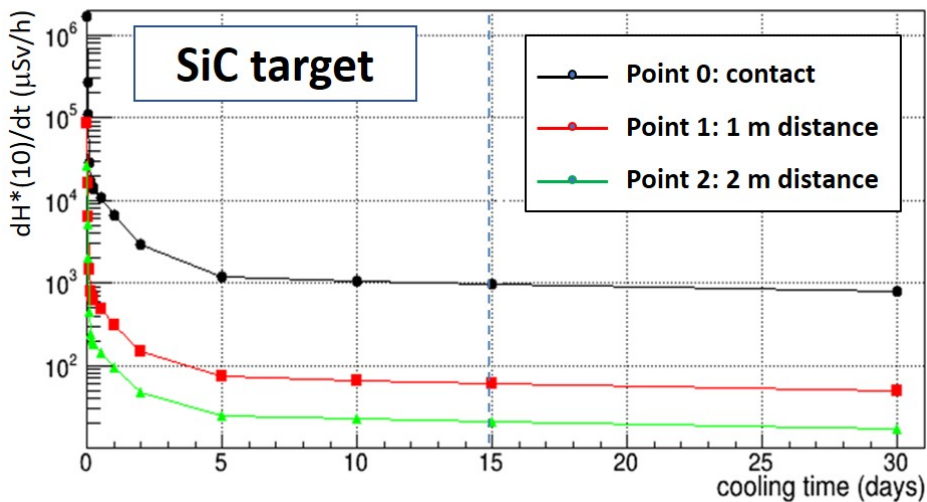The second simulation set describes the following production phase, in

Figure 8.5: Behavior of dH*(10)/dt in three points at different distances from the SiC target, during a cooling time period of 30 days.

which low intensity proton beams and small UC_x targets are foreseen to be used. Due to the high rate of fission reactions on the ^{238}U disks of the UC_x target (about 10^{12} fission/s in this SPES production phase), a shielding panel needs to be mounted on the MHM to reduce the exposure for the operator to acceptable levels, unlike the case of the SiC target.

Different configurations of parameters, representing the thickness of the panel and of the leaded glass windows, as well as the size and position of the windows, are evaluated. The final design adopted for the shielding panel, to optimize the dose and, at the same time, to guarantee the service functions of the MHM, is a 30 mm lead panel with three 40 mm leaded glass windows, suitably sized and positioned. These values take also into account the dose coming from the Front-End activation after a long period of irradiation (10 irradiation cycles), calculated with FLUKA in Section 6.5.3 and scaled for the difference in the proton beam intensity.

Figure 8.6 shows two meshes of ambient dose equivalent rate in the SPES production bunker, calculated with FLUKA on a horizontal and a vertical plane crossing the UC_x target, respectively. They refer to a complete irradiation cycle of 15 day beam on and 15 day cooling. The calculation has been performed implementing in the code a low intensity proton source, and with the final geometry of the MHM. In addition, the dose rate is calculated at different distances from the TIS unit, at 1 m behind the panel (point 1)
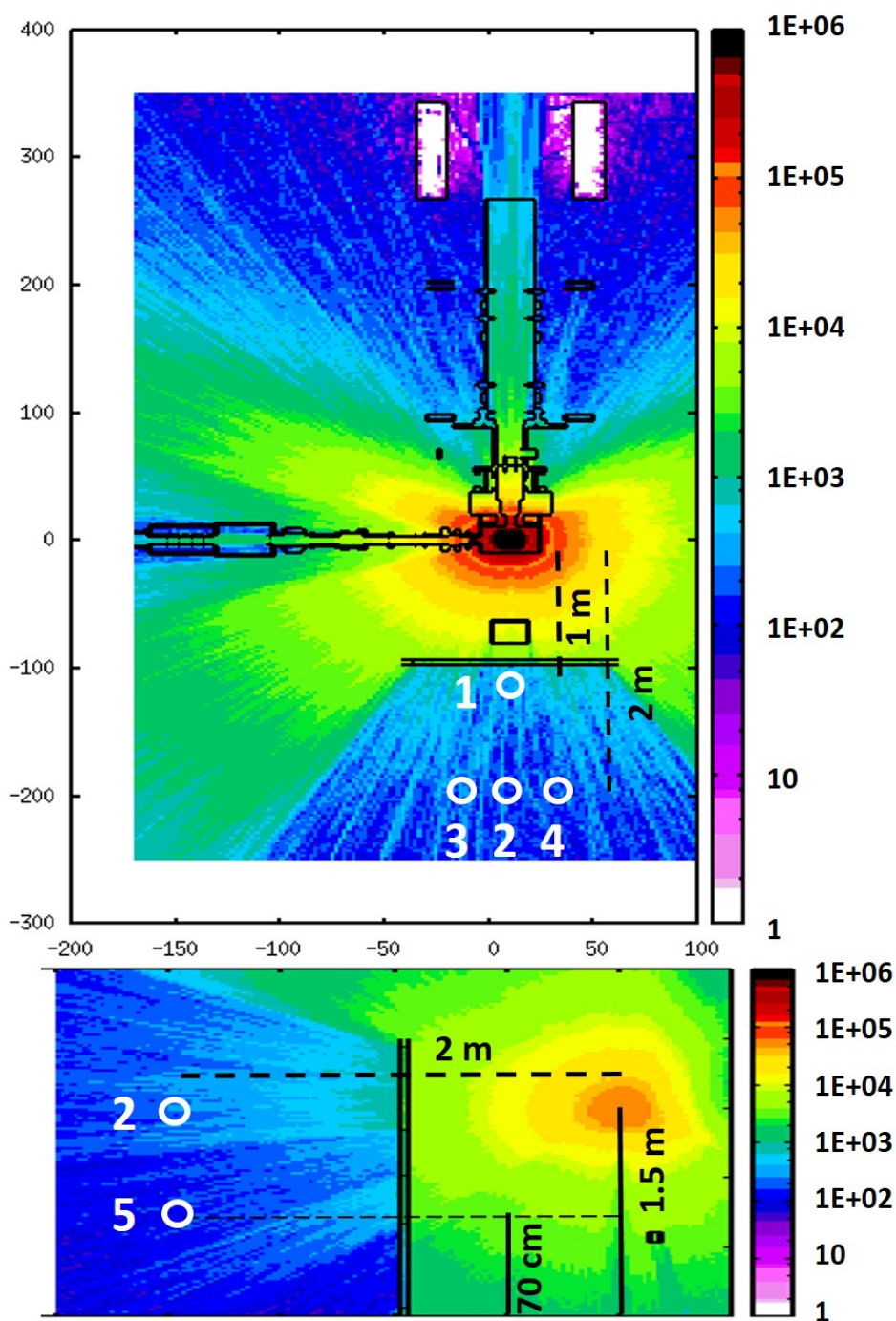
Figure 8.6: FLUKA spatial meshes of dH*(10)/dt in the SPES production bunker, on a horizontal (top) and vertical (bottom) plane crossing the UC$_x$ target, after a complete 30 day irradiation cycle at low intensity. The schematic design of the MHM is visible, with the positions for the dose rate calculation. Units of the color scale are in $\mu Sv/h$.

and at 2 m (points 2 to 5). All the positions are at the height of the source, except point 5, at 70 cm height. The dH*(10)/dt behavior versus the cooling time is illustrated in Figure 8.7 for all the positions considered in Figure 8.6.
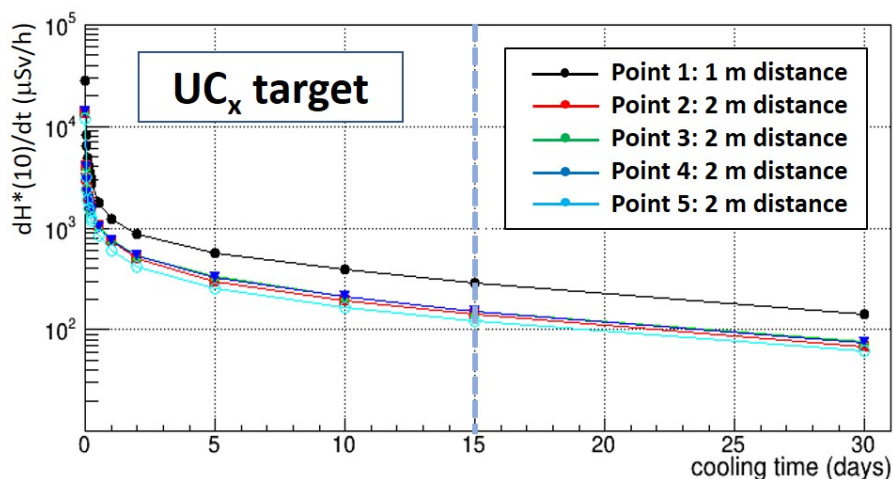
Figure 8.7: Behavior of dH(10)/dt in several points at 1 m and 2 m distance from the UC_x target and at different height, during a cooling time period of 30 days.*

As it appears from Figure 8.7, the designed panel ensures that the global value of dH*(10)/dt in the position occupied by the operator is below the dose rate constraint. The calculated dose rate is due to the presence of both the exhausted TIS unit and the Front-End system as activated after 10 irradiation cycles; note that the scattered component of the radiation coming from the source is not shielded by the panel.

Moreover, from the vertical mesh of Figure 8.6 appears that the height of the panel, fixed at 2 m in the FLUKA model of Figure 8.4, can be safely reduced a little, without increase the direct radiation in the position occupied by the operator.

8.4 The Temporary Storage System

8.4.1 The configuration of the temporary storage system

In ordinary SPES activities, with a 40 MeV energy and 200 μA intensity primary proton beam, full size UC_x targets will be used. The exhausted TIS unit replacement is planned to be performed in a completely automatic way, with the HHM device.

Given the SPES operation schedule, which plans the extraction of a TIS unit from the Front-End every 30 days, it is expected that about 50-60 highly radioactive TIS units will be produced over a few years. This time period matches with the period of activity of the SPES facility, before the total or partial substitution of the Front-End system structural components due to their progressive activation.

It is therefore necessary to design a temporary deposit that houses the exhausted TIS units extracted from the Front-End for several years, in order to allow the decay of short half-life radioactive nuclei and, therefore, reduce the level of radioactivity. After this period of time, the TIS units are extracted from the temporary storage and moved to the hot cell or to the other areas for a successive treatment.

The SPES "Temporary Storage System" (TSS) is hosted inside the room A8a (see Figure 8.1). It contains a storage rack with 54 locations, arranged in three rows of nine columns each, disposed on two levels. Each vertical compartment includes two superimposed TIS units and is closed on the top by a shielding cover.

The exhausted TIS unit is picked up from the Front-End system in room A6 (bunker) by the HHM device, inserted into the shielded sarcophagus and transported in a lateral corridor of the room A8a, passing through room A7 (prebunker) and room A8b (external corridor). The TIS unit is then positioned on a telescopic arm, composed of a translating and rotating support, that moves the chamber from the lateral HHM maneuver area to a Cartesian manipulator. After opening the upper cover, the Cartesian manipulator lowers the TIS unit in the storage area, inside the proper location, with a vertical movement.

The TSS system is illustrated Figure 8.8 [147], while the scheme of the storage sequence is described in [148].

The TSS represents an intense radiation source for the SPES building, being filled with all exhausted TIS units stored in a period of few years. Therefore, appropriate shielding elements have to be designed for the A8a room. Furthermore, several strategies for the TIS unit filling sequence inside the room are designed. The TIS units are lowered into the rack following the arrangement shown in Figure 8.9, based on the cooling time: a general reshuffling of the chambers already present is foreseen at each insertion, in order to position the last chamber as far away as possible from corridor A8b and from the internal maintenance areas.

To avoid potential dispersion in air of radioactive material escaped from the TIS units, two hermetically closed valves seal the TIS unit at the moment of the extraction from the Front-End. Moreover, the area A8a is maintained
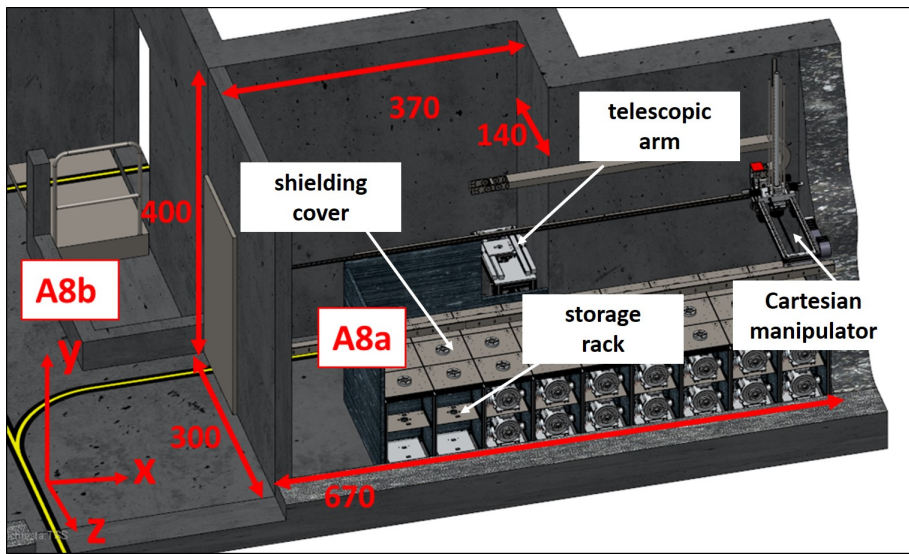
Figure 8.8: CAD image of the Temporary Storage System with the main elements. The distances are expressed in centimeters.

in depression at a lower pressure (-40 Pa) relative to the corridor A8b, which is at atmospheric pressure.

By Monte Carlo FLUKA calculations, a dose rate assessment has been performed to define the structure of the A8a room. Several configurations have been considered for the material and thickness of the external shielding walls and for the internal arrangement of the room.

The choice of the best configuration for the shielding of the A8a room has been made with the aim of optimizing the dose rate in the personnel access positions: in the external corridor A8b and in the internal area predisposed for TSS operations and maintenance. At the same time, logistical needs have been considered, such as facilitating vehicle entry and limitation of the weight of the lead shielding door. The simulation of the TSS is described in Section 8.4.2.

8.4.2 The FLUKA simulation of the TSS

A complex multi-step simulation of the TSS has been performed considering, as a safe approach, the most critical condition, that consists in a completely full storage, 5-6 years after the first beam start-up and with 54 TIS units housed inside, each one having different residual activity [63].

Considering the worst possible scenario, it is assumed that, for logistical reasons, the last TIS units entering the TSS are not placed at the lower
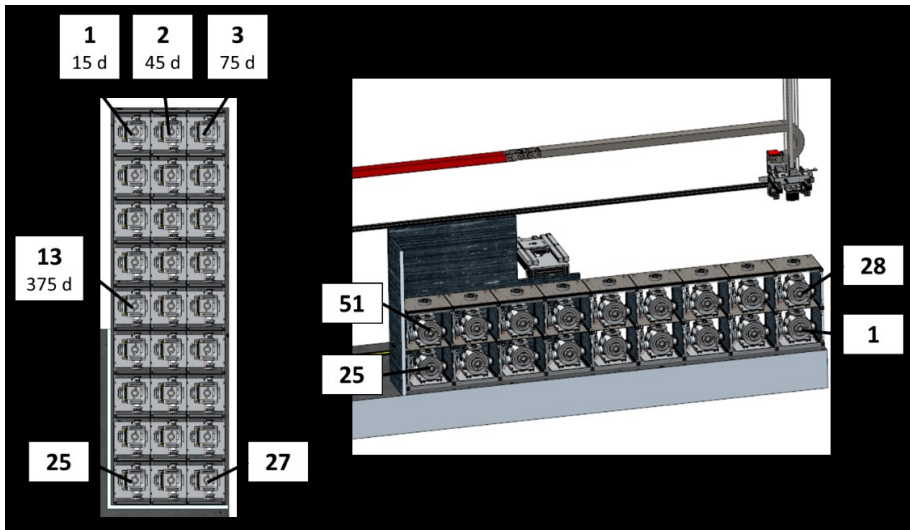
159

Figure 8.9: Arrangment of the TIS units in TSS, with full storage: three rows of nine columns each, disposed on two levels for a total of 54 units. On the left, a horizontal section on the lower level, on the right a vertical section. In the boxes the location order and the corresponding cooling time, in days, are indicated.

level, as suggested in Figure 8.9, but at the upper one.

The calculation procedure is based on the following steps:

1. characterization of the gamma spectrum emitted by every irradiated production target at the corresponding cooling time;

2. construction of the global gamma source in the TSS, starting from the contribution of all the TIS units stored at different cooling times;

3. building of the FLUKA model of the TSS;

4. calculation of the gamma ambient dose equivalent rate dH*(10)/dt inside and in the surrounding of the storage area.

Target gamma spectrum versus cooling time

After 15 days of irradiation of the UC_x target with high intensity proton beams, a large percentage of the produced radionuclides, just uder 90%, has decay half-lives less than 1 day, and an additional 10% has decay half-lives less than 1 month, as shown in Figure 8.10 [144]. Therefore, after 15 day cooling time, the residual radioactivity of the target is less than 10% of the radioactivity at the beam shutdown.
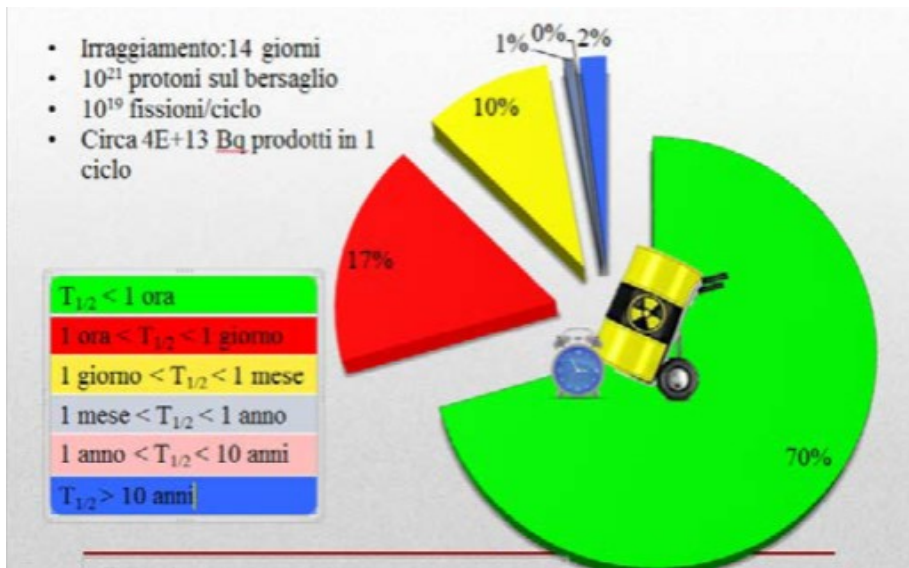
- Irraggiamento: 14 giorni
- 10^{21} protoni sul bersaglio
- 10^{19} fissioni/ciclo
- Circa 4E+13 Bq prodotti in 1 ciclo

1% 0% 2%

10%

17%

$T_{1/2} < 1$ ora

1 ora $< T_{1/2} < 1$ giorno

1 giorno $< T_{1/2} < 1$ mese

1 mese $< T_{1/2} < 1$ anno

1 anno $< T_{1/2} < 10$ anni

$T_{1/2} > 10$ anni

70%

Figure 8.10: Percentages of radionuclides produced within the UC_x target after a cycle of irradiation, depending on their half-life [144].

To characterize the single gamma source, a dedicate time evolution calculation has been carried out, using the FLUKA model of the SPES Front-End (see Section 6.2.1), to follow the decay processes on the activated target, generated by one 15 day proton beam irradiation, until long cooling times.

In the simulation, all the gamma energy spectra emitted by the target are constructed. Incremental time intervals of 30 days are considered, starting from a time of 15 days after the proton beam is turned off. This preliminary study shows that the "15-day cooling" source (T15) alone contributes almost 40% to the total radioactivity, and that after one year the residual activity drops to less than 1% of the activity due to T15. Therefore, to simplify the calculation procedure and, at the same time, to be on the safe side, the spectrum corresponding to one year cooling time is attributed to all the "oldest" targets, until five year cooling time.

Global TSS gamma source

Once the gamma sources for the different cooling times are available, a global gamma source is constructed with an external FLUKA routine. It reads the individual source contributions, it places the corresponding TIS units in the rack according to the radioactivity level and it samples the gamma energy from the individual spectra, with a position-dependent probability. The

arrangement of the single TIS units in the TSS is indicated in Figure 8.9, but, to be on the safe side, in the simulation the lower-upper levels are inverted.

Each single gamma source, considered point-like and placed in the center of the corresponding cell of the TSS rack, emits in isotropic way and is surrounded by a 10 mm thick aluminum cylinder that reproduces the supporting structure of the TIS unit. The geometric arrangement of the sources is shown in Figure 8.11.
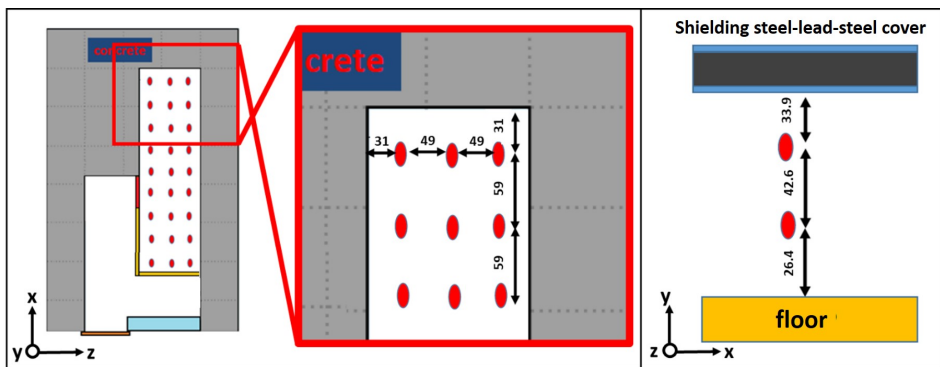

Figure 8.11: Position of the sources within the TTS. The distances are expressed in centimeters.

FLUKA model of the TSS

The global gamma source is implemented within a new static (with no time evolution enabled) FLUKA simulation code, containing the geometry of the A8a room. In Figure 8.12 the main shielding elements, as modelled by FLUKA, are shown.

Thick concrete walls, one meter or more thick and 400 cm high, shield the TSS on the side and rear walls, while the fourth side of the room, adjacent to the corridor A8b, is shielded by a 20 cm thick concrete wall. A 250 cm high and 20 mm thick lead sliding door, supported by a frame not present in the FLUKA geometry, closes the room on the corridor A8b.

Inside room A8a, a 190 cm high and 5 cm thick L-shaped lead wall separates the TIS unit storage area from both the lateral HHM access corridor, sufficiently wide to allow for the movement of the handling machine, and the internal space adjacent to corridor A8b. The latter is a 55 cm wide compartment, designed to safely carry out possible maintenance interventions inside the room A8a. In correspondence to the entrance window of the telescopic
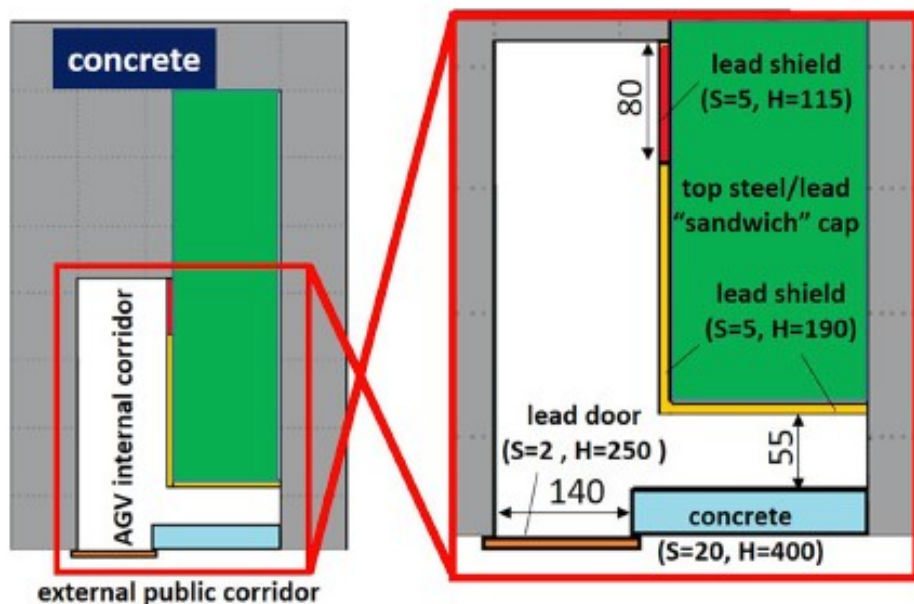
Figure 8.12: Main shielding elements implemented in the FLUKA geometry model of the A8a room. Dimensions and distances are expressed in centimeters.

arm, the height of the lead wall is 115 cm.

Each vertical compartment including two TIS units is covered by a 30 mm thick "sandwich" layer simulating the shielding caps (steel 2.5 mm - Pb 25 mm - steel 2.5 mm), at 106 cm from the floor. Vertical compartments are separated the one from the other by a vertical lead sheet 5 mm thick, starting from the bottom of the rack, 105 mm from the floor. These shielding elements are shown in Figure 8.13.

To avoid radiation leakages, the edges of the lead shielding sheets must be sealed, the upper covers must be designed with a snap-fitting structure, the lead sliding door must be superimposed where possible on the adjacent walls.

8.4.3 External exposure assessment for the Temporary Storage System

During the transport of the exhausted TIS unit towards the TSS, with the HHM vehicle, the access to the external corridor A8b is forbidden. Otherwise, the external corridor must be accessible to unexposed workers. Furthermore, the human presence is foreseen inside the storage, in the shielded area adjacent to the external A8b corridor, for ordinary and extraordinary
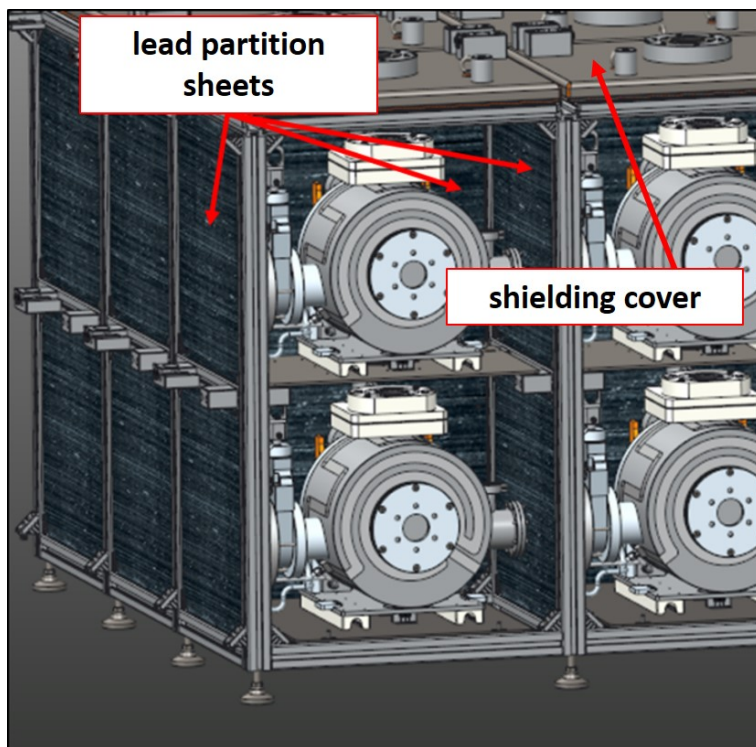
Figure 8.13: CAD representation of the shielding covers and of the lead dividing sheets that separate each vertical compartment of the TSS storage area.

maintenance. An emergency entrance inside the local, above the shielded covers of the TIS units, must also be planned in case of failure of the Cartesian manipulator.

Taking into account that the external corridor is not a work place but a controlled area at low occupancy, the dose rate constraint in the external corridor is set to 1 μSv/h. Instead, in the internal accessible areas of the A8a room, the dose rate constraint compatible with the maintenance operations is 25 μSv/h.

Figure 8.14 and Figure 8.15 show two horizontal meshes of ambient dose equivalent rate dH*(10)/dt, calculated at different heights in the FLUKA geometry of the TSS. The dose rate has been calculated also in several positions of access for the personnel, represented as white or black boxes: in corridor A8b, in the vehicle maneuver corridor and in the internal area adjacent to corridor A8b. A fourth group of boxes are positioned 30 cm above the covers of the storage area. In Figure 8.16 a vertical FLUKA mesh of ambient dose equivalent rate dH*(10)/dt, superimposed on the TSS geometry, is shown.

The dose rate value for each position on the meshes is shown in Table 8.1. Looking at the table, it can be seen that the dH*(10)/dt value in the external A8b corridor (positions 1-5 and 13-17) does not exceed the dose rate constraint of 1 μSv/h. Furthermore, in the first part of the internal maneuver corridor (positions 6-9 and 18-21) and in the internal maintenance area adjacent to the external A8b corridor (positions 11-12 and 23-24), the H*(10) rate is lower than the dose rate constraint of 25 μSv/h.

Instead, in the bottom part of the corridor (position 10), and mostly in correspondence to the window for the telescopic arm (position 22), the dose rate increases up to over 100 μSv/h. In addition, inside the storage area and above the shielding covers (positions 25-32), the values of dose rate are higher than 100 μSv/h, except in positions 25 and 26, the farthest from T15. The values reach a few mSv/h in proximity of the bottom wall, above the first two TIS units (positions 31 and 32). Therefore, strategies have to be implemented to confine interventions only in areas with limited dose rate levels.

The vertical lead sheets inside the storage area and the 5 cm L-shaped lead wall interposed up to the height of 190 cm, are elements relatively inexpensive and easy to install. They allow the dose rate in all positions outside the storage area, and in particular in the external corridor A8b, to be lower than the dose rate constraint. The presence of these lead shielding elements also makes it possible to minimize the thickness of the supporting concrete wall along the maneuver corridor and to lighten the lead sliding
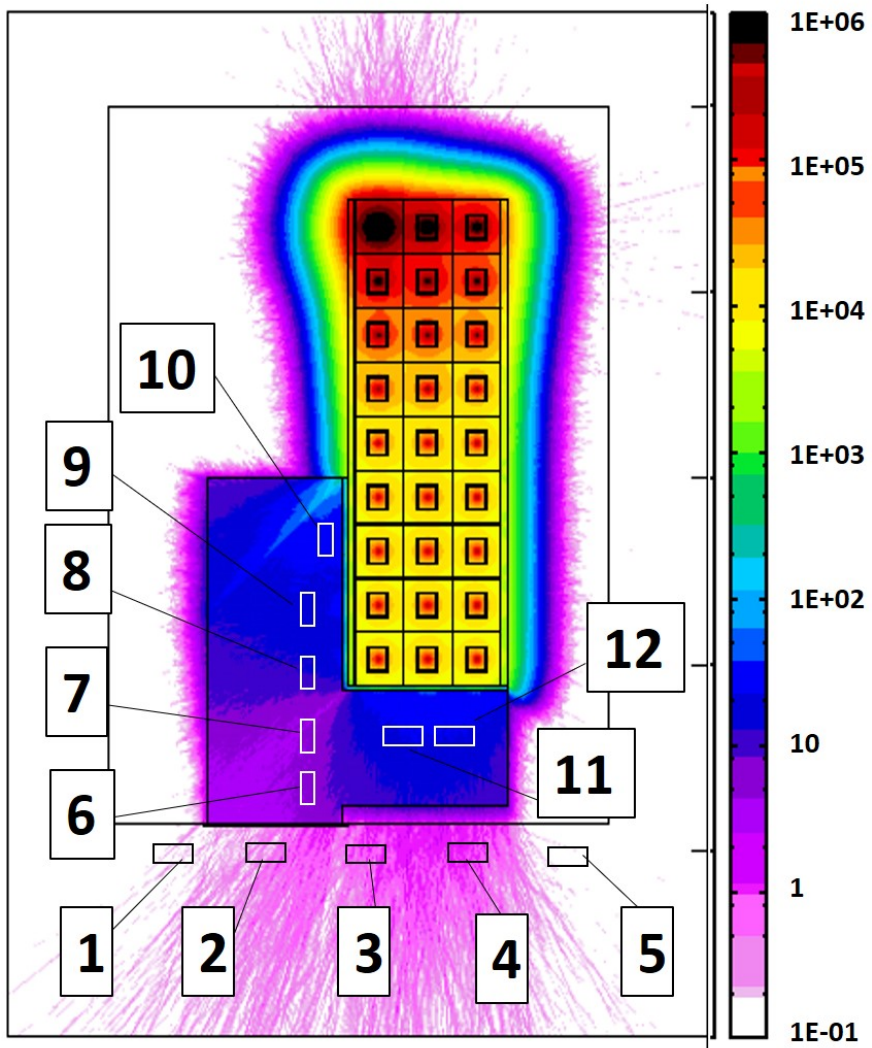
Figure 8.14: FLUKA spatial mesh of dH*(10)/dt in the A8a room, averaged over a horizontal section in correspondence of the upper level of storage containing the T15 chamber (70-100 cm). The white and black boxes represent positions for the calculation of dH*(10)/dt. Units of the color scale are in $\mu Sv/h$.
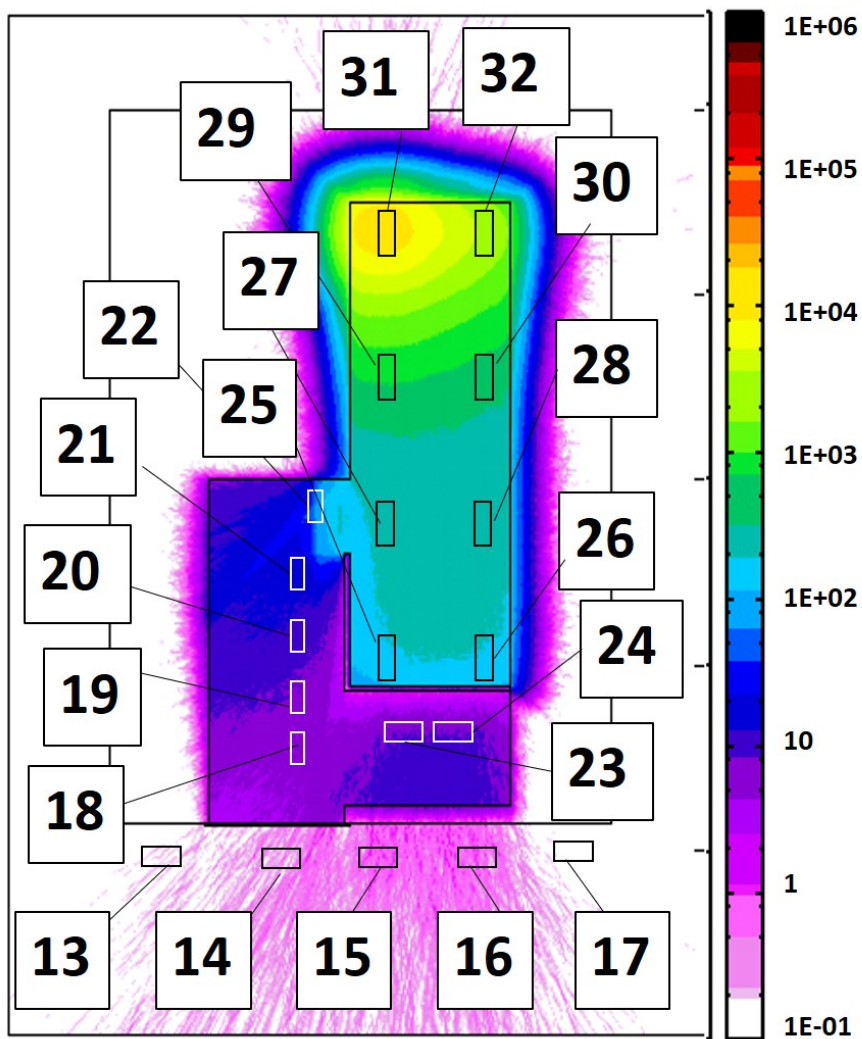
Figure 8.15: FLUKA spatial mesh of dH*(10)/dt in the A8a room, averaged over a horizontal section in correspondence of a level above the storage area (130-160 cm). The white and black boxes represent single positions for the calculation of dH*(10)/dt. Units of the color scale are in $\mu Sv/h$.
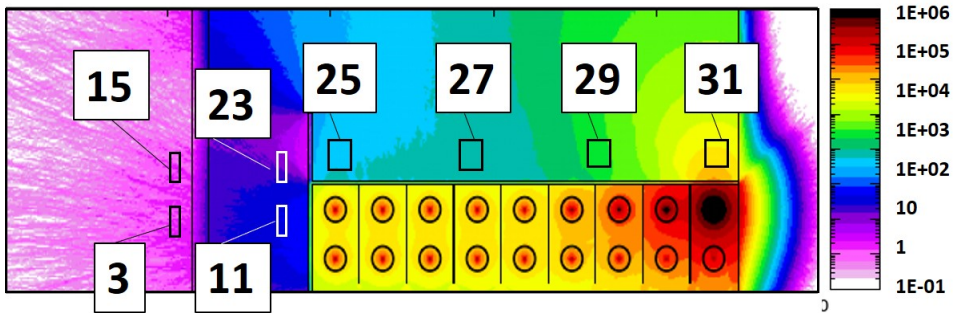
Figure 8.16: FLUKA spatial mesh of dH*(10)/dt in the A8a room, averaged over a vertical section in correspondence of the first raw of locations containing the T15 chamber. The white and black boxes represent single positions for the calculation of dH*(10)/dt. Units of the color scale are in μSv/h.

door. In addition, the internal separation between vertical compartments is fundamental to protect the operator in case of extraordinary intervention above the storage area in the presence of an open cap, especially if the most active TIS units are placed in the upper locations of the rack.

Finally, the shielding contribution of the aluminum supporting structures of the TIS units has been evaluated. For this purpose, only the six most active TIS units have been simulated, those positioned in the first row on the bottom of the A8a room. The calculation of the ambient dose equivalent rate has then been repeated in the same positions as in Table 8.1. The result of the simulation shows that, in almost all sampled positions, the dose rate is up to 10-15 times lower than the value calculated with the TSS completely filled. Only in positions 31 and 32, placed above the two most active TIS units (which in this calculation are positioned one above the other), the dose rate is about 30% higher than the one obtained with the storage full of TIS units. Therefore, the overall shielding effect of all the supporting structures interposed between the TIS units of the first row and the operator is not able to compensate for the dose increase coming from the TIS units themselves.

8.5   Final sequences for the TIS unit handling

Before being transported in a hot cell or being re-treated after a few years of permanence into the temporary storage, the TIS unit has to be extracted from the TSS, coupled to the MHM vehicle, the same one used in the first SPES operation phases and described in Section 8.3, and placed in a shielded

Table 8.1: *Values of the ambient dose equivalent rate dH*(10)/dt, calculated in the positions indicated in Figure 8.14 and Figure 8.15. Units of dH*(10)/dt are μSv/h. Monte Carlo errors are less than 5% for values greater than 1 μSv/h.*

point N.	height	dH*(10)/dt (μSv/h)	point N.	height	dH*(10)/dt (μSv/h)
1	85	$0.13 \pm 20\%$	17	145	$0.04 \pm 26\%$
2	85	$0.48 \pm 11\%$	18	145	$4.9 \pm 2.5\%$
3	85	$0.77 \pm 7.2\%$	19	145	$5.0 \pm 2.2\%$
4	85	$0.87 \pm 6.8\%$	20	145	$7.9 \pm 1.8\%$
5	85	$0.04 \pm 31\%$	21	145	$14 \pm 1.5\%$
6	85	$4.7 \pm 3.2\%$	22	145	$120 \pm 0.60\%$
7	85	$4.5 \pm 2.9\%$	23	145	$6.3 \pm 2.5\%$
8	85	$13 \pm 2.0\%$	24	145	$6.2 \pm 2.3\%$
9	85	$19 \pm 1.5\%$	25	155	$3.6 \pm 2.6\%$
10	85	$37 \pm 1.2\%$	26	155	$3.6 \pm 2.5\%$
11	85	$23 \pm 1.4\%$	27	155	$180 \pm 0.57\%$
12	85	$23 \pm 1.3\%$	28	155	$200 \pm 0.48\%$
13	145	$0.14 \pm 20\%$	29	155	$510 \pm 0.36\%$
14	145	$0.29 \pm 13\%$	30	155	$400 \pm 0.33\%$
15	145	$0.68 \pm 7.6\%$	31	155	$6.4 \cdot 10^3 \pm 0.11\%$
16	145	$0.57 \pm 8.2\%$	32	155	$2.3 \cdot 10^3 \pm 0.15\%$

sarcophagus mounted on a light trolley. Taking into account that the operation involves manual steps, the best strategy has to be implemented to safeguard the operator by optimizing the dose rate during the whole handling sequence. For example, the optimum delay for the extraction of the TIS unit from the TSS must be defined, as well as the optimum distance of the operator from the source, or how long the operation can take.

Therefore, an assessment of the radiation exposure of the operator during the whole handling operations of the exhausted TIS unit has been performed using the FLUKA Monte Carlo model of the temporary storage, described in Section 8.4.2. The model simulates the most conservative scenario from the radiation protection point of view. This is a global gamma radiation source coming from all the 54 TIS units contained in the TSS.

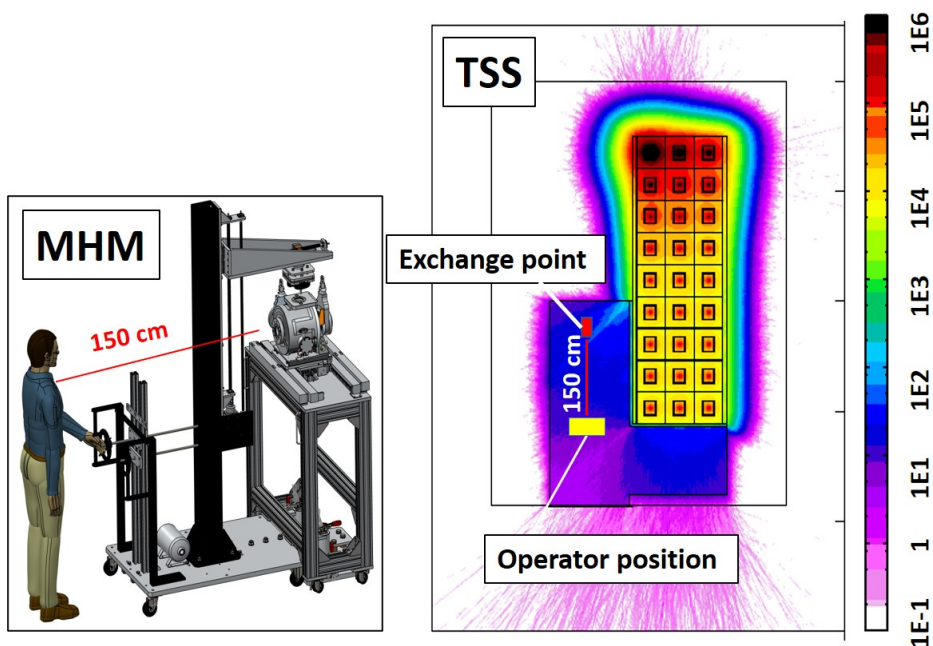The first step of the handling operation consists in the manual retrieval

Figure 8.17: Scheme of the retrieval operation of an exhausted TIS unit from the TSS.

of the exhausted TIS unit from the temporary storage. The operator enters in the lateral maneuver corridor of the A8a room with the MHM vehicle and picks up the TIS unit, once the telescopic arm has extracted it from its location inside the storage rack. During this operation, the MHM configuration is such that the worker stays 150 cm away from the TIS unit. It is exposed to two radiation sources: the radiations coming from the TSS completely filled and those coming from the extracted TIS unit itself: the two contributions have to be added to assess the external exposure in the position occupied by the operator. In Figure 8.17 the retrieval operation of the TIS unit from the TSS is illustrated.

After the extraction from the A8a room, the MHM deposits the TIS unit in a shielded trolley, that allows the operator stay at 1 m distance from the TIS unit. This operation occurs in the external corridor A8b. The trolley is then transported back to the production laboratories for the final treatment, using the elevator, since the laboratory area is at a different floor respect to the production area (see Section 8.1). In this case the only relevant contribution to the dose rate is due to the shielded TIS unit located on the trolley, being the dose rate in the corridor A8b less that 1 μSv/h.

Table 8.2 reports the ambient dose equivalent rate due only to the ex-

Table 8.2: Values of the ambient dose equivalent rate dH*(10)/dt, calculated at two distances from an exhausted TIS unit after different cooling times. Monte Carlo errors are less than 1%.

cooling time (year)	d=100 cm (μSv/h)	d=150 cm (μSv/h)
1	290	250
2	91	89
3	62	60
4	45	43
5	35	34

hausted TIS unit, at different distances and at different cooling times. The contribution of the TSS to the dose rate during the first operation, in the most conservative hypothesis of completely filled storage, is of about 18 μSv/h in the position indicated in Figure 8.17.

Considering that the dose rate constraint for both these operations, inside and outside the A8a room, is of 150 μSv/h, after 2 years of storage in the TSS, the TIS unit can be safety extracted.

The duration of each of the two operations, excluding the time for the ascent of the trolley in the elevator, where the worker is not present, is about 3-10 min. Therefore, the total dose incurred by the operator during the whole handling intervention, considering a duration of about 10 min for each operation, is less than 40 μSv. If the same operator performs the intervention ten times per year, the annual dose received is less than 0.5 mSv, the annual value of effective dose assumed at LNL for unexposed workers.

Chapter 9

Final considerations about the sustainability of the SPES project

9.1 Introduction

A complete study of the radiation protection aspects for nuclear facilities for the production of RIBs, such as the SPES apparatus, is a complex effort and is certainly out of the scope of this work. It requires an accurate description of all the possible radiation issues for operators, population and the surrounding environment [98, 143, 144, 149, 150]. A detailed analysis of the risks related to the SPES project is being performed by a specialized company, with special regard to the radiation protection aspects, but also to specific hazards such as earthquake, fire, overflow, explosion.

The study carried out in the previous chapters of this thesis addresses several radiation "hot spots" related to the SPES project, with the purpose of quantify the radiological hazard in the most critical areas of the facility and to provide useful information on the impact of the facility on the environment. The work only considers external irradiation; it doesn't consider air, soul and wall contamination, or area contamination caused by tool break and/or other accidents.

To assess the external exposure in the most critical SPES radiation areas, a map of dose rate present in the production bunker has been obtained, originating from all contributions coming from the residual activation of the Front-End, as a function of time. The different sequences of the handling of the TIS unit during its life cycle, as well as the system for the temporary storage of the exhausted targets have been studied and their radiation

impact has been evaluated as well.

In a broad sense, the present study can be considered part of the most complete risk analysis of the project. For this reason I believe it is important, upon completion of the thesis work, to draw some general considerations about the sustainability of the SPES project. Therefore, on the end of this thesis, an overview on the main radiation hazards and optimization procedures connected with the SPES activities, and on the environmental impact of the project throughout its whole life cycle, is provided.

9.2 SPES Radiation Protection Issues

The generation of radioactivity at a RIB facility like SPES is intrinsic to the production of RIBs. A not exhaustive list of the principal SPES radiation issues contains the following aspects:

- radiation from the primary proton beam;

- radioactivity induced by protons and neutrons in the Front-End structures;

- radioactivity induced by isotope deposition along the RIB line;

- radioactivity induced by fission fragments in the production target;

- loose radioactivity containment (in vacuum systems).

Such aspects are briefly discussed in the following of the section, as well as the strategies adopted for the containment of the radioactive hazard.

9.2.1 Radiation from the primary proton beam

The first issue is present in each facility equipped with a proton or heavy ion accelerator. In fact, the intense proton beam emitted by the cyclotron to bombard the production target, may give rise to high neutron and gamma radiation fields. At SPES this could occur in case of unexpected proton beam losses or when the beam interacts with the structures of the PPB line of the Front-End, like the collimators and mainly the production target [143].

Therefore, massive concrete layers, of the order of 3 m thickness, are required in the cyclotron area and in the production bunker to shield the neutron component of the radiation, that is the most critical. A shield suitable for the neutrons is in fact suitable also for the other secondary radiation components produced.

A "Radiation System Security" (SSR) is implemented in SPES, including the "Access Control System" (SCA). The system controls the shutdown of the cyclotron whenever high losses or failure occur or whenever an attempt is made to access in any areas interested by the path of the proton beam: the cyclotron compartment, the production bunker and the areas where the handling and storage of targets are performed.

Moreover, the high fluxes of neutrons generated by the proton beam interaction with the target activate both the floor and the concrete of the shielding walls and the air in the production bunker which, therefore, has to be properly released into the external environment to avoid potential intake of radionuclides. When the UC_x target is mounted into the TIS unit, the waiting and storage time required for the concentration of radioactive gases in air to decrease so that they can be safely released in atmosphere is of the order of 20 min [143]. Furthermore, on the underground floor, a ventilation system is present; it allows a negative pressure within the areas of the cyclotron and the irradiation bunker to be maintained. The residual radioactivity in the closed water refrigerant systems is another issue to be taken in account.

On the underground floor, the cyclotron compartment, the production bunker and the areas of handling and storage of the exhausted targets are classified as controlled areas. The areas placed on the ground floor and all the remaining areas of the SPES building should be classified as supervised areas, except the laboratory of preparation of uranium carbide targets, which is classified as a controlled area (see Chapter 8). The personnel will be classified based on the planned activities and the workload, and the consequent potential radiation exposure [144].

9.2.2   Radioactivity induced in the Front-End system

The second and the third issues of the previous crucial item list have been described in detail in Chapter 6 and Chapter 7. The assessment of the external radiation exposure received by the personnel and its evolution with the time, is necessary to plan operations and maintenance interventions on the Front-End system. These interventions are often performed manually, during the short or extended technical stops of the apparatus.

It has to be stressed that the radiation protection of the personnel during the maintenance interventions on the Front-End system, represents one of the most important issues related to the SPES operation. Therefore, a big effort is required to set-up good practices for the interventions, by carefully specifying action protocols for each single maintenance operation, strictly

respecting the ALARA principle.

As an example of ALARA optimization, the SPES operating management body, with the involvement of the radiation protection expert and possible of the workers, could decide to produce only the beams that are less impacting, depending on the type of isotopes that deposit on the Front-End structures and their deposition position, or to chose those that don't spread radioactivity outside the bunker.

Furthermore, the study of the Front-End residual activity is important to manage the decommissioning phase of the installation (see next Section 9.3.2). In fact, the study evidences the most critical elements of the Front-End system, based on the materials they are made of and on the activation level reached. For example, critical items are the graphite of the collimators that intercept the beam, the steel elements that contain long half-life isotopes, the aluminum elements of which many components of the apparatus are constituted. However, these latter are less problematic for disposal, due to the short half-life of most composing isotopes (see Section 6.5.2).

9.2.3 Radioactivity induced by fission fragments in the production target

The fourth issue of the previous list is connected to the irradiation of the production target and to the life cycle of the Target and Ion Source unit. It has been discussed in Chapter 8.

After the closure of the sealing valves, subsequent the shutdown of the beam, the TIS unit becomes a close system until the final treatment, after removal from the temporary storage. Therefore it shouldn't represent an issues concerning the release of radioactivity. However, possible radiation losses can potentially occur during the removal of the TIS unit from the Front-End, or across the valves during the storage period inside the TSS. Anyway, to avoid uncontrolled releases of volatile radioactive species, both production bunker and TSS maintain a depression of 40-80 Pa with respect to the adjacent external areas.

Furthermore, to detect the possible presence of radioactive material inside the production bunker, coming from the irradiated target, the air of the bunker is continuously monitored and an interlock signal is generated if a fixed concentration threshold is exceeded.

9.2.4 Loose radioactivity containment

An issue connected to the production in target is the formation of radioactive volatile species in the beam pipes. The most severe problems are encountered when UC_x targets are used, because they are capable of producing the greatest variety of radioactivity.

The radioactive volatile species produced, and the gases generated thanks to the high working temperature of the production system, migrate along the beam lines, thus potentially contaminating both pipe lines and beam intercepting devices. Moreover, accelerated volatile RIBs and their progeny carry radioactivity along the RIB line, even if the level of contamination attenuates gradually moving away from the source. One of the major constraints might be the potential alpha emitter gas release, especially the radioactive isotopes of the noble gas radon. In fact, although they don't pose particular radiation protection problems, they decay to products (children of radon) that are of considerable radiological importance for their high radiotoxicity, such as ^{210}Po. However, due to the low energy of the protons used at SPES, the production of long half-life alpha emitters is extremely limited [144].

A "Gas Recovery System" (HA-GRS) is adopted at SPES, to capture and hold all the gases exhausted inside a vacuum system during the proton irradiation [151]. The delivered gasses are checked and eventually stored up until their radioactivity has dropped to acceptable levels to permit the release in atmosphere. The estimated time for the release to take place is no less than 2 months. The HA-GRS system is suitably shielded with concrete blocks/walls not less than 50 cm thick. In addition, the entire system of storage is controlled by interlock gates.

Since vacuum pumps act as a filter for the radioisotopes, they could concentrate significant amounts of radioactivity. Moreover, the level of radioactivity affects the reliability of all the pump components, as electro-pneumatic valves, lubricants and polymeric gaskets. Periodical maintenance interventions on the vacuum pumps have to be carefully planned, since they represent an hazard for the operator, both for the external exposure and also for the contamination risk.

9.3 The SPES environmental impact

In this final section, tentative considerations on the environmental impact of the SPES facility during its life cycle are made.

At a RIB facility like SPES, substantial inventories of radioactivity is accumulated during the apparatus operation. Therefore, containment of

the radioactivity has to be ensured over the entire life cycle of the facility, from the very early stage of the design to the final decommissioning.

External and internal exposure for workers and population, waste production, radiation activation and damage of structures and materials, all these aspects and their management strategies have to be carefully considered. They must refer the Italian legislation on the radiological protection [82], the ALARA principle and the ethical values of the radiation protection (see Section 4.4). Moreover, the choice between different possible solutions to the numerous radiation protection issues, could strongly affect the total cost of the facility and its social and environmental impact. For this reason, the success of a facility such as SPES depends on cost-effective solutions to these issues.

9.3.1 External and internal exposure for workers and population

The assessment of dose levels and strategies for the containment of the radioactivity spread have been illustrated in the previous sections of this thesis, considering ordinary operation situations. In these conditions, the main LNL objectives regarding effective dose constraints for unexposed workers and members of the public are not to exceed 0.5 mSv/year, and for workers classified as exposed workers, not to exceed 5 mSv/year.

Potential unexpected exposure scenarios, as proton beam losses, block of the automatic handling system of the irradiated TIS unit, radioactive losses from the sealed TIS unit during the transport and storage period, have been analyzed in the SPES context and different radiation protection scenarios have been proposed [144].

As one of the worst potential accident scenery, the instantaneous release of all gaseous and volatile products generated in the target, due to a sudden break of the TIS unit, has been considered. To be conservative, the time of the observation refers to the end of the two weeks of irradiation. Accidental release of radioactivity to the atmosphere has been simulated and estimated using standard computation models. Considering the worst possible meteorological conditions, the effective dose calculated for the population 400 m away, where the closest buildings of the LNL laboratories are located, is less than 20 μSv/year [144].

Finally, the effectiveness of safety and emergency instrumentation for radiation monitoring related to the SPES operation, is controlled by the radiation protection expert of the LNL laboratories [144]. Personnel will be informed on the specific risks to which they will be exposed and training

programs for the radiation protection will be developed.

9.3.2   Waste production and decommissioning

Decommissioning typically generates a certain amount of radioactive material [98]. Some of it can be potentially recycled and reused, while the rest is destined to waste.

The TIS units extracted from the TSS system after the storage period are not considered as a significant radioactive waste. Indeed, the targets can be reused under beam and reassembled on the Front-End system. Only after their reuse is completed, they are disassembled in hot cell. At this point, only a very small fraction of transuranic elements with very long half-life will remain in the target material, that will be finally disposed in a proper way, by an authorized company [145].

A radiochemistry method for the extraction and reuse of radionuclides from the exhausted targets, mostly ^{99}Mo of interest to nuclear medicine, is under study. In fact, ^{99}Mo, having a half-life of about 66 h, decays in ^{99m}Tc metastable, which has a half-life of 6 h. This latter radioisotope is used in over 70% of nuclear medicine procedures for functional studies, diagnostic and therapy. Currently, the worldwide production of ^{99}Mo occurs by fission of ^{235}U induced by thermal neutrons in nuclear reactors using enriched ^{235}U, a strategic material used predominantly for military purposes.

The interesting thing is that ^{99}Mo is produced in the UC_x SPES target, and, being refractory, remains trapped in the target material. However, its recovery is possible after dismounting of the TIS unit in a hot cell, using conventional chemical methods. At this time, from an economic point of view, the method is not competitive with the standard one used in nuclear reactor. Nevertheless, in the future, the SPES targets could be considered an alternative source for the production of radioisotopes interesting for nuclear medicine [152].

As illustrated in Chapter 6, the interaction of the proton beam with structures and materials, both inside the cyclotron area and along the beam lines of the Front-End system, as well as the fission neutrons produced in the target, induce material activation.

The components of the cyclotron don't represent a major concern for activation, with respect to others high neutron environments, for example a nuclear reactor. However the activation of these components is not completely negligible, so they need to be properly handled as a radioactive waste.

Conversely, in the design of the structures and materials of the SPES

179

Front-End system, the material activation has to be carefully taken into account for the waste management, in particular if some materials need to be separated to be sent to waste (like aluminum compounds, silver and copper).

After some year of SPES operation, the activated parts of the Front-End which require maintenance can be removed and, after a suitable cooling period, reused. The amount of time to wait before reusing the activated Front-End materials depends on the lifetime of the radioisotopes produced by the materials themselves. Some materials that cannot be reused will be removed by LNL through an authorized company. In the same way, other activated materials will be removed because their proper functioning will no longer be guaranteed. They will be temporarily placed in a special shielded space on the underground floor, where they will be appropriately identified and reported in a register [144].

Methods and calculations for the management of the decommissioning phase consider 20 years of operation of the apparatus. The radioactivity induced after such a period in the cyclotron and in the Front-End structures, in the concrete of the shielding walls, in the ground below the facility and in the cooling water systems has been evaluated. This is because safety conditions for the dismantling operations must be planned [143].

The radioactive ions deposited on the RIB line of the Front-End system can present a hazard for the generated contamination (see Chapter 7). The implementation of the ALARA principle suggests that only the beams less impacting for the Front-End structures and for the spread of radioactivity outside the bunker should be produced. Anyway, the deactivation operations have to be carried out with extreme caution, following the good practice rules [144].

The temporary storage system has been carefully defined, since it represents a strong impact on the project cost(see Chapter 8). In fact, an overestimate of the storage area might lead to huge overcosts for the building, and an underestimate might stop the operation of the facility for lack of storage zones. Anyway, the storage system necessary for the operation of the SPES project has to be considered temporary and functional to the radioactive cooling of the TIS units before their subsequent treatment.

9.3.3   SPES and sustainable development

Sustainable development is for a long time one of the fundamental projects of the European Commission, therefore, a continuous forum for sustainable development issues has been instituted within the European framework [153].

"Development must meet the needs of the present without compromising the ability of future generations to meet their own needs. A life of dignity for all within the planet's limits and reconciling economic efficiency, social inclusion and environmental responsibility is at the essence of sustainable development" [154].

In the SPES context, sustainability means optimize the project in all its parts, with the aim to reduce the costs and the radioactive wastes, at the same time maintaining a high degree of scientific competitiveness and providing a research facility capable of satisfy both scientific and application needs, without represent an issue for the environment.

Speaking about sustainable development, a study on the "Life Cycle Assessment" (LCA) of the SPES project could be imagined. The LCA method provides the best framework to evaluate the environmental aspects and the potential environmental impacts related to a process or an activity, along the entire life cycle of that process or activity, from the extraction and treatment of raw materials until the final disposal [155, 156].

A possible application of the LCA method to SPES is a complex matter. In fact, also for standard processes or activities, choosing the correct impact indicators of products and finding the information necessary to quantify these impacts, is not always easy. Furthermore, SPES is a prototype of research apparatus unique in space and over time, and not a commercial product, therefore ever more so its impact is not directly quantifiable.

The optimization of the radioactive confinement and the waste management passes through the application of the ALARA principle and of the radiation protection ethical values (see Section 4.4). This approach includes the concern for the future generations and the environment, complying the maximum limitation of waste in each phase of the facility life cycle. This, of course, means also a reduction of the waste management costs.

On the other hand, due to both energy and intensity of beams produced with the ISOL technique, interdisciplinary foreground applications can be developed at SPES, from astrophysics to material studies, from biology to medicine. Production of innovative radioisotopes for nuclear medicine, diagnostics and radiotherapy can be performed in the framework of the ISOL-PHARM project.

SPES contributes significantly to the national and international development of nuclear physics research. INFN has included the SPES project in its road map for the development of nuclear physics in Italy. Moreover, it participates to the definition of the European project EURISOL, addressing the study and realization of innovative ISOL direct targets. What's more, SPES is connected to an international framework of scientific research and

181

technological development, in collaboration with important laboratories in the world.

For all these reasons, looking at the preservation of the environment, but also to the future of the scientific research and knowledge and to the capability to improve the human health and the technological progress, the global impact of the SPES project on the external environment can certainly be considered positive.

Chapter 10

Summary and Conclusions

The present work has been developed in the framework of the SPES (Selective Production of Exotic Species) project, a second generation nuclear facility for the production of Radioactive Ion Beams (RIBs), currently under construction at INFN-LNL (Istituto Nazionale di Fisica Nucleare, Laboratori Nazionali di Legnaro), Padua, Italy.

The production of radioactive ion beams at SPES is based on the "Isotope Separation On-Line" (ISOL) method. A intense proton beam, driven by a cyclotron accelerator, interacts with a thick UC_x target, heated to high temperature. The radioactive fragments produced through ^{238}U fission in the target diffuse out towards an ion source, and the produced ions are then accelerated at low energy. This ion beam is analyzed by mass, to select specific species which are then accelerated. Such a method, in conjunction with the improvement of the technology developed at the second generation RIB facilities, allows beams with high intensity and purity, with good timing and optical qualities and with a large range in mass to be produced.

The worldwide interest in producing accelerated beams of unstable nuclei is proven by the national and international network of collaborations between the SPES project and a large number of research institutions and RIB facilities, both in Europe and in the world. This is because multidisciplinary applications, from nuclear physics to astrophysics, from engineering to material science, from radiochemistry to medicine, can be developed at a RIB facility such as SPES.

However, the high biological hazard of the radioactivity generated imposes severe radiological constraints to the design and operation of RIB facilities. The success of such types of nuclear physics projects depends also on cost-effective solutions to such problems.

The work developed in the present thesis provides a study of the radi-

ation hazard and environmental impact for a radioactive ion beam facility, considering the SPES project as the case study. Anyway, in a more general extent, the approach followed in the work can be applied to any existent of future RIB facility.

Several radiation "hot spots" related to the SPES project activity are addressed in the thesis. The first case study consists in the assessment of the radioactivity induced in the structures of the production apparatus, and of the consequent external radiation exposure inside the SPES production bunker. The radioactivity is generated by the activation of the materials caused by the primary proton beam and by fission neutrons coming out of the target, as well as by the deposition of radioactive ions in the electromagnetic devices of the radioactive ion beam line.

The second case study regards the assessment of the external radiation exposure related to the handling operations on the exhausted "Target and Ion Source" (TIS) units. Radiation issues are present in different stages of the TIS life cycle, from the removal from the production lines after irradiation, until the final treatment after a proper cooling period in a temporary storage.

In both study cases, strategies to optimize the radiation dose during the necessary accesses and maintenance interventions in the most critical areas of the facility are discussed. These considerations refer to the "International Commission on Radiological Protection" (ICRP) recommendations, and are in compliance with the Italian legislation on relevant basic safety standards for protection against the hazard from radiation exposure, and with the radiation safety constraints implemented at INFN-LNL laboratories.

An overview on the themes concerning the environmental impact of the facility during its whole life cycle, from initial design to final decommissioning, is addressed. Underlying to the whole process, are the SPES R&D policies and the increasing interest of the national and international community of nuclear physics towards sustainable development of such research projects.

Bibliography

[1] Available at https://www.britannica.com/science/nuclear-binding-energy.

[2] Available at https://www.eurisol.org.

[3] A. Andrighetto *et al.*, Eur. Phys. J. A 25, 41 (2005).

[4] V. A. Rubchenya *et al.*, Nuclear Instrum. Methods Phys. Res. A 463, 653 (2001).

[5] H. Penttilä *et al.*, Eur. Phys. J. A 52, 104 (2016).

[6] K. H. Schmidt *et al.*, Nucl. Data Sheets 131, 107 (2016).

[7] A. Andrighetto *et al.*, Eur. Phys. J. A 30, 591 (2006).

[8] G. Prete *et al.*, Eur. Phys. J. Web of Conf. 66, 11030 (2014).

[9] A. Monetti *et al.*, Eur. Phys. J. A 51, 128 (2015).

[10] A. Monetti *et al.*, Eur. Phys. J. A 52, 168 (2016).

[11] A. Andrighetto *et al.*, J. Phys. Conf. Ser. 966, 012028 (2018).

[12] F. Gramegna *et al.*, Il Nuovo Cimento 41C, 195 (2018).

[13] R. Catherall *et al.*, J. Phys. G Nucl. Part. Phys. 44 9, 094002 (2017).

[14] G. C. Ball, G. Hackman and R. Krücken, Phys. Scr. 91 9, 93002 (2016).

[15] F. Ibrahim, The ALTO facility at IPN Orsay, in XXI International School on Nuclear Physics, Neutron Physics and Applications (2015).

[16] J. R. Beene *et al.*, J. Phys. G Nucl. Part. Phys. 38 2, 024002 (2011).

[17] Available at https://www.ganil-spiral2.eu.

[18] Available at https://fair-center.eu.

[19] Available at https://www.kek.jp/en/.

[20] Available at https://tlabs.ac.za.

[21] M. Lindroos, CERN-AB-2004-086 (2004).

[22] S. Corradetti *et al.*, Ceram. Int. 43, 10824 (2017).

[23] F. M. Marqués *et al.*, Phys. Rev. C 64 no.6, 61301 (2001).

[24] C. Shen, G. Kosenko and Y. Abe, Phys. Rev. C 66 no.6, 61602 (2002).

[25] E. M. Burbidge *et al.*, Rev. Mod. Phys. 29, no.4, 547 (1957).

[26] H. Hofsäss, Hyperfine Interact. 97, no.1, 247 (1996).

[27] R. Abbe, "The use of Radium in malignant disease", Lancet (1913).

[28] S. Chaturvedi and A.K. Mishra, Front. Med. 3, 5 (2016).

[29] M. Ballan *et al.*, Appl. Radiat. Isot. 164, 109258 (2020).

[30] Available at http://jens-maus.de/ftp/langner_mscthesis.pdf.

[31] A. Vértes *et al.*, Handbook of Nuclear Chemistry, Vol. 1-4, Chem. Springer US (2010).

[32] Available at https://home.cern/tags/medicis.

[33] A. Andrighetto *et al.*, Int. J. Mod. Phys. Conf. Ser. 48, 1860103 (2018).

[34] D. Scarpa *et al.*, Eur. Phys. J. A 47, 32 (2011).

[35] Y. Blumenfeld *et al.*, Phys. Scr. T152, 014023 (2013).

[36] T. Nilsson, Nucl. Instr. Methods Phys. Res. B 317, 194 (2013).

[37] O. Kofoed-Hansen and K.O. Nielsen, Phys. Rev. 82, 96 (1951).

[38] I. Tanihata *et al.*, Phys. Lett. B 160, 380 (1985).

[39] T. Stora, Nucl. Instr. Methods Phys. Res. B 317, 402 (2013).

[40] L. Popescu, D. Houngbo and M. Dierckx, Nucl. Instr. Methods Phys. Res. B 463, 262 (2020).

[41] Y. Blumenfeld, The EURISOL Project, AIP Conf. Proc. 891, no.1, 147 (2007).

[42] S. Corradetti *et al.*, Eur. Phys. J. A 47, 119 (2011).

[43] S. Corradetti *et al.*, Eur. Phys. J. A 47, 32 (2011).

[44] S. Corradetti *et al.*, Nucl. Instr. Methods Phys. Res. B 488, 12 (2021).

[45] R. Kirchner, Nucl. Instr. Methods Phys. Res. B 204, 179 (2003).

[46] R. Köster *et al.*, Nucl. Instr. Methods Phys. Res. B 266, 4229 (2008).

[47] SPES Technical Design Report, INFN-LNL-223 (2008).

[48] M. Manzolaro *et al.*, Rev. Sci. Instrum 87, 02B502 (2016).

[49] B. Marsh, Proceedings of the CAS-CERN Accelerator School: Ion Sources, edited by R. Bailey, CERN-2013-007, 203-254 (2012).

[50] https://www.bestcyclotron.com.

[51] M. Ferrari *et al.*, A residual activation study on the SPES Front-End: dosimetry and radiation protection calculations, SPES-Note-WPB06_04_0004 (2017).

[52] R. L. Seliger, J. Appl. Phys. 43, 2352 (1972).

[53] K. Jensen and E. Veje, Nucl. Instrum. Methods 122, 511 (1974).

[54] E. Leal-Quiros and M. A. Prelas, Rev. Sci. Instrum 60, 350 (1989).

[55] A. Monetti, Design and development of the target-ion source system for the SPES project, Ph.D. Thesis, Dipartimento di Ingegneria Industriale, Università degli Studi di Padova. Italy (2017).

[56] Available at https://www.ptc.com/en/products/cad/creo.

[57] M. Manzolaro, Engineering of the INFN SPES target - ion source system, LAP Lambert Academic Publishing (2012).

[58] M. Manzolaro, F. D' Agostini, A. Monetti, and A. Andrighetto, Rev. Sci. Instrum. 88, no. 9, 93302 (2017).

[59] M. Manzolaro *et al.*, Rev. Sci. Instrum. 83, no. 2, 02A907 (2012).

[60] M. Ballan *et al.*, Nucl. Instr. Methods Phys. Res. B 376, 28 (2016).

[61] E. Madenci and I. Guven, The Finite Element Method and Applications in Engineering Using ANSYS®, Springer US (2015).

[62] M. Ferrari *et al.*, RadJ. 3(2), 98 (2018).

[63] A. Donzella *et al.*, Nucl. Instr. Methods Phys. Res. B 463, 169 (2020).

[64] A. Donzella *et al.*, Eur. Phys. J. A 56, 54 (2020).

[65] ICRP, 2007. The 2007 Recommendations of the International Commission on Radiological Protection. ICRP Publication 103, Ann. ICRP 37 (2-4).

[66] Los Alamos Science 23, 116 (1995).

[67] IXRPC, 1928. X ray and Radium Protection. Recommendations of the 2nd International Congress of Radiology, 1928. Br. J. Radiol. 12, 359-363.

[68] IXRPC, 1934. International Recommendations for X ray and Radium Protection. Revised by the International X ray and Radium Protection Commission and adopted by the 4th International Congress of Radiology, Zurich, July 1934. Br. J. Radiol. 7, 1-5.

[69] ICRP, 1955. Recommendations of the International Commission on Radiological Protection. Br. J. Radiol., Suppl. 6.

[70] ICRP, 1957. Reports on Amendments during 1956 to the Recommendations of the International Commission on Radiological Protection (ICRP). Acta. Radiol. 48, 493-495.

[71] Y. Socol and L. Dobrzyński, Dose-Response 13, 1 (2015).

[72] ICRP, 1959. Recommendations of the International Commission on Radiological Protection. ICRP Publication 1. Pergamon Press, Oxford, UK.

[73] ICRP, 1966. Recommendations of the International Commission on Radiological Protection. ICRP Publication 9, Pergamon Press, Oxford, UK.

[74] ICRP, 1973. Implications of Commission Recommendations that Doses Be Kept As Low As Readily Achievable. ICRP Publication 22. Pergamon Press, Oxford, UK.

[75] ICRP, 1977. Recommendations of the International Commission on Radiological Protection. ICRP Publication 26, Ann. ICRP 1 (3).

[76] ICRP, 1991b. The 1990 Recommendations of the International Commission on Radiological Protection. ICRP Publication 60, Ann. ICRP 21 (1-3).

[77] ICRP, 2012. ICRP Statement on Tissue Reactions and Early and Late Effects of Radiation in Normal Tissues and Organs - Threshold Doses for Tissue Reactions in a Radiation Protection Context. ICRP Publication 118, Ann. ICRP 41 (1-2).

[78] NEA International Radiological Protection School (IRPS), Stockholm University (2018).

[79] I. Turai *et al.*, BMJ 328, 568 (2004).

[80] J.C. Nénot, J. Radiol. Prot. 29, 301 (2009).

[81] D. Forkel-Wirth *et al.*, arXiv:1303.6519. doi:10.5170/CERN-2013-001.415 (2013).

[82] Decreto Legislativo 31 luglio 2020, n. 101. Attuazione della direttiva 2013/59/Euratom.

[83] ICRU, 1993b. Quantities and units in radiation protection dosimetry. ICRU Report 51. ICRU Publications: Bethesda, MD.

[84] ICRU, 2001b. Determination of operational dose equivalent quantities for neutrons. ICRU Report 66. Journal of ICRU 1 (3).

[85] EU, 1996. Council of the European Union: Council Directive on laying down the Basic Safety Standards for the protection of the health of workers and the general public against the dangers arising from ionising radiation. Official. J. Eur. Community 39, No. L, 159.

[86] IAEA, 1996. International Basic Safety Standards for Protection against Ionizing Radiation and for the Safety of Radiation Sources. Safety Series 115. STI/PUB/996. International Atomic Energy Agency, Vienna, Austria.

[87] M. Najafi *et al.*, J. Biomed. Phys. Eng. 4, 163 (2014).

[88] E.G. Dimova *et al.*, Genetics and Molec. Biol. 31 2, 396 (2008).

[89] UNESCO, 2005. The Precautionary Principle. United Nations Educational, Scientific and Cultural Organization, Paris, France.

[90] ICRP, 2005d. Low dose extrapolation of radiation-related cancer risk. ICRP Publication 99. Ann. ICRP 35 (4).

[91] UNSCEAR, 2008. Effects of Ionizing Radiation. United Nations Scientific Committee on the Effects of Atomic Radiation Report to the General Assembly with Scientific Annexes. United Nations, New York, NY.

[92] Council Directive 2013/59/EURATOM of 5 December 2013, laying down basic safety standards for protection against the dangers arising from exposure to ionising radiation, and repealing Directives 89/618/Euratom, 90/641/Euratom, 96/29/Euratom, 97/43/Euratom and 2003/122/Euratom.

[93] ICRP, 2018. Ethical Foundations of the System of Radiological Protection. ICRP Publication 138, Ann. ICRP 47 (1).

[94] W.K. Frankena, Ethics. Prentice Hall, Englewood Cliffs, NJ (1963).

[95] UNECE, 2001. Public Participation. The Århus Convention on Access to Information, Public Participation in Decision-making and Access to Justice in Environmental Matters. United Nations Economic Commission for Europe, New York. Available at https://www.unece.org/env/pp/welcome.html.

[96] United Nations, 1948. The Universal Declaration of Human Rights. Adopted 10 December 1948. United Nations, New York. Available at https://www.un.org/en/universal-declaration-human-rights/.

[97] D. Benini and S. Canella, Quality-Safety Management and Protective Systems for SPES, INFN-LNL, Legnaro, Italy. Proceedings of ICALEPCS 2011, Grenoble, France.

[98] D. Benini, Analisi dei rischi del progetto SPES, Internal report DOC-00000002, SPES Document Repository, Laboratori Nazionali di Legnaro (2012).

[99] MCNPX User's Manual, Version 2.7.0, April 2011, LA-CP-11-00438.

[100] A Manual for CINDER'90, Version 07.4 Codes and Data, LA-UR-07-8412.

[101] A. Ferrari, P.R. Sala, A. Fassò and J. Ranft, FLUKA: a multi-particle transport code, CERN-2005-10 (2005), INFN TC05/11, SLAC-R-733.

[102] T.T. Böhlen et al., The FLUKA Code: Developments and Challenges for High Energy and Medical Applications, Nuclear Data Sheets 120, 211-214 (2014).

[103] Available at https://mcnp.lanl.gov.

[104] H.W. Bertini, Phys. Rev. 131, 1801 (1963).

[105] J. Barish *et al.*, HETFIS High-Energy Nucleon-Meson Transport Code with Fission, ORNL-TM-7882 (1981).

[106] ICRP, 1996. Conversion Coefficients for use in Radiological Protection Against External Radiation. ICRP Publication 74, Ann. ICRP 26 (3-4).

[107] ICRU, 1998. International Commission on Radiation Units and Measurements, Conversion Coefficients for use in Radiological Protection Against External Radiation. ICRU Report 57, Bethesda, MD: ICRU Publications.

[108] M. Pelliccioni, Radiat. Prot. Dosim. 88(4), 279 (2000).

[109] ICRP, 2010. Conversion Coefficients for Radiological Protection Quantities for External Radiation Exposures. ICRP Publication 116, Ann. ICRP 40 (2-5).

[110] M. Halász and M. Szieberth, Annals of Nuclear Energy 121, 429 (2018).

[111] H. Bateman, The solution of a system of differential equations occurring in the theory of radioactive transformations. In Proc. Cambridge Philos. Soc. v.15, 423 (1910).

[112] J.D. Cossairt, Radiation Physics for Personnel and Environmental Protection, Fermilab Report TM-1834, Rev. 13 (2014).

[113] V. Vlachoudis, FLAIR: A Powerful But User Friendly Graphical Interface For FLUKA, Proc. Int. Conf. on Mathematics, Computational Methods & Reactor Physics (M&C 2009), Saratoga Springs, New York (2009).

[114] Available at https://www.fluka.org.

[115] S. Agostinelli *et al.*, Geant4-a simulation toolkit, Nucl. Instrum. Methods Phys. Res. A 506 n. 3, 250 (2003).

[116] M. Ballan, Development of targets for the production of radionuclides of medical interest according to the ISOL technique, Ph.D. Thesis, Doctoral Course in Physics, Università degli Studi di Ferrara. Italy (2018).

[117] G. Battistoni *et al.*, J. Phys. Conf. Ser. 408 no. 1, (2013).

[118] G. Battistoni *et al.*, Annals of Nuclear Energy 82, 10 (2015).

[119] A. Ferrari *et al.*, *The physics of high energy reactions.* In: Gandini, A., Reffo, G. (Eds.), Workshop on Nuclear Reaction Data and Nuclear Reactors Physics, Design and Safety. p. 424 (1998).

[120] G. Battistoni *et al.*, *The physics of high energy reactions.* In: Gadioli, E. (Ed.), 11th Int. Conf. on Nuclear Reaction Mechanisms. p. 483 (2006).

[121] M. Cavinato *et al.*, Nucl. Phys. A679, 753 (2001).

[122] M. Cavinato *et al.*, Phys. Lett. B382, 1 (1996).

[123] 5th FLUKA Advanced Course and Workshop, Boulogne-Billancourt, France (2019).

[124] F. Atchinson, A Revised calculational model for fission, P. Scherrer Intitut, PSI Bericht Nr. 98-12 (1998).

[125] I. V. Ryzhov *et al.*, Phis. Rewiew C 83, 054603 (2011).

[126] K. B. Gikal *et al.*, Phys. Atomic Nuclei, 79, No. 9-10, 1367 (2015).

[127] P. Sala, FLUKA Collaboration Meeting, Milano (2020).

[128] Available at https://www.ptc.com/en/products/cad/creo.

[129] C. G. Denise *et al.*, A Los Alamos Multigrouped Activation File, Los Alamos National Laboratory, preprint LA-UR-94-1471 (1994).

[130] P. Andreetto *et al.*, J. Phys.: Conf. Ser. 898, 052007 (2017).

[131] A. Zenoni *et al.*, Review Sci. Instrum. 88, 113304 (2017).

[132] D. Battini *et al.*, Materials and Design 156, 514 (2018).

[133] P. Bricault *et al.*, Proceedings of the 15th International Conference on Cyclotrons and their Applications, Caen, France (1998).

[134] J. Dilling, R. Kr*ü*cken and L. Merminga, Hyperfine Interact. 225, 1-3 (2014).

[135] A. Monetti, private communication.

[136] J. Vollaire , talk at SPES Safety TAC 2014.

[137] L. Centofante *et al.*, to be submitted to Eur. Phys. J. A.

[138] L. Sarchiapone and D. Zafiropoulos, Int. J. Mod. Phys. Conf. Ser. 44, 1660238 (2016).

[139] O. Almén and G. Bruce, Nuclear Instrum. Methods 11, 257 (1961).

[140] F. Brown and J.A. Davies, Can. J. Phys 41, 844 (1963).

[141] G. Carter *et al.*, Radiation Effects 53, 143 (1980).

[142] B.M. Oliver, G.C. Eiden and N.E. Ballou, Implantation and Release of Krypton with Copper Foils, PNNL-13642 (2001).

[143] D. Zafiropoulos, Relazione Tecnica in Materia di Radioprotezione Relativa al progetto SPES - Fase Alfa - dei Laboratori Nazionali di Legnaro dell'INFN, 2010.

[144] D. Zafiropoulos, Relazione Tecnica dell'Esperto Qualificato in Materia di Radioprotezione Relativa al progetto SPES - Fase Beta - dei Laboratori Nazionali di Legnaro dell'INFN, 2018.

[145] G. Prete, Descrizione del ciclo di vita del bersaglio di SPES Utilizzi successivi al primo irraggiamento, Internal report DOC-00000092, SPES Document Repository, Laboratori Nazionali di Legnaro (2017).

[146] A. Zanettin, Progettazione meccanica e test di una macchina per l'estrazione orizzontale del bersaglio di produzione del progetto SPES, Tesi di Laurea, Corso di Laurea Magistrale in Ingegneria Meccanica, Dipartimento di Ingegneria Industriale, Università degli Studi di Padova. Italy (2018).

[147] A. Donzella, Valutazioni preliminari sulle dosi del deposito temporaneo TIS, Internal report DOC-00000103, SPES Document Repository, Laboratori Nazionali di Legnaro (2019).

[148] F. D'Agostini, Il Temporary Storage System del progetto SPES, Internal report DOC-00000113, SPES Document Repository, Laboratori Nazionali di Legnaro (2018).

[149] G. Prete, Presentazione Progetto SPES, Ref. 170724, Laboratori Nazionali di Legnaro (2017).

[150] ISPRA - Centro Nazionale per la Sicurezza Nucleare e la Radioprotezione, Parere di competenza in merito alla richiesta di modifica del Nulla Osta di categoria A, Reg. I.0019030.26-07-2018.

[151] G. Prete, Il sistema di recupero gas di SPES (HA-GRS), Internal report DOC-00000045, SPES Document Repository, Laboratori Nazionali di Legnaro (2018).

[152] A. Andrighetto *et al.*, An alternative method to produce isotopes for medical applications in the framework of the SPES Project: Mo-99 from the UC_x target, Internal report Report DOC-00000237, SPES Document Repository, Laboratori Nazionali di Legnaro (2012).

[153] Directive 2001/42/EC of the European Parliament and of the Council, of 27 June 2001, on the assessment of the effects of certain plants and programmes on the environmental.

[154] Available at https://ec.europa.eu/environment/sustainable-development/.

[155] UNI EN ISO 14040:2006, Gestione ambientale - Valutazione del ciclo di vita - Principi e quadro di riferimento.

[156] UNI EN ISO 14044:2018, Gestione ambientale - Valutazione del ciclo di vita - Requisiti e linee guida.

Ringraziamenti

Non è mai troppo tardi per ricominciare...

Giunta oramai alla fine di questa avventura, ho il piacere di ringraziare tutte le persone che mi hanno sostenuto in questi tre anni molto belli e intensi della mia vita.

Il primo ringraziamento va al Prof. Aldo Zenoni. Caro Aldo, nei tanti anni di appartenenza al gruppo di ricerca di cui sei responsabile, ho sempre molto apprezzato il tuo grande talento, la professionalità, il rigore e la correttezza scientifica con cui affronti ogni attività. Mi hai trasmesso dei valori che giudico fondamentali per una persona: la passione per il proprio lavoro, il rispetto e la tolleranza nei confronti del prossimo.

Un particolare ringraziamento va al Dott. Alberto Andrighetto, responsabile del gruppo SPES Target dei Laboratori Nazionali di Legnaro dell'INFN. Il clima di serenità che respiro ogni volta che vengo ai LNL, e il modo in cui dirigi i "tuoi" ragazzi in questo importante progetto, con grande senso di responsabilità ed instancabile entusiasmo, hanno contribuito alla mia decisione di intraprendere questa strada.

Non posso non ringraziare Matteo, per me sempre un importante punto di riferimento. Nelle molteplici discussioni durante i periodi del (nostro) dottorato, sei stato un interlocutore attento e molto preparato, sensibile, capace di stupirti e di entusiasmarti per le cose che mano a mano sei riuscito a costruire.

Grazie ai miei colleghi Germano e Davide. Pur non lavorando direttamente sui temi della mia tesi, vi siete resi sempre disponibili a darmi preziosi consigli e a supportarmi nei momenti importanti.

Ringrazio i colleghi del DIMI, Ileana, Valerio e Diego, per l'entusiasmo e la professionalità nella collaborazione ai progetti SPES e ISOLPHARM. Grazie Diana per i preziosi consigli e per il tempo che mi hai dedicato leggendo parti della mia tesi. Grazie per il tuo rigore ma anche per la tua segreta passione per la "fisica nucleare".

Ed ora lasciatemi ringraziare i giovani colleghi di SPES, che mi hanno